Ph. D. DISSERTATION

Study on the internal structure of ferroelectric $Hf_{1-x}Zr_xO_2$ thin film systems

by

Han Joon Kim

February 2018

Department of Materials Science and Engineering
College of Engineering
Seoul National University

Study on the internal structure of ferroelectric $Hf_{1-x}Zr_xO_2$ thin film systems

Advisor : Prof. Cheol Seong Hwang

By

Han Joon Kim

A thesis submitted to the Graduate Faculty of Seoul National University in partial fulfillment of the requirements for the Degree of Doctor of Philosophy

Department of Materials Science and Engineering

February 2018

Approved

by

Chairman of Advisory Committee : Hyeong Joon Kim

Vice-chairman of Advisory Committee : Cheol Seong Hwang

Advisory Committee : Ho Won Jang

Advisory Committee : Deok Sin Kil

Advisory Committee : Seong Keun Kim

Abstract

Ferroelectric (FE) property of HfO_2 thin films was first reported in 2011 NaMLab in Dresden, Germany, which had a fluorite structure, doped with a few amounts of Si. It was a very intriguing issue on the FE community because the fluorite-type film has only ~ 10 nm thickness, whereas the conventional perovskite type ferroelectrics have > 100 nm thickness. It has merit for fabrication of 3-dimensional structure due to its small thickness. Also, the band gap of the HfO_2 thin film is 5.5 eV which is high enough to prevent leakage currents flowing through devices. Having titanium nitride as a metal electrode, combined with an excellent compatibility with Si, HfO_2 as a thin film could be the representative industrial-friendly materials for the adoption of memory production technology. It has been widely accepted that the emergence of unexpected ferroelectricity in HfO_2 thin films is due to the formation of non-centrosymmetric orthorhombic $Pca2_1$ phase. However, it still lacks researches on the emergence of ferroelectricity in this material systems.

Therefore, this dissertation aims to resolve the ambiguity of the origin of the emergence of ferroelectricity in thin films through researches on the internal structure of the FE HfO_2 thin films. For its robust ferroelectricity, many dopants were induced. (Si, Zr, Y, Al, Gd, Sr, La, etc.) Among these dopants, Zr doped HfO_2 has its wide composition range for emerging various electrical characteristics and lower processing temperature for crystallization of films.

Therefore, $Hf_{1-x}Zr_xO_2$ thin films are up-and-coming FE materials for analyzing the mechanism of emerging ferroelectricity.

As the first step, the degradation of the FE properties of atomic layer deposited $Hf_{0.5}Zr_{0.5}O_2$ films with increasing thickness was examined. When the thickness of the film increases over 20 nm, the FE properties of the films start to degrade whereas the 10 nm-thick film shows robust FE properties in previous reports. The origin of the degradation was elucidated by phase transition of non-FE monoclinic phase. According to general thin film growth theory, meanwhile, the grain size of the film increases with increasing film thickness. The grain size is the critical factor to get FE properties of $Hf_{0.5}Zr_{0.5}O_2$ films because the surface energy and volumetric energy are affected by the grain size. Therefore, control of the grain size of films is key point to interrupt degradation of FE properties despite of increasing film thickness. In this dissertation, the grain size is successfully controlled by inserting 1nm-thick Al_2O_3 interlayer at the middle position of the thickness of the FE film. The Al_2O_3 interlayer could hinder the continual growth of $Hf_{0.5}Zr_{0.5}O_2$ films, and the resulting decrease of grain size prevented the formation of the non-FE monoclinic phase. The Al_2O_3 interlayer also principally decreased the leakage current of the $Hf_{0.5}Zr_{0.5}O_2$ films.

As the next step, a “wake-up effect” on the FE $Hf_{0.5}Zr_{0.5}O_2$ films was examined which refers to the increase in remanent polarization with increasing electric field cycling number before the occurrence of fatigue effect. In this work, the wakeup effect from the $Hf_{0.5}Zr_{0.5}O_2$ was carefully examined by the pulse-switching experiment. At the pristine state, the $Hf_{0.5}Zr_{0.5}O_2$ film mostly

showed the FE-like behavior with a small contribution of antiferroelectric(AFE)-like distortion, which could be ascribed to the involvement of AFE phase. The field cycling of only 100 cycles almost wholly transformed the AFE phase into FE phase by depinning the pinned domains. The influence of field cycling on the interfacial layer was also examined through the pulse-switching experiments.

In addition to that, the broken FE hysteresis loops achieved from a $Hf_{0.4}Zr_{0.6}O_2$ film was interpreted based on the first order phase transition theory. The two-step polarization switching, which was expected from the theory, could be observed by dynamic pulse switching measurement. The variations in the interfacial capacitance values along with switching time and number of switching cycles could also be estimated from the pulse switching test. Being different from the one-step polarization switching in other FE films, two-step polarization switching produced two slanted plateau regions where the estimated interfacial capacitance values were different from each other. This could be understood based on the quantitative model of the two-step polarization switching with the involvement of an intermediate nonpolar phase. The $Hf_{0.4}Zr_{0.6}O_2$ film changed from AFE-like to FE-like with increasing number of electric field cycling, which could be induced by the field driven phase change.

Finally, this thesis presents a new strategy for extending conventional scaling trend in dynamic random access memory (DRAM) by utilizing newly found morphotropic phase boundary (MPB) of solid solution of the HfO_2-ZrO_2

system. For the purpose, the schematic phase diagram of HZO films with various thickness and Hf:Zr ratio was presented based on the previous works, and the MPB of tetragonal and orthorhombic phase for an abnormal increase in dielectric constant (ε_r) was found. From the C-V characterizations, the extraordinary ε_r values could be observed in the MPB, and it could be confirmed that the composition of films changes with changing film thickness. The Zr contents for MPB decreased with decreasing film thickness owing to the relative decrease of the free energy of o-phase compared to that of t-phase. The minimum t_{ox} of 0.59nm could be achieved for 8.1 nm-thick $Hf_{0.5}Zr_{0.5}O_2$ films.

Keywords : Ferroelectric, HfO_2, $(Hf,Zr)O_2$, ZrO_2, $Pca2_1$, Wake-up effect, Microstructure, First order phase transition theory, FeRAM, Capacitor, Nonvolatile memory, Atomic Layer Deposition

Student ID : 2012-24158

Han Joon Kim

Table of Contents

[1] H. J. Kim, et al., *Appl. Phys. Lett.,* **105**, 192903 (2014)

[2] H. J. Kim, et al., *Nanoscale,* **8**, 1383-1389 (2016)

[3] M. H. Park and H. J. Kim, et al., *Nanoscale,* **8**, 13898-13907 (2016)

[4] H. J. Kim, et al., Submission preparation

List of Tables

List of Figures

(with error bars whose magnitudes refer to the standard deviation of the average grain sizes from three measurements), and (c) in the relative ratio of the o(111)/{m(-111) + o(111) + m(111)} of the $Hf_{0.5}Zr_{0.5}O_2$ films on the Ir and TiN electrodes, respectively.

Figure 2. 5. Polarization-electric field curves of the $Hf_{0.5}Zr_{0.5}O_2$ films with various thicknesses on the (a) TiN electrode and the (b) Ir bottom electrode with a Pt/TiN top electrode, and (c) change in the double remanent polarization ($2P_r$) as a function of the film thickness, respectively.

Figure 2. 6. (a) Glancing incidence angle X-ray diffraction spectra of the 9.8-, 19.6-, and 24.5-nm-thick $Hf_{0.5}Zr_{0.5}O_2$ films on the TiN BE. (b) Normal X-ray diffraction spectra of the 13.0-, 18.1-, and 24.9-nm-thick $Hf_{0.5}Zr_{0.5}O_2$ films on the Pt BE. (c) Change in the in-plane strain calculated from the shift of the t(111) diffraction peaks as a function of film thickness, respectively.

Figure 2. 7. Grazing incidence x-ray diffraction measurements of two Si:HfO_2 samples of the same composition where crystallization was induced with and without capping. The molar SiO_2 content is approximately 3%, a composition where ferroelectricity was observed in MIM capacitors.

Figure 2. 8. Polarization-voltage characteristics of ~ 10-nm-thick $Hf_{0.5}Zr_{0.5}O_2$ films after (a) FGA with Pt TE, (b) FGA with Pt/TiN TE, and (c) NA with Pt TE. (d) Summary of the changes in $2P_r$ as a function

of annealing temperature. (FGA: forming gas (95% N_2 + 5% H_2) annealing and NA: N_2 annealing.)

Figure 2. 9. Polarization hysteresis (black) and AC C-V characteristics (thick red) of a set of "capped" MIM capacitors with 8.5 nm insulator thickness. The shape of the polarization loops changes from ferroelectric to antiferroelectric with increased SiO_2 admixture. This is reflected in one or two peaks in the AC C-V sweeps, respectively.

Figure 2. 10. (A) P-V curve at 1 kHz and small signal CV hysteresis at 10 kHz (50 mV level) of 9 nm thin HfO_2–ZrO_2 based metal–insulator–metal capacitors at room temperature. An evolution from paraelectric HfO_2 to ferroelectric HfO_2–ZrO_2 to an antiferroelectric-like behavior in ZrO_2 can be observed in PV as well as in C-V characteristics. (B) Current response to a triangular voltage excitation reveals polarization switching to be clearly separable from leakage current contributions at high fields. (C) Remanent polarization, dielectric constant, and monoclinic phase fraction in the HfO_2–ZrO_2 solid solution with respect to the mixing ratio of the oxides. With increasing ZrO_2 content the dielectric constant increases due to a reduction in monoclinic phase fraction, whereas the remanent polarization is maximized in the transition region.

List of Abbreviations

AC	Alternating Current
AES	Auger Electron Spectroscopy
AFM	Atomic Force Microscope
ALD	Atomic Layer deposition
BE	Bottom Electrode
BFO	$BiFeO_3$
BL	Bit Line
BTO	$BaTiO_3$
CMOS	Complementary Metal Oxide Semiconductor
C-E	Capacitance-Electric field
C-V	Capacitance-Voltage
D_{avg}	Average grain size
d_{hkl}	Inter-planar distance of (hkl) planes
DRAM	Dynamic Random Access Memory
DC	Direct Current
E_c	Coercive field
E_g	Bandgap
FeRAM	Ferroelectric Random Access Mermory
GAXRD	Grazing Angle incidence X-ray Diffraction
HRTEM	High Resolution Transmission Electron Microscopy
HZO	$Hf_{0.5}Zr_{0.5}O_2$
I-V	Current-Voltage
MFM	Metal-Ferroelectric-Metal

MIM	Metal-Insulator-Metal
MPB	Morphotropic Phase Boundary
m-phase	$P2_1/c$ m-phase
MOSFET	Metal-Oxide-Semiconductor Field-Effect-Transistor
o-phase	$Pbc2_1$ orthorhombic phase
P-E	Polarization-Electric field
P-V	Polarization-Voltage
PcRAM	Phase-change Random Access Mermory
PDA	Post-Deposition Annealing
PMA	Post-Metallization Annealing
PZT	$Pb(Zr,Ti)O_3$
RAM	Random Access Memory
P_r	Remanent Polarization
PUND	Positive Up Negative Down
ReRAM	Resistive Random Access Mermory
RTA	Rapid Thermal Annealing
SBT	$SrBi_2Ta_2O_9$
SEM	Scanning Electron Microscope
TE	Top Electrode
TEMA-Hf	Tetrakis-Ethyl-Methyl-Amino-Hafnium
TEMA-Zr	Tetrakis-Ethyl-Methyl-Amino-Zirconium
T_c	Curie Temperature
t_{ox}	Equivalent oxide thickness
t_f	Film thickness
t-phase	$P4_2/nmc$ tetragonal phase
V_c	Coercive voltage
XRD	X-ray Diffraction

ε_r	Dielectric constant
ε_r-E	Dielectric constant-Electric field

1. Introduction

1.1. Overview and Issues on ferroelectrics

Ferroelectricity has been reported by Valsek in the early 1920s as Rochelle salt and has been extensively studied in a variety of application including microelectromechanical systems (MEMS), radio frequency identification (RFID) chips and semiconductor memory devices. [1-4]

The ferroelectric (FE) material has two different remanent polarization states ($\pm P_r$) even if the electric field applied to the device is removed. When applied to memory applications, “0” and “1” information can be input. [3, 4] FE materials can also be applied to other applications such as pyroelectricity, piezoelectricity and high-k characteristics. In recent years, many researches have been conducted to apply energy-related applications using characteristics such as an electrocaloric effect. [5-8]

In order to use FE thin films for ferroelectric random access memory (FeRAM) application, materials having a perovskite structure such as $Pb(Zr,Ti)O_3$ (PZT), $BaTiO_3$ (BTO) and $SrBi_2Ta_2O_9$ (SBT) have been used. [4] However, the interface quality between the FE layer and the Si substrate is not good due to the difference in the crystal structure. Because the Si compatibility with the conventional FE materials, which is the fundamental template for

contemporary memory technology, was weak. [9] In general, when an interfacial SiO_2 layer is formed, this layer generates a depolarization field, making it difficult to maintain two bi-stable polarization states. Therefore, the direct integration of the conventional FE thin films on Si substrate has not been successful. Consequently, in order to solve above problem, a noble metal such as Pt or Ir was introduced as the bottom and top metal electrodes. [10] However, these noble metal electrodes have been inappropriate for commercial and mass-productive memory technology. In general, the conventional FE materials have a relatively small bandgap (E_g, 3 ~ 4 eV), which induces a Schottky barrier height of only ~ 1 eV with respect to the metal electrodes. It has a disadvantage that it is vulnerable to leakage current and electrical breakdown. Therefore, a relatively large film thickness (t_f ~ 100nm) is required for the charge-based FeRAM to be successfully used, which has a significant obstacle for manufacturing a three-dimensional capacitor structure for a technology node of several tens of nanometers. [11] Conventional FE materials can cause problems such as fatigue, imprint, and retention failure because the bond energy between metal ions and oxygen is relatively weak. [4, 12] Also, lead-containing materials such as PZT, despite of having shown excellent performance, are prohibited in many countries due to environmental issues. [12] Therefore, it is an urgent problem to develop an FE material having good compatibility with a Si substrate, high E_g and P_r, and high bonding energy between metal ions and oxygen. The FE thin film based on HfO_2 has been interesting because it is a simple binary oxide and has a relatively low permittivity as non-perovskite

structure materials.

In addition to the FE materials, other materials have a stable polarization-aligned state under certain bias conditions. In the vicinity of a specific ordered polarization state within the materials, it should be aligned with the opposite polarization state for systematically stable. A material having such properties is referred to as an antiferroelectric (AFE) material. The phenomenological study of antiferroelectricity was first initiated by Kittel in the early 1950s. [13] Unlike FE materials, AFE materials are not suitable for operation in memory applications because they do not have a residual polarization at zero-bias. Nonetheless, the AFE materials show double hysteresis loops in their polarization-electric field curve. Therefore, these properties can be applied to applications such as energy storage, [14-17] pyroelectric energy harvesting (PEH), [14, 18] solid-state cooling based on electrocaloric effects (ECE), [14, 17, 19] and IR sensing. [5, 20] Another application area is the materials which can measure the mechanical deformation by using the piezoelectric effects. This requires a large transition electric field, a large breakdown field, and a large piezoelectric constant. Therefore, Zr-rich PZT-based inorganic materials and poly(vinylidene fluoride) (PVDF) based polymer materials were the most likely candidates. [5-8, 18-20] However, the PZT thin film has environmental problems as aforementioned above, and the PVDF-based polymer has a low melting point and is unsuitable for use at high temperatures. [7, 19] Therefore, there is a need to develop a new lead-free AFE materials with a large transition electric field, a large breakdown field, and excellent thermal stability for the

above applications.

HfO_2-based FE and AFE materials were first reported in NaMLab, Dresden, Germany. [21] Figure 1. 1 shows the polarization – electric field (P - E, top row) curve and the piezoelectric displacement – electric field (bottom row) results of FE (left column) and AFE (right column) 10nm-thick Si-doped HfO_2 thin films. HfO_2 thin films with a doping concentration of Si 3.8 mol% showed ferroelectricity with a remanent polarization of 10 $\mu C/cm^2$. On the other hand, the HfO_2 thin film with 5.6 mol% doping concentration of Si showed AFE behavior. Surprisingly, the HfO_2-based thin films exhibit robust ferroelectricity at a film thickness of about 10nm, but the PZT films should have a thickness of 10^2-10^4 nm to achieve the same performance due to their small bandgap. Therefore, the use of 10nm-thick HfO_2 films enables the fabrication of three-dimensional capacitors for memory and energy storage applications. The HfO_2-based FE thin films have a much larger bandgap than that of the conventional perovskite-based FE materials, and the bonding force between oxygen and Hf (and their partner dopants) is much larger than that of conventional FE materials. [21-23] Therefore, leakage currents of HfO_2 films can be small even though they are thin films, and the reliability issues can be solved. Also, HfO_2 is already suitable for mass production and have been fabricated by highly matured atomic layer deposition (ALD). [23] TiN electrodes, which play a crucial role in the emerging ferroelectricity of HfO_2 thin films, are also standard materials in the semiconductor industry. [23] Because of this, HfO_2-based FE thin films offer significant advantages for industrialization and mass production.

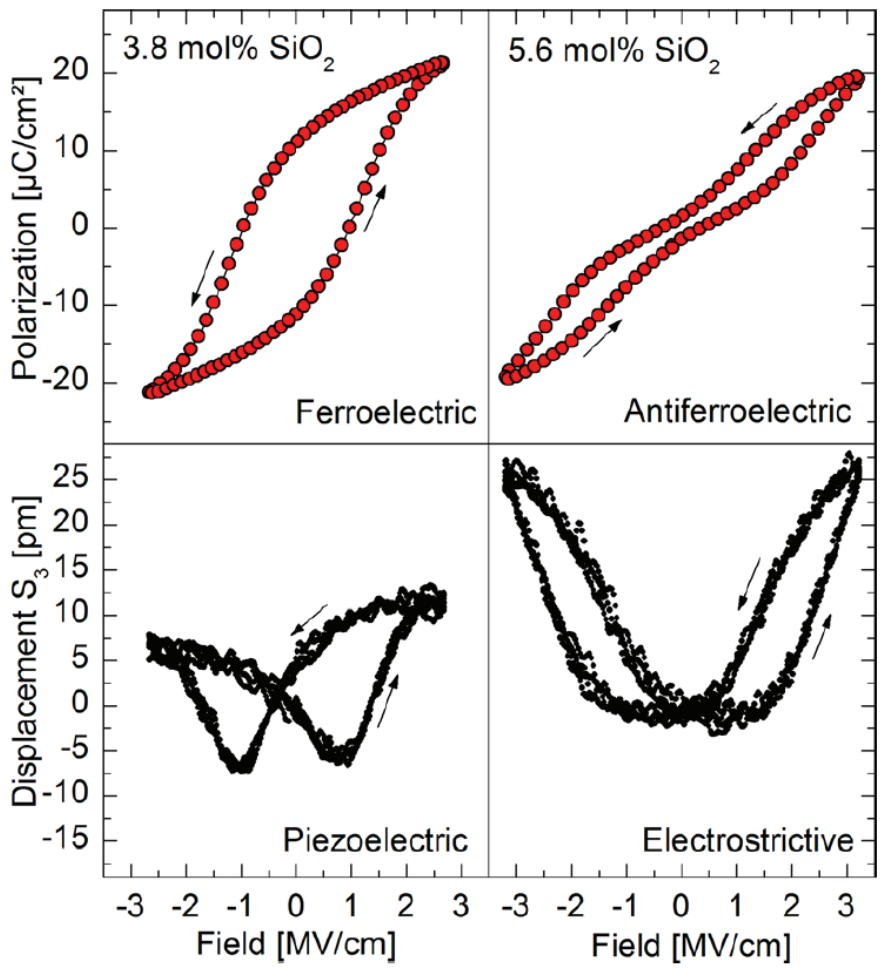

Figure 1. 1. Polarization (top row) and piezoelectric displacement (bottom row) measurement of TiN/Si:HfO_2/TiN capacitor sample with ferroelectric (left column) and antiferroelectric (right column) composition.

1.2. Objective and Chapter Overview

The objective of the present thesis is to study the internal structure of ferroelectric $Hf_xZr_{1-x}O_2$ thin film systems.

Chapter 3 presents that the degradation of ferroelectric properties of atomic layer deposited $Hf_{0.5}Zr_{0.5}O_2$ films with increasing thickness was mitigated by inserting 1 nm-thick Al_2O_3 interlayer at the middle position of the thickness of the FE film. The Al_2O_3 interlayer could interrupt the continual growth of $Hf_{0.5}Zr_{0.5}O_2$ films, and the resulting decrease of grain size prevented the formation of non-ferroelectric monoclinic phase.

Chapter 4 covers the wake-up effect from $Hf_{0.5}Zr_{0.5}O_2$ was carefully examined by the pulse switching experiment. The wake-up effect refers to the increase in remanent polarization with increasing electric field cycling number before the occurrence of the fatigue effect. In the pristine state, the $Hf_{0.5}Zr_{0.5}O_2$ film mostly showed FE-like behavior with a small contribution from AFE-like distortion, which could be ascribed to the involvement of the AFE phase. The field cycling of only 100 cycles almost completely transformed the AFE phase into the FE phase by depinning the pinned domains. The influence of field cycling on the interfacial layer was also examined through the pulse-switching experiments.

Chapter 5 reports the broken ferroelectric hysteresis loop achieved from a $Hf_{0.4}Zr_{0.6}O_2$ film, which was interpreted based on the first order phase transition

theory. The two-step polarization switching, which was expected from the theory, could be observed by dynamic pulse switching measurement. This could be understood based on the quantitative model of the two-step polarization switching with the involvement of an intermediate nonpolar phase. The $Hf_{0.4}Zr_{0.6}O_2$ film was changed from antiferroelectric-like to ferroelectric-like with the increasing number of electric field cycles, which could be induced by the field driven phase change.

Chapter 6 covers a new strategy for extending conventional scaling trend in dynamic random access memory by utilizing newly found morphotropic phase boundary of a solid solution of the HfO_2-ZrO_2 system.

Finally, in chapter 7, the conclusion of the thesis is made.

1.3. References

[1] J. Valasek, *Phys. Rev.,* **15**, 527 (1920).

[2] J. Valasek, *Phys. Rev.,* **17**, 475 (1921).

[3] M. E. Lines, A. M. Glass, Principles and Applications of Ferroelectrics and Related Materials, Oxford University Press, New York, USA 2001.

[4] J. F. Scott, Ferroelectric Memories, Springer-Verlag, Berlin, Germany 2000.

[5] R. W. Whatmore, *J. Electroceram.*, **13**, 139 (2004).

[6] A. S. Mischenko, Q. Zhang, J. F. Scott, R. W. Whatmore, N. D. Mathur, *Science*, **311**, 1270 (2006).

[7] B. Neese, B. Chu, S.-G. Lu, Y. Wang, E. Furman, Q. M. Zhang, *Science*, **321**, 821 (2008).

[8] C. R. Bowen, H. A. Kim, P. M. Weaver, S. Dunn, *Energy Environ. Sci.*, **7**, 25 (2014).

[9] M. Takahashi, S. Sakai, *Jpn. J. Appl. Phys.*, **44**, L800 (2005).

[10] T. Yamaguchi, M. Koyama, A. Takashima, S. Takagi, *Jpn. J. Phys. Lett.*, **39**, 2058 (2000).

[11] D. S. Jeong, R. Thomas, R. S. Katiyar, J. F. Scott, H. Kohlstedt, A. Petraru, C. S. Hwang, *Rep. Prog. Phys.*, **75**, 076502 (2012).

[12] N. Setter, D. Damjanovic, L. Eng, G. Fox, S. Gevorgian, S. Hong, A. Kingon, H. Kohlstedt, N. Y. Park, G. B. Stephenson, I. Stolitchnov, A. K. Taganstev, D. V. Taylor, T. Yamada, S. Streiffer, *J. Appl. Phys.*, **100**, 051606 (2006).

[13] C. Kittel, *Phys. Rev.*, **82**, 729 (1951).

[14] X. Hao, J. Zhai, L. B. Kong, Z. Xu, *Prog. Mater. Sci.*, **63**, 1 (2014).

[15] K. Yao, S. Chen, M. Rahimabady, M. S. Mirshekarloo, S. Yu, F. E. H. Tay, T. Sritharan, L. Lu, *IEEE T. Ultrason. Ferr.*, **58**, 1968 (2011).

[16] J. Li, S. Tan, S. Ding, H. Li, L. Yang, Z. Zhang, *J. Mater. Chem.*, **22**, 23468 (2012).

[17] S. E. Reyes-Lillo, K. F. Garrity, K. M. Rabe, arXiv:cond-mat/1403.3878, (2014).

[18] G. Sebald, S. Pruvost, D. Guyomar, *Smart Mater. Struct.*, **17**, 015012 (2008).

[19] S.-G. Lu, Q. Zhang, *Adv. Mater.*, **21**, 1983 (2009).

[20] A. J. Holden, *IEEE T. Ultrason. Ferr.*, **58**, 1981 (2011).

[21] T. S. Böscke, J. Müller, D. Bräuhaus, U. Schröder, U. Böttger, *Appl. Phys. Lett.*, **99**, 102903 (2011).

[22] M. H. Park, H. J. Kim, Y. J. Kim, W. Lee, H. K. Kim, and C. S. Hwang, *Appl. Phys. Lett.*, **102**, 112914 (2013).

[23] C. S. Hwang, Atomic Layer Deposition for Semiconductors, Springer US, New York (2013).

2. Literature

2.1. Conventional FE materials

Most ferroelectric materials for memory applications are based on perovskite or laminated perovskite structures, and their chemical structure is ABO_3. Typically, the A site cation is monovalent or divalent and the B site one is tetravalent or pentavalent. The perovskite structure is based on a cubic structure, with the cube corner (A), body center (B) and face center (oxygen ion) when the temperature (T) is higher than the Curie temperature (T_c). In low symmetric structures such as polynomial and rhombohedral systems, T can be lower than T_c. Figure 2.1 shows the crystal structure of PZT in a cubic structure (left panel, $T > T_c$) and a tetragonal structure (right panel, $T < T_c$). It should be noted that a cubic perovskite structure cannot be a ferroelectric due to its symmetric center. Of the various ferroelectric materials based on the perovskite structure, BTO is the first ferroelectric perovskite discovered, and only complex hydrogen-bonded crystals are known which can exhibit ferroelectricity before being discovered. The simple physics of ferroelectricity in perovskite structural materials provided physicists with the opportunity to study the beginning of ferroelectricity for the first time at a simple high symmetric prototype stage. BTO exhibits ferroelectricity below 120 °C and can be present in three ferroelectric phases such as 4mm tetragonal (5 - 120 ° C), mm orthorhombic (-90 - 5 ° C) and 3m trigonal phase (below - 90 ° C). The polar axes of the three

phases are [001], [011], and [111]. [1] PZT can be a widely used material in today's industry. It has a large P_r of ~ 80 μC / cm^2, which is also the strength for ferroelectric memory applications. Even in the thin film form, the P_r of PZT is generally 30 - 50 μC / cm^2 and the thickness is several hundred nanometers. Scott et al., in the mid-1970s, in a study entitled "Ferroelectric Memories" in the United States and Western Europe, found that PZT is the most important material in ferroelectric memory in its initial state. [2] However, since PZT has many problems such as deterioration due to hydrogen annealing, a poor interface with Si, and environmental issues of Pb contents, SBT can be free from this problem has been suggested. Araujo et al. SBT has been reported to feel fatigue after 10^{12} cycles which are larger than that of PZT several order of the magnitude. $BiFeO_3$ (BFO) is another important material with multiferroic properties, which means coexistence of ferroelectricity and ferromagnetism. [4,5] Several ferromagnetic phenomena can be found in other materials, but they are far from practical applications due to temperature limitations. The P_r (~50 - 60 μC/cm^2) of the thin BFO thin film is larger than the that of the bulk BFO due to P4mm tetragonal phase in thin film, different from R3c rhombohedral in bulk form. Its anti-ferromagnetic properties can also be found on magnetic properties.

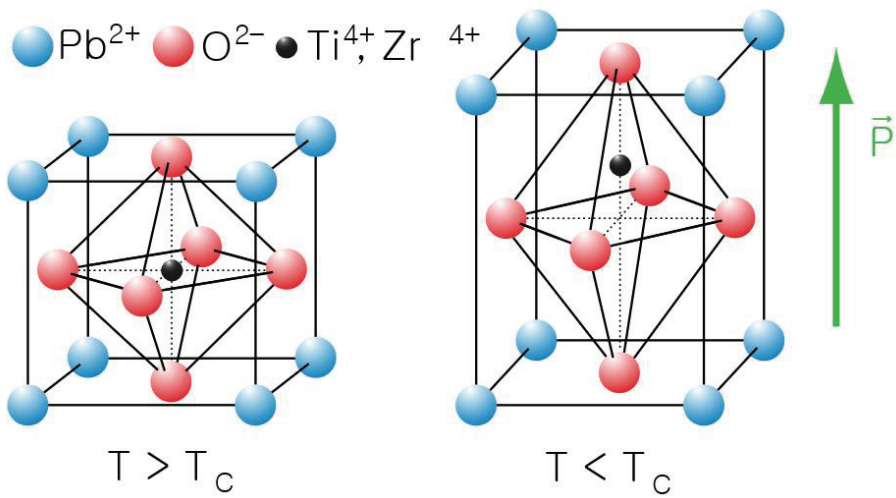

Figure 2. 1. The crystal structure of $Pb(Zr,Ti)O_3$ with cubic structure (Left panel, $T>T_c$) and that with tetragonal structure (Right panel, $T>T_c$), respectively.

2.2. HfO_2 based FE materials [7]

2. 2. 1. Identification of FE phase

It is very plausible that the origin of ferroelectricity in the doped HfO_2 film is o- phase formation because it is challenging to experimentally identify the phase, especially in thin films using conventional X-ray diffraction techniques [8-10]. This is mostly the same in the phases of o- and t- (doped) HfO_2 and ZrO_2, which can be easily understood from the symmetry of the phase structure shown in Fig. 1b. Also, diffraction patterns become very complicated because of the widened peak shape due to the coexistence of random directions of different phases in small grain size (D_{ave}) and $t_f \sim 10$ nm films. Grazing incident X-ray diffraction (GIXRD) is advantageous to increase the intensity of diffracted X-rays, but is not sufficient to intelligently and quantitatively identify phases in HfO_2 based films. Despite these difficulties, Böscke et al. reported a clear difference between m-, t-, and o- GIXRD patterns in Si-doped HfO_2 thin films. [8] After that, the diffraction pattern in the 2-theta range of 80-90° was also adopted to identify the phases for Y, Gd, Al and Zr doped HfO_2. [10-13] Among these results, S. Müller et al. reported that Al-doped HfO_2 was the most systematic and clear by showing the difference of XRD patterns. Figure 2. 2 shows a GIXRD diffraction diagram for an Al-doped HfO_2 film having various Al-doping concentrations of 0 to 11.4% deposited by an ALD process and having a post-annealed at a temperature of 800-1000 °C for crystallization. Pure HfO_2 is m-phase, whereas phase transition from m- to o- to c-phase can be

clearly observed as the Al content increases. [10] In particular, the data for the 2θ range 80-90 ° of HfO_2 with different Al doping concentrations was enlarged in Fig. 2. 2(b), which showed the clearest differences over the entire 2θ range. They observe the diffraction peaks from the positive (331), (133) and (421) planes of o- phase, which can be distinguished from the diffraction peaks from the t- and m- phases. [10] On the contrary, Park et al. reported that GIXRD data in the 2θ range of 27-33° could be very useful for quantitatively identifying not only the types of steps involved but also the related parts using deconvolution techniques. The peaks of the various compositions for $Hf_{1-x}Zr_xO_2$ films appear over a broad composition and t_f range. [14]

In contrast, in a recent report on Y-doped HfO_2 films grown by a sol-gel solution process, Starschich et al. could not observe any evidence for the formation of o- phases in the 2θ range of 80-90°. [9] They were able to observe a unique diffraction peak from the known c-phase for the structure of Y-doped HfO_2. [9] In this study, the thickness of the Y-doped HfO_2 film (up to ~ 70 nm) was the largest reported among the reported results for structural analysis using XRD. However, they clearly showed the FE characteristic P-E hysteresis curve. This will be discussed in more detail in the next section.

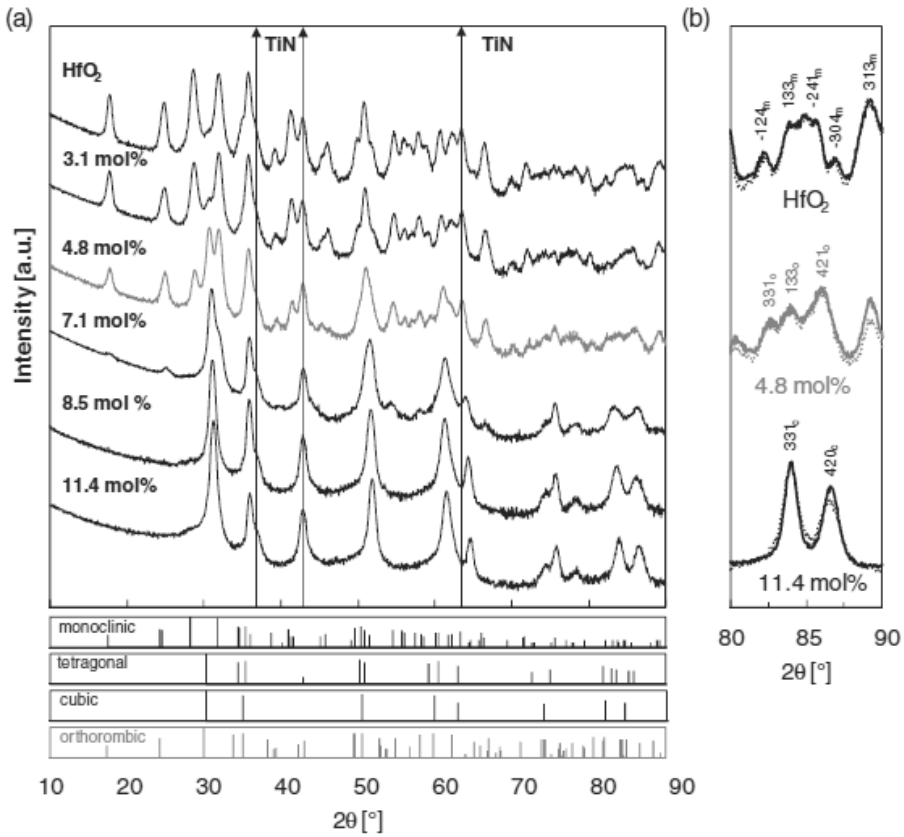

Figure 2. 2. (a) GAXRD diffractograms for PMA samples having different aluminium concentrations. A monoclinic-to-cubic phase transition is clearly visible for increasing aluminium content. The powder diffraction patterns as well as the calculated orthorhombic $Pbc2_1$ reference pattern are shown below the diffractograms. The composition which possesses the purest ferroelectric properties is highlighted in blue. (b) Enlarged 2θ scans from 80 ° to 90 ° for paraelectric HfO_2 containing no aluminium, ferroelectric HfO_2 containing 4.8 mol% aluminium, and, again, paraelectric HfO_2 containing 11.8 mol% aluminium. The diffractogram of the ferroelectric composition shows a triplet which would not be expected for monoclinic, tetragonal, or cubic phases. The dotted lines show results for PDA samples of the same composition. [9]

2. 2. 2. The effect of film thickness and grain size

The FE characteristics are highly dependent on the particle formation process, and t_f and T budgets are generally known to affect the average grain size. So far, it appears important that the dielectric layer is deposited on an amorphous phase that is crystallized in a subsequent annealing step. Böcke et al. reported that the capped top electrode reduces m- phase formation by avoiding cell shear and volume expansion during the crystallization process. [15] Si and Gd-doped films exhibited stable P_r values in the t_f range accessible by ALD deposition (5 to 30 nm). [16, 17] Yurchuk et al. initially reported a decrease in P_r for higher thicknesses, but thicker films already crystallized during deposition which results in a higher amount of the m-phase. [18] Similar results were obtained in the $Hf_{0.5}Zr_{0.5}O_2$ layer. [19] Here, the deposition temperature is very close to the crystallization temperature. It also prefers a higher amount of m-phase grains and a lower P_r value for the thicker layer.

Park et al. investigated the effect of t_f on FE characteristics of $Hf_{0.5}Zr_{0.5}O_2$ films. [20] They tested $Hf_{0.5}Zr_{0.5}O_2$ films with various t_f (5.5-25 nm) and annealing temperatures (400-800 °C). Figure 2. 3(a) showed that the P_r of $Hf_{0.5}Zr_{0.5}O_2$ films was maximum (~ 15 $\mu C/cm^2$) at ~ 10 nm thickness and ~ 12 $\mu C/cm^2$ and ~ 5 $\mu C/cm^2$ when the t_f increased to 17 and 25nm, respectively. This can be understood from the fact that the portion of the m-phase increases as the t_f of $Hf_{0.5}Zr_{0.5}O_2$ increases. [14] The effect of the t_f on the change of P_r can be attributed to a change in the grain size of the $Hf_{0.5}Zr_{0.5}O_2$ film having an

increased thickness. (Figures 2. 4 and 2. 5) Polymorphic HfO_2 and ZrO_2 polymorphisms are dominated by size effects, especially when the grain size is <~ 100 nm. [21-26] The critical grain size for obtaining tetragonal phase is ~ 4, and for HfO_2 and ZrO_2 ~ 32nm, the grain size of $Hf_{0.5}Zr_{0.5}O_2$ is estimated to be ~ 18nm by interpolation method based on Vegard's law. [23, 24] When the grain size of the HfO_2 based film is maintained, the tetragonal phase can be induced by surface or grain boundary effects below the critical dimension. The specific surface area of the o- phase is not known experimentally, but it can be assumed that this can contribute to o- phase stabilization. This can be a mechanism to compensate for the appropriate asymmetric stress known to cause an o- phase. The effect of grain size on phase stability is described by Materlik et al. [27] Obviously, obtaining a grain size smaller than a critical dimension that does not induce the formation of a stable m- phase is a prerequisite for achieving FE or AFE behavior from HfO_2 based films. It is clear that when $Hf_{1-x}Zr_xO_2$ films (and other doped HfO_2 films) are grown by ALD, the grain size is highly dependent on the t_f: the thicker the t_f, the higher the m- phase and the lower the FE performance. [14, 18] Therefore, the maximum t_f for possible FE and AFE performance is limited to ~ 20 nm for $Hf_{1-x}Zr_xO_2$ and to a minimum of 30 nm for Si or Gd-doped HfO_2. However, this is not necessary when other deposition techniques are used. Starschich et al. have reported that Y-doped HfO_2 thin films can exhibit feasible FE performance of up to 70 nm t_f when grown by chemical solution deposition (CSD). [9] Although the source of this

phenomenon is not exclusively known, a step by step process of coating-annealing-crystallization that produces a layer about 7 nm thick per step can induce perturbations of columnar crystal growth to a total of t_f. A desirable aspect of this thick FE Y-doped HfO_2 thin film is that it is advantageous for clearly identifying the phase and obtaining a clear piezoelectric response signal in laser interferometer measurements which are direct evidence of FE interference distortion. [28] Interestingly, both the 18 nm and 70 nm thick films exhibited a c- phase structure with no o- phase, but the laser interferometer measurements revealed that the films exhibited piezoelectric properties as expected for the FE material. Phase shift during on-site cycling may be the cause of this effect. Another important point of this study is that Pt is used for the bottom electrode and top electrode for solution-based processes that produce undesirable results for ALD-based $Hf_{1-x}Zr_xO_2$ thin films. (Fig. 2. 3(b)) [20] Therefore, there is still much work to fully understand the basic principles of FE performance and phase transitions.

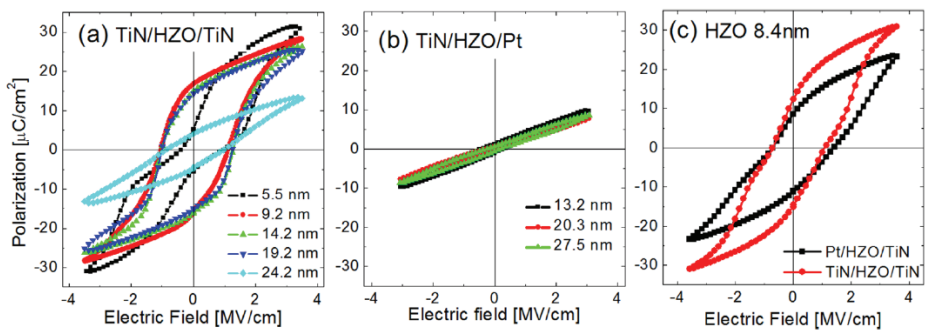

Figure 2. 3. (a) P-E characteristics of the $Hf_{0.5}Zr_{0.5}O_2$ capacitors with various film thicknesses on TiN, and (b) those on Pt, respectively. The TE was Pt(60 nm)/TiN(20 nm) for both cases. (c) P-E characteristics of the 8.4-nm-thick $Hf_{0.5}Zr_{0.5}O_2$ capacitor on TiN with Pt(60 nm)/TiN(20 nm) and Pt(80 nm). [20]

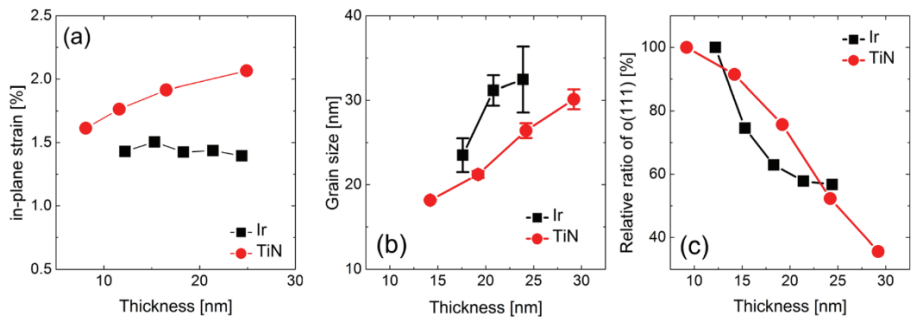

Figure 2. 4. (a) Variations in the in-plane strain, (b) in the average grain size (with error bars whose magnitudes refer to the standard deviation of the average grain sizes from three measurements), and (c) in the relative ratio of the o(111)/{m(-111) + o(111) + m(111)} of the $Hf_{0.5}Zr_{0.5}O_2$ films on the Ir and TiN electrodes, respectively. [44]

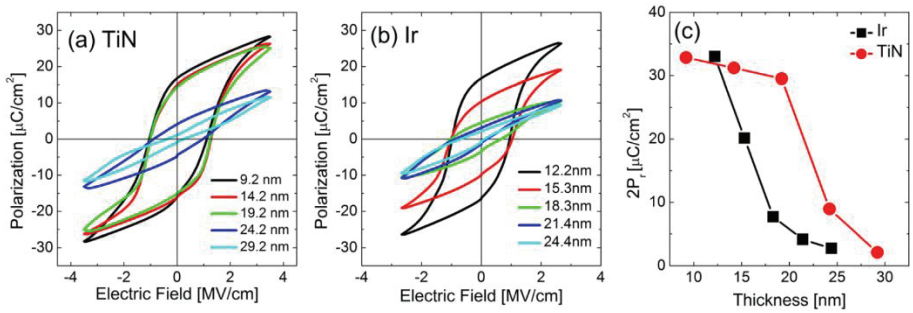

Figure 2. 5. Polarization-electric field curves of the $Hf_{0.5}Zr_{0.5}O_2$ films with various thicknesses on the (a) TiN electrode and the (b) Ir bottom electrode with a Pt/TiN top electrode, and (c) change in the double remanent polarization ($2P_r$) as a function of the film thickness, respectively. [44]

2. 2. 3. The effects of asymmetric stress

Park et al. systematically investigated the origin of unexpected FE phase formation regarding asymmetric stress action during thin film growth of $Hf_{0.5}Zr_{0.5}O_2$ thin films. [20] In the knowledge of the crystal structure at various stages of HfO_2 and ZrO_2, they investigated the c / a ratio of the t- phase and 2b / (a + c) ratio of the o- phase of ZrO_2 and HfO_2 to the bulk phase. It can be seen that the c-axis of o- phase which is the direction of P_r has the shortest lattice parameter but the non-polar b-axis has the longest. On the other hand, in the case of t- phases, since the c-axis has the longest lattice parameter, the c-axis on the t- phase becomes the b-axis on the o- phase during the phase transition. It can be seen that the ratio of 2b / (a + c) of the o- phase (both ZrO_2 and HfO_2) is higher than the c / a ratio of t- phase system. [11, 14, 29-33] In addition to the difference in the ratio of o- and t- phases, there is another subtle difference between HfO_2 and ZrO_2, which can play an important role in understanding the phase transition behavior induced by strain. The difference between 2b / (a + c) of o- phase and c / a ratio of t- phase were higher for ZrO_2 than that of HfO_2. [19, 20, 30-34] Therefore, in the case of ZrO_2, much higher stress (~4 GPa) would be required for the transition from t- to o- phases, which is why Zr-rich $Hf_xZr_{1-x}O_2$ thin films cannot be FE. Zr-rich $Hf_xZr_{1-x}O_2$ films tend to retain t-phase and become AFE. [35]

On the other hand, in the case of HfO_2, it is challenging to prevent the formation of a stable m- phase because the critical grain size for the transition to t- phase

(~ 4 nm) is much smaller. [36] Therefore, the FE o- phase can hardly be formed despite the small strain required to induce the transition to the o- phase. Therefore, Hf-rich $Hf_xZr_{1-x}O_2$ films are left in a m- phase, which is a high-k dielectric, and the FE phase can usually be obtained from a composition around Hf: Zr ~ 0.5: 0.5. [11] These considerations take into account possible variations based solely on the difference in lattice parameters on the t- and o- phases, but in practice, this is, in fact, similar to the theoretical considerations proposed by Reyes-Lillo et al. [35]. They suggested that the in-plane compressive stress on the a-b plane of a t- phase originated from an unexpected FE o- phase that could induce tensile strain along the c-axis of the t- phase. [35] However, the polarization component caused by such a mechanism is parallel to the film surface and cannot be measured. In thin film growth, in-plane tensile stress can be induced by several mechanisms, but in the case of ALD $Hf_{0.5}Zr_{0.5}O_2$ films, it has been suggested that compressive stress is an appropriate reason to impose a film at the desired stress state. [20, 37, 38] Zipping stress is the stress imposed on the entire film when adjacent nuclei begin to contact each other, causing the grain (or amorphous cluster) boundary to become "zipped". [37, 38]

The crystallographic orientation of the $Hf_{0.5}Zr_{0.5}O_2$ particles was another important factor for this mechanism to work. Since the growth nuclei have a t-phase structure before being compressed, the surface energy effects must be different in the deformed state due to nuclear compression depending on the original crystallographic orientation. Park et al. can use the in-plane stress

conditions of thin films to calculate the strain along the a, b, and c axes for various directions of the grains. [20] As a result, 110-orientation was most favorable for the formation of o- phase from t-phase, while 111-orientation was worst because the almost uniform strain was formed along a-, b- and c-directions. This actually produced a 111-highly oriented $Hf_{0.5}Zr_{0.5}O_2$ film as a result of the experiment on the ALD $Hf_{0.5}Zr_{0.5}O_2$ film on the 111-direction Pt electrode. [20] A highly 111-oriented 9.2 nm thick $Hf_{0.5}Zr_{0.5}O_2$ film showed neither an FE nor AFE even though 111 characteristic $Hf_{0.5}Zr_{0.5}O_2$ films meet the above conditions for the appearance of FE characteristics (grain size, stress, and composition) (Fig. 2. 3(a)). In contrast, the $Hf_{0.5}Zr_{0.5}O_2$ film grown at the same time on the TiN electrode exhibited FE performance without exhibiting the preferred orientation and possible P-E hysteresis (Fig. 2. 3(b)). [20] As shown in Fig. 2. 6(c), the in-plane strain in the $Hf_{0.5}Zr_{0.5}O_2$ thin film deposited on the Pt bottom electrode is the same as that of the TiN bottom electrode. Thus, the formation of the FE o- phase is very sensitive to film orientation in addition to the grain size determined by the t_f in the case of ALD. It should also be noted that the FE (and AFE) performance can be further enhanced by appropriate control of the film growth direction, perhaps by adopting other substrates and growth methods/conditions, since the current level of FE performance is obtained from the mostly randomly oriented films.

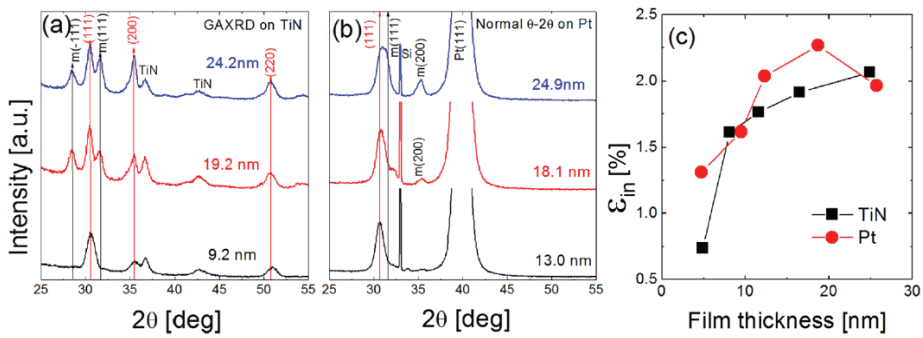

Figure 2. 6. (a) Glancing incidence angle X-ray diffraction spectra of the 9.8-, 19.6-, and 24.5-nm-thick $Hf_{0.5}Zr_{0.5}O_2$ films on the TiN BE. (b) Normal X-ray diffraction spectra of the 13.0-, 18.1-, and 24.9-nm-thick $Hf_{0.5}Zr_{0.5}O_2$ films on the Pt BE. (c) Change in the in-plane strain calculated from the shift of the t(111) diffraction peaks as a function of film thickness, respectively. [20]

2. 2. 4. The effect of TiN capping and annealing

TiN is known as the best electrode material for FE HfO_2-based films. In a related report on this subject, a FE HfO_2-based film was sandwiched between the top and bottom TiN electrodes. [8, 10-15, 18-20, 39-48] Figure 2. 7 shows compared the GIXRD patterns of crystallized Si-doped HfO_2 thin films before and after deposition of the top TiN capping layer. [8] When annealing the thin film before depositing the upper TiN capping layer, the intensity of the diffraction peak from the m- phase is much greater than that from the o- phase. [8] On the other hand, in the case of the thin film crystallized with the TiN capping layer, the diffraction peak from the m- phase was hardly observed. The TiN capping layer can mechanically clamp the film to prevent volumetric expansion and shear of monoclinic unit cells, thus acting as a mechanical confinement to suppress non-ferroelectricity formation. However, this may be one of several factors and may not be the cause of ferroelectricity as in other experiments. Although not explicitly described, this may involve inhibiting ion migration at the film surface during annealing, which can lead to m-phase formation with grain growth. In the case of the doped HfO_2 thin film, the crystallized thin films without the capping layer showed a relatively smaller P_r value than those with the capping layer. [10, 12, 13]

In contrast, for the $Hf_{0.5}Zr_{0.5}O_2$ film, the role of the TiN capping layer was reported to be less important than Si-doped HfO_2. Park et al. reported that the P_r values of $Hf_{0.5}Zr_{0.5}O_2$ capacitors with or without a TiN capping layer are

nearly equal when the TiN layer deposition process is carefully optimized. [38] This may be related to lower annealing temperatures than Si-doped HfO_2 (1000 °C) compared to $Hf_{0.5}Zr_{0.5}O_2$ (400 - 600 °C). [11, 14, 19, 20, 38, 42-44] Since the low annealing temperature did not cause any significant grain growth, the m-phase formation was suppressed even without the capping TiN layer. Lomenzo et al. reported that Ir could be used as a capping layer instead of TiN in a report on Si-doped HfO_2 thin films. [49] In this experiment, they used Si and Ir, which are heavily doped with the bottom electrode and the top electrode, respectively. [49] Capacitors without TiN exhibit strong ferroelectricity, indicating that TiN is not the only bottom electrode materials in Si-doped HfO_2 thin films. Schenk et al. reported an improved P_r value by replacing the TiN electrode with TaN for Gd: HfO_2 where the P_r value was increased from 20 $\mu C/cm^2$ to 30 $\mu C/cm^2$ by changing the two electrodes. [50]

On the other hand, considering that the bottom electrode hardly changes to obtain the desired crystal structure, the top electrode, especially the conductive oxide electrode, was an important asset for improving the reliability of the FE PZT layer. [51, 52] Park et al. have attempted to improve the durability characteristics of the $Hf_{0.5}Zr_{0.5}O_2$ capacitor by replacing the TiN top electrode with RuO_2, which is well known for improving the durability of existing FE materials such as PZT. [43] However, in the crystallization process, the RuO_2 decreased due to the oxygen scavenging effect of the lower TiN layer, and the FE characteristic of the $Hf_{0.5}Zr_{0.5}O_2$ capacitor was greatly reduced. [43] Figure

2. 8 showed that the TiN layer can serve as a barrier to H bonding during molding gas annealing, although $Hf_{0.5}Zr_{0.5}O_2$ is generally much more immune to decomposition by hydrogen gas annealing than conventional FE materials. [19]

The TiN and TaN capping layers are generally believed to improve the FE characteristics of HfO_2-based films in general when the crystallization is carried out at high temperatures (800-1000 ^oC). [10, 12, 13] Ir capping layers are similar. [49] So far, the FE HfO_2-based films sandwiched by the top and bottom TiN electrodes appear to be the best structure in practical applications. When the electrode is RuO_2, the oxygen scavenging effect of TiN should be carefully controlled. [43] The role of cost-effective H-matching, Si compatibility and barrier layers for TiN is more attractive for electrode materials in HfO_2-based films. [19]

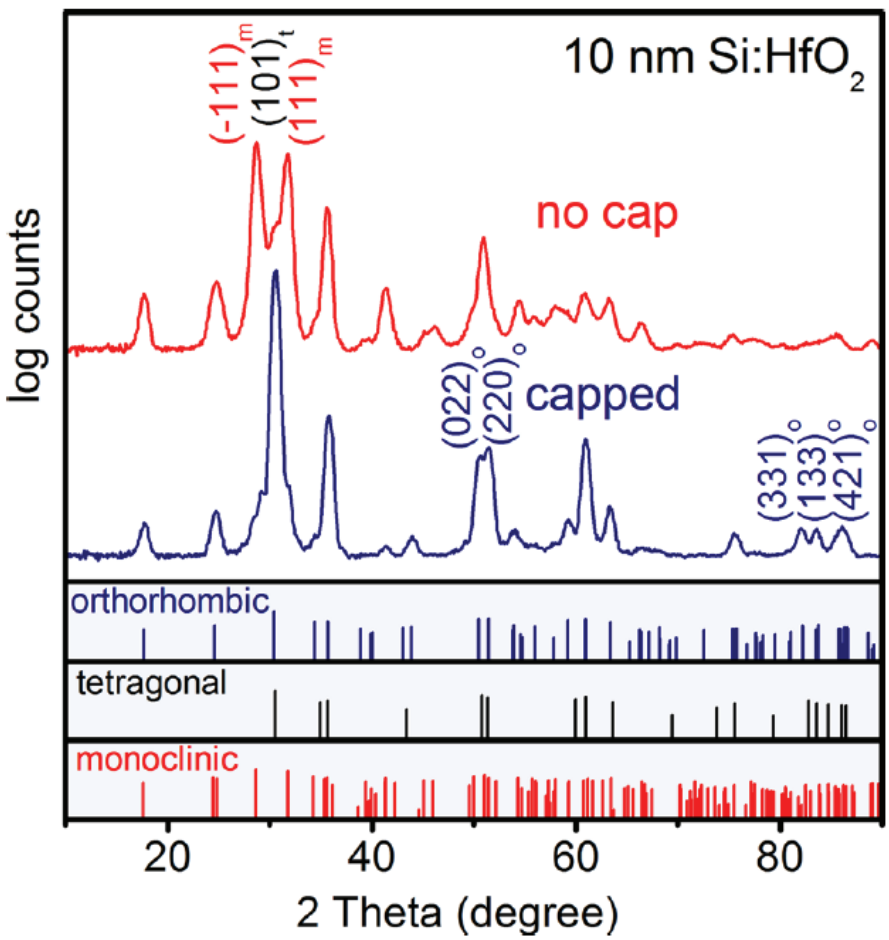

Figure 2. 7. Grazing incidence x-ray diffraction measurements of two Si:HfO_2 samples of the same composition where crystallization was induced with and without capping. The molar SiO_2 content is approximately 3%, a composition where ferroelectricity was observed in MIM capacitors. [8]

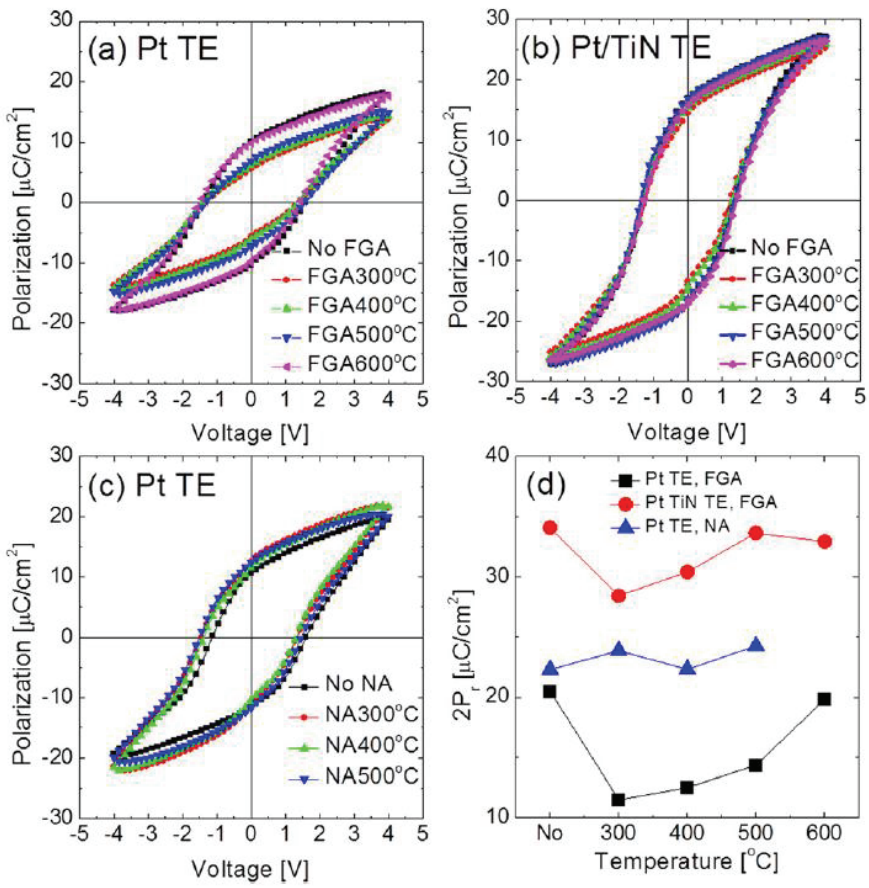

Figure 2. 8. Polarization-voltage characteristics of ~ 10-nm-thick $Hf_{0.5}Zr_{0.5}O_2$ films after (a) FGA with Pt TE, (b) FGA with Pt/TiN TE, and (c) NA with Pt TE. (d) Summary of the changes in $2P_r$ as a function of annealing temperature. (FGA: forming gas (95% N_2 + 5% H_2) annealing and NA: N_2 annealing.) [19]

2. 2. 5. The effects of dopants

Various dopants such as Si, Al, Zr, Y, Sr, La and Gd have been reported to induce ferroelectricity in the HfO_2 films. [8-15, 18-20, 39-48] This is known to enhance t- or c- phase formation to obtain higher ε_r in the field of high-k gate dielectrics, [53] which is a prerequisite for the final transition to the well-known o- phase. This section summarizes the FE and AFE characteristics of HfO_2 thin films with various dopants.

2. 2. 5. 1. Si-doped HfO_2 films

The FE characteristics of Si-doped HfO_2 were first reported in 2011 and had been primarily studied in the Namlab / Fraunhofer CNT collaboration. [8, 15-18, 40, 41, 49] The AFE properties of Si-doped HfO_2 have also been reported, but there is a report mostly focused on FE characteristics. (Figure 2. 9) Because Si is the base material for the semiconductor industry, adopting Si as a doping material is preferred regarding maturity and contamination control of semiconductor mass production processes.

Si is a tetravalent material whose atomic radius (110 μm) is about 29% smaller than the atomic radius of Hf (155 μm). [54] Si doping is known to stabilize the t- phase of HfO_2, and it is known that the maximum solubility of Si in HfO_2 is about 9%. [56] When the atomic ratio of Si and Hf is 1: 1, $HfSiO_4$ is known as Hafnon and is stabilized, but hardly seen in studies of Si-doped HfO_2 films. [16] Hoffmann et al. reported a comparison of P_r values for two different t_f at 12 and 36 nm. [17] These result shows the ε_r change of a 12 nm thick film as a function

of Si concentration. For both thicknesses the maximum polarization is achieved in the region of AFE properties of ~ 3.8% Si, then 5 to 8% Si, the material shows paraelectric properties only at high Si concentration. One indication of the transition is the position of the (111) o- phase or the (011) t- phase peak of the XRD pattern. This position shifts from about 30.6 ° in the FE o- phase to 30.8 ° to 31.3 ° in the AFE t- phase, indicating expansion of the lattice. The thick 30 nm film is larger than the 10 nm film. In parallel with this phase transformation, ε_r in the material increases from ~20 in the m- phase to ~38 in the t- phase. [16, 40] In this dopant, the annealing condition causes similar grain formation and the stable P_r value. Richter et al. found that there is a clear correlation between the dopant concentration of the 10 nm thick film and the electric field cycle behavior. [16] Between 2 and 3%, the film is paraelectric and can cause ferroelectricity in these layers during the field cycle and can be seen by hysteresis measurement. Furthermore, when the Si concentration was increased, the field inducing the FE polarization of these AFE layers showed the complete polarizability of the FE layer [39, 57]. The rectangular pattern can be polarized at the surface in both polarization directions. A typical domain size was determined to be 100 - 300 nm. Zhou et al. reported that the leakage current density of a 10 nm thick Si-doped HfO_2 film under a huge electric field of 3 MV/cm is less than 4×10^{-5} A/cm^2. [40] J. Muller and colleagues investigated the cycling reliability of Si-doped HfO_2 capacitors sandwiched between the TiN top electrode and the bottom electrode. [58] On the other hand, the both positive

and negative P_r state did not decrease until 10^3 hours at 125 °C. [58] Therefore, the durability of the Si-doped HfO_2 film needs to be improved for the semiconductor memory field. One of the common problems with doped HfO_2-based FE layers is the very high coercive fields (E_c) of ~ 1 MV/cm. When the t_f of the thin film is 10 nm, the coercive voltage (V_c) can be ~ 1 V, but a drive field high enough (~ 3 MV/cm) is required to get the full P_r. Therefore, because of the high binding energy between oxygen and metal ions, it is inherently more reliable than conventional FE materials, but the intrinsic life cycle of new FE materials has not been studied yet. [14]

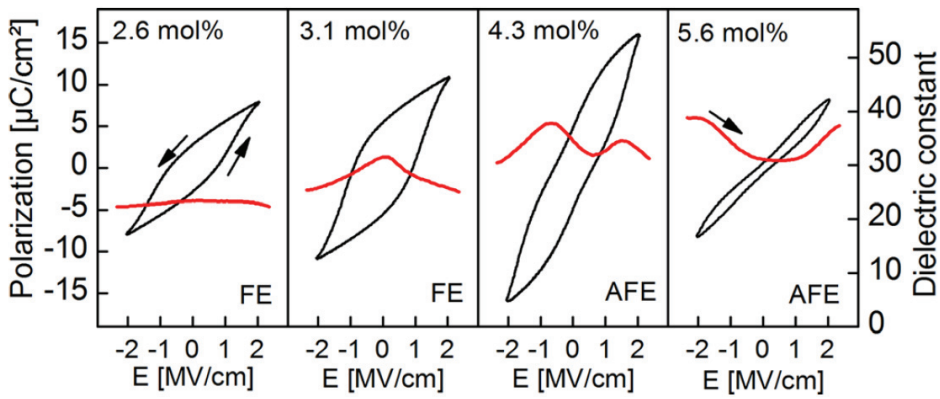

Figure 2. 9. Polarization hysteresis (black) and AC C-V characteristics (thick red) of a set of "capped" MIM capacitors with 8.5 nm insulator thickness. The shape of the polarization loops changes from ferroelectric to antiferroelectric with increased SiO_2 admixture. This is reflected in one or two peaks in the AC C-V sweeps, respectively. [8]

2. 2. 5. 2. $Hf_{1-x}Zr_xO_2$ films

ZrO_2 and HfO_2 exhibit very similar physical and chemical properties. Zr is tetravalent, and its atomic radius (155 pm) is almost equal to that of Hf (155 pm). [54] And they have almost the same crystal phase with almost the same lattice constant. Because of their similarity, the HfO_2-ZrO_2 system forms a single-phase solid solution over the entire composition range. [11] HfO_2 and ZrO_2 are used as standard materials in high-k gate dielectric layers of advanced metal oxide semiconductor field effect transistors (MOSFETs) and DRAM capacitors. This means that these materials are highly matured in the semiconductor industry. [59] J. Muller et al. first reported the FE characteristics of $Hf_{0.5}Zr_{0.5}O_2$ films. [42] Their typical P_r values are ~ 15 $\mu C/cm^2$, and E_c is 1 MV/cm. For the Hf- and Zr- rich composition, paraelectric (ε_r = ~ 20) and AFE characteristics are achieved, respectively. Figure 2. 10(a) shows P-E hysteresis and ε_r-E curves for $Hf_{1-x}Zr_xO_2$ (x = 0, 0.3, 0.4, 0.5, 0.7 and 1.0) films. Figure 2. 10(b) shows that the leakage current through the thin FE and AFE layers has little effect on P-E hysteresis curve. As shown in Figure 2. 10(c), the maximum P_r value of ~ 16 $\mu C/cm^2$ can be obtained for the $Hf_{0.5}Zr_{0.5}O_2$ film. [11] The lower panel in Figure 2. 10(c) shows that the value increases as the ZrO_2 content increases and the m-phase fraction decreases. $Hf_{1-x}Zr_xO_2$ thin films can be crystallized at 400-600 ^oC compared to HfO_2 containing Si. [11, 14, 19, 20, 42-44, 60-63] Lower annealing temperatures than Si-doped HfO_2 can be an advantage of $Hf_{1-x}Zr_xO_2$ thin films in the integration process. The ε_r of 10 nm-

thick-FE-$Hf_{0.5}Zr_{0.5}O_2$ films was ~ 30, and that of the AFE-$Hf_{0.3}Zr_{0.7}O_2$ film was ~ 40. [11, 14, 60] The leakage current density of $Hf_{1-x}Zr_xO_2$ thin film was slightly larger than that of the Si-doped HfO_2 thin film. The endurance of the FE-$Hf_{0.5}Zr_{0.5}O_2$ film was investigated, 5.5 nm and 10 nm-thick-$Hf_{0.5}Zr_{0.5}O_2$ thin films were able to withstand up to 10^9 and 10^8 times the cycling electric field strength of 3 MV/cm, respectively. [43] The endurance characteristics of the $Hf_{0.5}Zr_{0.5}O_2$ thin film were superior to the that of the Si-doped HfO_2 thin film at the cycling field strength of 3MV/cm. According to J. Muller et al., positive and negative P_r values did not decrease after 10^5 seconds in the retention test. [42] In conclusion, the $Hf_{0.5}Zr_{0.5}O_2$ film is expected to be a Si-doped HfO_2 film.

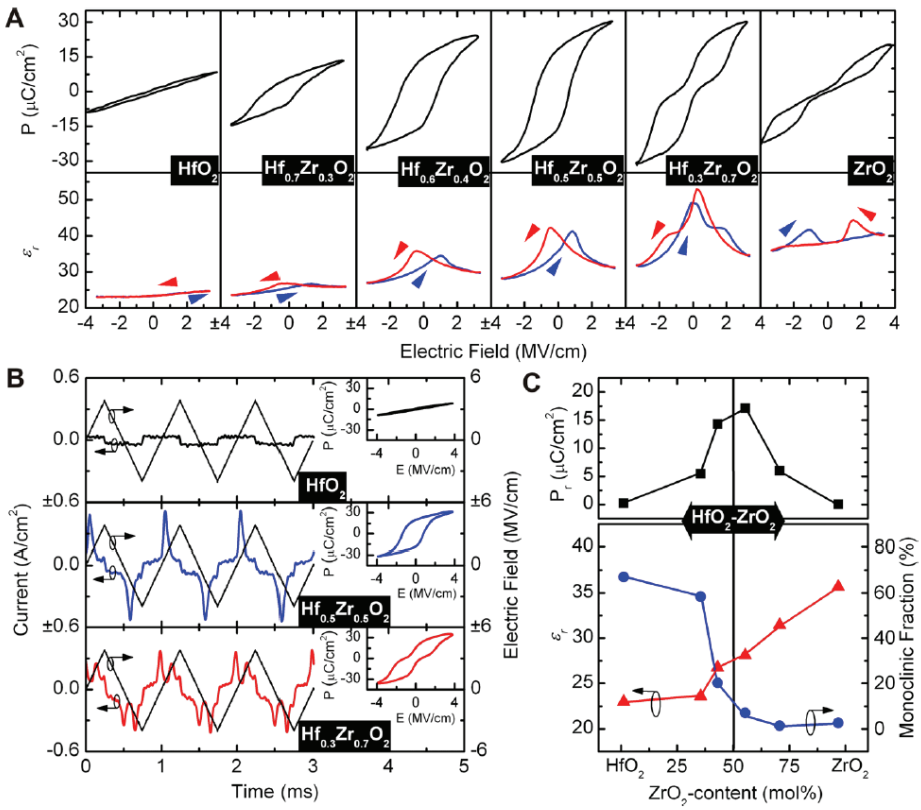

Figure 2. 10. (A) P-V curve at 1 kHz and small signal CV hysteresis at 10 kHz (50 mV level) of 9 nm thin HfO_2–ZrO_2 based metal–insulator–metal capacitors at room temperature. An evolution from paraelectric HfO_2 to ferroelectric HfO_2–ZrO_2 to an antiferroelectric-like behavior in ZrO_2 can be observed in PV as well as in C-V characteristics. (B) Current response to a triangular voltage excitation reveals polarization switching to be clearly separable from leakage current contributions at high fields. (C) Remanent polarization, dielectric constant, and monoclinic phase fraction in the HfO_2–ZrO_2 solid solution with respect to the mixing ratio of the oxides. With increasing ZrO_2 content the dielectric constant increases due to a reduction in monoclinic phase fraction, whereas the remanent polarization is maximized in the transition region. [11]

2.3. References

[1] M. E. Lines and A. M. Glass, "Principles and applications of ferroelectrics and related materials", Oxford, New York, USA (1977).

[2] J. F. Scott and C. A. P. de Araujo, *Science* **246**, 1400 (1989).

[3] C. A. P. de Araujo, J. D. Cuchiaro, L. D. McMillan, M. C. Scott, and J. F. Scott, *Nature* **374**, 627 (1995).

[4] E. K. H. Salje, Phase Transitions in Ferroelastic and Co-elastic Crystals (Cambridge Univ. Press, Cambridge, 1990).

[5] G. A. Smolenskii, I. Chupis, *Sov. Phys. Usp.* **25**, 475 (1982).

[6] G. Catalan and J. F. Scott, *Adv. Mater.* **21**, 2463 (2009).

[7] M. H. Park, Y. H. Lee, H. J. Kim, Y. J. Kim, T. Moon, K. D. Kim, J. Muller, A. Kersch, U. Schroeder, T. Mikolajick, C. S. Hwang, *Adv. Mater.* **11**, 1181 (2015)

[8] T. S. Böscke, J. Müller, D. Bräuhaus, U. Schröder, U. Böttger, *Appl. Phys. Lett.,* ***99***, 102903 (2011).

[9] S. Starschich, D. Griesche, T. Schneller, R. Waser, U. Böttger, *Appl. Phys. Lett.,* **104**, 202903 (2014).

[10] S. Mueller, J. Mueller, A. Singh, S. Riedel, J. Sundqvist, U. Schroeder, T. Mikolajick, *Adv. Funct. Mater.,* **22**, 2412 (2012).

[11] J. Müller, T. S. Böscke, U. Schröder, S. Mueller, D. Bräuhaus, U. Böttger, L. Frey, T. Mikolajick, *Nano Lett.,* **12**, 4318 (2012).

[12] J. Müller, U. Schröder, T. S. Böscke, I. Müller, U. Böttger, L. Wilde, J.

Sundqvist, M. Lemberger, P. Kücher, T. Mikolajick, L. Frey, *J. Appl. Phys.,* **110**, 114113. (2011)

[13] S. Mueller, C. Adelmann, A. Singh, S. V. Elshocht, U. Schroeder, T. Mikolajick, *ECS J. Solid St. Sci.,* **1**, N123 (2012).

[14] M. H. Park, H. J. Kim, Y. J. Kim, W. Lee, T. Moon, and C. S. Hwang, *Appl. Phys. Lett.,* **102**, 242905 (2013).

[15] T. S. Böscke, St. Teichert, D. Bräuhaus, J. Müller, U. Schröder, U. Böttger, T. Mikolajick, *Appl. Phys. Lett.* **99**, 112904 (2011).

[16] C. Richter, T. Schenk, U. Schroeder, T. Mikolajick, Baltic ALD conference, Helsinki, 2014

[17] M. Hoffmann, T. Schenk, I. Kulemanov, C. Adelmann, M. Popovici, U. Schroeder, T. Mikolajick, *Ferroelectrics*, **480**, 16 (2015).

[18] E. Yurchuk, J. Müller, S. Knebel, J. Sundqvist, A. P. Graham, T. Melde, U. Schröder, T. Mikolajick, *Thin Solid Films,* **533**, 88 (2013).

[19] M. H. Park, H. J. Kim, Y. J. Kim, W. Lee, H. K. Kim, and C. S. Hwang, *Appl. Phys. Lett.,* **102**, 112914 (2013).

[20] M. H. Park, H. J. Kim, Y. J. Kim, T. Moon, and C. S. Hwang, *Appl. Phys. Lett.,* **104**, 072901 (2014).

[21] R. C. Garvie, *J. Phys. Chem.,* **69**, 1238 (1965).

[22] R. C. Garvie, *J. Phys. Chem.,* **82**, 218 (1978).

[23] M. W. Pitcher, S. V. Ushakov, A. Navrotsky, B. F. Woodfield, G. Li, J. Boerio-Goates, *J. Am. Ceram. Soc.,* **88**, 160 (2005).

[24] M. Shandalov, P. C. McIntyre, *J. Appl. Phys.,* **106**, 084322 (2009).

[25] D. Y. Cho, H. S. Jung, I. H. Yu, J. H. Yoon, H. K. Kim, S. Y. Lee, S. H. Jeon, S. W. Han, J. H. Kim, T. J. Park, B. G. Park, C. S. Hwang, *Chem. Mater.,* **24**, 3534 (2012).

[26] S. K. Kim, C. S. Hwang, *Electrochem. Solid St.,* **11**, G9 (2008).

[27] R. Materlik, A. Kersch, C. Künneth, *J. Appl. Phys.,* **117**, 134109 (2015).

[28] A. Gruverman, O. Kolosov, J. Hatano, K. Takahashi, H. Tokumoto, *J. Vac. Sci. Technol. B,* **13**, 1095 (1995).

[29] J. E. Lowther, J. K. Dewhurst, J. M. Leger, J. Haines, *Phys. Rev. B,* **60**, 14485 (1999).

[30] M. V. Nevitt, Y. Fang, S. K. Chan, *J. Am. Ceram. Soc.,* **73**, 2502 (1990).

[31] T. Tojo, T. Atake, T. Mori, H. Yamamura, *J. Chem. Thermodyn.,* **31**, 831 (1999).

[32] J. E. Jaffe, R. A. Bachorz, M. Gutowski, *Phys. Rev. B,* **72**, 144107 (2005).

[33] P. Simoncic A. Navrosky, *J. Mater. Res.,* **22**, 876 (2007).

[34] C. J. Howard, E. H. Kisi, O. Ohtaka, *J. Am. Ceram. Soc.,* **74**, 2321 (1991).

[35] S. E. Reyes-Lillo, K. F. Garrity, K. M. Rabe, arXiv:cond-mat/1403.3878, (2014**).**

[36] M. Shandalov, P. C. McIntyre, *J. Appl. Phys.,* **106**, 084322 (2009).

[37] W. D. Nix, B. M. Clemens, *J. Mater. Res.,* **14**, 3467 (1999).

[38] M. H. Park, Ph. D thesis, Seoul National University (Seoul, Korea), Feb., (2014).

[39] U. Schroeder, E. Yurchuk, J. Müller, D. Martin, T. Schenk, P. Polakowski, C. Adelmann, M. I. Popovici, S. V. Kalinin, T. Mikolajick, *Jpn. J. Appl. Phys.,* **53**, 08LE02 (2014).

[40] D. Zhou, J. Müller, J. Xu, S. Knebel, D. Bräuhaus, U. Schröder, *Appl. Phys. Lett.,* **100**, 082905 (2012).

[41] D. Zhou, J. Xu, Q. Lu, Y. Guan, F. Cao, X. Dong, J. Müller, T. Schenk, U. Schröder, *Appl. Phys. Lett.,* **103**, 192904 (2013).

[42] J. Müller, T. S. Böscke, D. Bräuhaus, U. Schröder, U. Böttger, J. Sundqvist, P. Kücher, T. Mikolajick, L. Frey, *Appl. Phys. Lett.,* **99**, 112901 (2012).

[43] M. H. Park, H. J. Kim, Y. J. Kim, W. Jeon, T. Moon, and C. S. Hwang, *Phys. Status Solidi RRL,* **8**, 532 (2014).

[44] M. H. Park, H. J. Kim, Y. J. Kim, W. Lee, T. Moon, K. D. Kim, C. S. Hwang, *Appl. Phys. Lett.,* **105**, 072902 (2014).

[45] T. Olsen, U. Schröder, S. Müller, A. Krause, D. Martin, A. Singh, J. Müller, M. Geidel, T. Mikolajick, *Appl. Phys. Lett.,* **101**, 082905 (2012).

[46] P. Polakowski, S. Riedel, W. Weinreich, M. Rudolf, J. Sundqvist, K. Seidel, J. Müller, IEEE 6th International Memory Workshop (IMW), 1 (2014).

[47] T. Schenk, S. Mueller, U. Schroeder, R. Materlik, A. Kersch, M. Popovici, C. Adelmann, S. V. Elshocht, T. Mikolajick, Proceedings of the European Solid-State Device Research Conference (ESSDERC), 260 (2013).

[48] J. Müller, T. S. Böscke, Y. Yurchuk, P. Polakowski, J. Paul, D. Martin, T. Schenk, K. Khullar, A. Kersch, W. Weinreich, S. Riedel, K. Seidel, A. Kumar, T. M. Arruda, S. V. Kalinin, T. Schlosser, R. Boschke, R. van Bentum, U. Schröder, T. Mikolajick, IEEE International Electron Devices Meeting (IEDM), 10.8.1 (2013).

[49] P. D. Lomenzo, P. Zhao, Q. Takmeel, S. Moghaddam, T. Nishida, M. Nelson, C. M. Fancher, E. D. Grimley, X. Sang, J. M. LeBeau, J. L. Jones, *J. Vac. Sci. Technol. B,* **32**, 03D123 (2014).

[50] M. Hoffmann, U. Schroeder, T. Schenk, C. Adelmann, M. Popovici, T. Mikolajick, Unpublished. ISAF 2014 conference proceeding; J. Appl. Phys., special edition (2015)

[51] J. F. Scott, M. Dawber, *Appl. Phys. Lett.,* **76**, 3801 (2000).

[52] I. K. Yoo, S. B. Desu, *Phys. Status. Solidi A,* **133**, 565 (1992).

[53] C.-K. Lee, E. Cho, H.-S. Lee, C. S. Hwang, and S. Han, *Phys. Rev. B,* **78**, 012102 (2008).

[54] J. C. Slater, *J. Chem. Phys.* **41**, 3199 (1964).

[55] L. Zhao, M. Nelson, H. Aldridge, T. Iamsasri, C. M. Fancher, J. S. Forrester, T. Nishida, S. Moghaddam, J. L. Jones, *J. Appl. Phys.,* **115**, 034104 (2014).

[56] J. A. Speer, B. J. Cooper, *American Mineralogist*, **67**, 804 (1982).

[57] D. Martin, J. Mueller, T. Schenk, T. M. Arruda , A. Kumar , E. Strelcov, E. Yurchuk, S. Mueller, D. Pohl, U. Schroeder, S. V. Kalinin, T. Mikolajick, *Adv. Mater.,* **26**, 8198 (2014).

[58] S. Mueller, J. Müller, U. Schroeder, T. Mikolajick, *IEEE T. Mater. Re.,* **13**, 93 (2013).

[59] C. S. Hwang, *Atomic Layer Deposition for Semiconductors*, Springer US, New York, (2013).

[60] M. H. Park, H. J. Kim, Y. J. Kim, T. Moon, K. D. Kim, C. S. Hwang, *Adv. Energy Mater.,* **4**, 1400610 (2014).

[61] M. H. Park, H. J. Kim, Y. J. Kim, T. Moon, K. D. Kim, C. S. Hwang, *Nanoenergy*, **12**, 131 (2015).

[62] M. H. Park, H. J. Kim, Y. J. Kim, T. Moon, K. D. Kim, Y. H. Lee, S. D. Hyun, C. S. Hwang, *J. Mater. Chem. C.,* **3**, 6291 (2015).

[63] M. H. Park, H. J. Kim, Y. J. Kim, T. Moon, K. D. Kim, C. S. Hwang, *Phys. Status Solidi RRL*, **8**, 857 (2014).

3. Grain size engineering for ferroelectric $Hf_{0.5}Zr_{0.5}O_2$ films by an insertion of Al_2O_3 interlayer

3.1. Introduction

Recently, it was reported that HfO_2 can show ferroelectric (FE) properties when doped with various dopants such as Zr, Si, Y, Al, Gd, La, and Sr. [1-7] Compared to the conventional ferroelectrics based on perovskite or layered perovskite structure, such as $Pb(Zr,Ti)O_3$ and $SrBi_2Ta_2O_9$, the FE HfO_2-based films showed quite distinctive physical and electrical properties. The HfO_2-based films can be extremely thin (film thickness, $t_f < 10$ nm) with feasible ferroelectricity (remanent polarization, $P_r \sim 10 - 40\ \mu C/cm^2$), whereas the much thicker thicknesses ($t_f > 100$ nm) are required for the stable FE properties of conventional ferroelectrics thin films, especially with the metal-ferroelectric-metal (MFM) configuration.[8-10] Due to their small thickness, the HfO_2-based films are considered promising for the three-dimensional capacitor structure which is highly required for the future ferroelectric random-access-memory (FeRAM) device according to International Technology Roadmap for Semiconductors.[11] This results from the relatively large bandgap ($E_g \sim 5.5$ eV),

[12, 13] high compatibility with Si, and matured atomic layer deposition (ALD) technique of HfO_2-based films. In fact, due to their high Si-compatibility, the non-FE HfO_2 thin film has been used as the buffer layer in ferroelectric field-effect-transistor (FeFET) to solve the interfacial problems of conventional ferroelectrics and Si substrate. [14] Furthermore, the authors recently reported that the feasible FE performance of $Hf_{0.5}Zr_{0.5}O_2$ (HZO) films could be maintained after the hydrogen annealing at temperatures as high as 600 °C due to the absence of weak metal-oxygen bonding such as Pb-O. [15]

It is generally accepted that the ferroelectricity within these materials originates from the formation of non-centrosymmetric $Pca2_1$ ($Pbc2_1$ in some references) orthorhombic phase (o-phase), which is not a stable phase under the usual temperature and pressure conditions. The authors suggested that this unusual FE phase can be formed due to the huge tensile stress ascribed to the island coalescence process of Volmer-Webber-type thin film growth, [16, 17] which is the general growth mechanism for the most of dielectric film growth on metal substrate, as in this work. In addition, sufficiently small grain size is required to prevent the formation of the stable monoclinic phase (m-phase, space group: $P2_1/c$). The small grain size is accompanied with the high surface to volume ratio, and the smaller surface energy of the tetragonal phase (t-phase, space group: $P4_2/nmc$) induced the formation of t-phase when the nuclei size is smaller than the critical value (~26nm for $Hf_{0.5}Zr_{0.5}O_2$). During the initial stage of film growth, nuclei of t-phase were formed on the bottom electrode layer and

they transformed into the o-phase at the moment of zipping occurs, which is accompanied with the asymmetric strain that was necessary to induce the unusual phase transition. [16]

The feasible ferroelectricity (P_r >20μC/cm^2) with extremely small t_f (<10 nm) is considered highly promising for various applications. In contrast, such a small t_f can be a critical barrier for exploring the physics behind the unexpected FE phenomenon, including domain dynamics and structural analysis. However, it was already reported that the ferroelectricity of HZO thin films is significantly degraded when the thickness of the thin films increases over 20nm, [18] which was also observed in Si-doped HfO_2 films. [19] The reason for the degradation is that the FE o-phase transforms into non-FE m-phase with the increasing film thickness which must be accompanied with the grain growth (increase in grain size) for polycrystalline HfO_2-based FE thin films. [20, 21] Thus, it is highly required to suppress the formation of the m-phase by independently controlling the grain size of HZO films to achieve the feasible ferroelectricity in films thicker than 20nm.

In $ZrO_2/Al_2O_3/ZrO_2$ stack system, which has been widely used as high-k dielectric layer in capacitors for dynamic random access memory, the Al_2O_3 interlayer can reduce the grain size of the adjacent ZrO_2 layers by interrupting continuous grain growth of the ZrO_2 layer. [22] When the physical and chemical similarities of ZrO_2 and HZO are considered, the Al_2O_3 interlayer is also expected to effectively control the grain size and produce polymorphism with

the layered structure of HZO/Al_2O_3/HZO (HZAHZ). In this study, therefore, the stacked HZAHZ film with various HZO layer thicknesses were prepared, and the physical and FE properties of HZAHZ system were compared to those of single layer HZO films. It was observed that the transformation into the m-phase resulting from grain growth could be effectively suppressed by inserting a 1-nm-thick Al_2O_3 layer between HZO layers. Moreover, it could be confirmed that the HZO layers on and under the Al_2O_3 interlayer had different crystallographic orientations via high resolution transmission electron microscopy (HRTEM). As a result, the ferroelectricity (P_r ~11.4μC/cm^2) of HZAHZ film was not degraded with increasing total thickness up to ~40nm.

3.2. Experimental

The HZO films were deposited on a 50-nm-thick TiN bottom electrode (BE) formed on SiO_2/Si substrate via thermal ALD at a 280°C substrate temperature using $Hf[N(C_2H_5)CH_3]_4$ (TEMAH), $Zr[N(C_2H_5)CH_3]_4$ (TEMAZ), $Al_2[CH_3]_6$ (TMA) and ozone (170 g/cm^3) as the precursor of Hf, Zr, Al, and oxygen source, respectively. The TiN BE was deposited via DC reactive sputtering. The growth per cycle of HfO_2 and ZrO_2 were almost identical (~0.12 nm/cycle), so the HZO films with a 0.5:0.5 Hf:Zr ratio could be deposited using a 1:1 HfO_2:ZrO_2 ALD cycle ratio. 1nm-thick Al_2O_3 layers were inserted between adjacent HZO layers having various t_f. Totally, 20, 30 and 40nm-thick HZAHZ films with the Al_2O_3 interlayer were prepared, where the 1-nm-thick Al_2O_3 layer located at the center position of the film thickness. For comparison, the HZO films without the Al_2O_3 interlayer were also deposited under the identical conditions.

For electrical characterization, a Pt(30 nm)/TiN(5 nm) top electrode (TE) was deposited via DC sputtering through a shadow mask with a 300 μm hole diameter (TiN contacted the HZO film). After the TE deposition, post-metallization-annealing was performed for 30s at 500°C in a N_2 atmosphere using rapid thermal annealing, for the films' crystallization. The composition and t_f of the HZO films were examined via X-ray fluorescence (Quant'X, Thermo SCIENTIFIC) and ellipsometry (L-116d, Gaetner), respectively. The cross-sectional images of HZO film were obtained by HRTEM (JEM-3000F,

JEOL) and the focused ion beam (Helios 650, NanoLab) in the NCIRF of Seoul National University was used to prepare the sample for HRTEM analysis. The crystal structure of the HZO films was analyzed using an X-ray diffractometer (X'pert Pro, Panalytical) via grazing-angle incidence X-ray diffraction (GIXRD, incidence angle=0.5°). The grain size of HZO films was calculated from in-plane image of scanning electron microscope (SEM, S-4800, Hitachi). For electrical characterization, the polarization-electric field (P-E) characteristics were measured using a ferroelectric tester (TF Analyzer 2000, Aixacct Systems) at a 1 kHz frequency and current density-electric field (J-E) characteristics were measured using pA meter/DC voltage source (HP 4140D, Hewlett Packard). An endurance test was performed using a ferroelectric tester (TF Analyzer 2000, Aixacct Systems) with 2.5MV/cm electric field and 100 kHz electrical cycling frequency. For the transient switching current analysis, the pulse/pattern generator (81110A, Agilent) and digital oscilloscope (TDS684c, Tektronix) were used.

3.3. Results and Discussions

Figure 3. 1(a) shows the cross-sectional TEM image of the Pt/TiN/HZO/Al_2O_3/HZO/TiN structure, confirming the uniform and flat HZO films with clean interfaces. The 1nm-thick Al_2O_3 interlayer was well deposited between adjacent top and bottom 15nm-thick HZO layers, clearly separating them. The HZO films consist of many separate grains, which are well crystallized, of which average vertical and lateral grain sizes are ~15 and ~30 nm, respectively. It is believed that the vertical grain growth of the bottom HZO film was interrupted by the Al_2O_3 interlayer, and the grain size of HZO films would have been increased with the increasing t_f if there was no Al_2O_3 interlayer. [23] As mentioned in the introductory part, the polymorphism of HZO films are strongly influenced by their microstructure, so the structural properties of HZO and HZAHZ films were examined via GIXRD. Figures 3. 1(b) and (c) show the GIXRD spectra in the 2θ range of 25°-65° for the HZO and HZAHZ films having various thickness, respectively. The diffraction peaks from the (111), (200), and (220) planes of the o-phase HZO could be clearly observed in the diffraction patterns. In fact, it is very challenging to unambiguously assign those peaks to only o-phase because of its structural similarity to t-phase. The peaks assigned to (111), (200), (220) planes of o-phase could be actually a signature of mixed o- and t-phases ((101), (110), and (200) planes of t-phase). Therefore, this must be taken as the indication that m-phase formation was

suppressed. The more notable difference in the GIXRD patterns of the HZO and HZAHZ films could be identified from the enhanced and suppressed, respectively, increase in the (111) peak (m(111) peak) intensity of m-phase ($2\theta = 31.7^{o}$). It could be readily understood that the increase in the intensity of this peak with the increasing t_f is quite largely suppressed for the case of HZAHZ compared with the HZO. This could be more quantitatively understood in figure 3. 2(a).

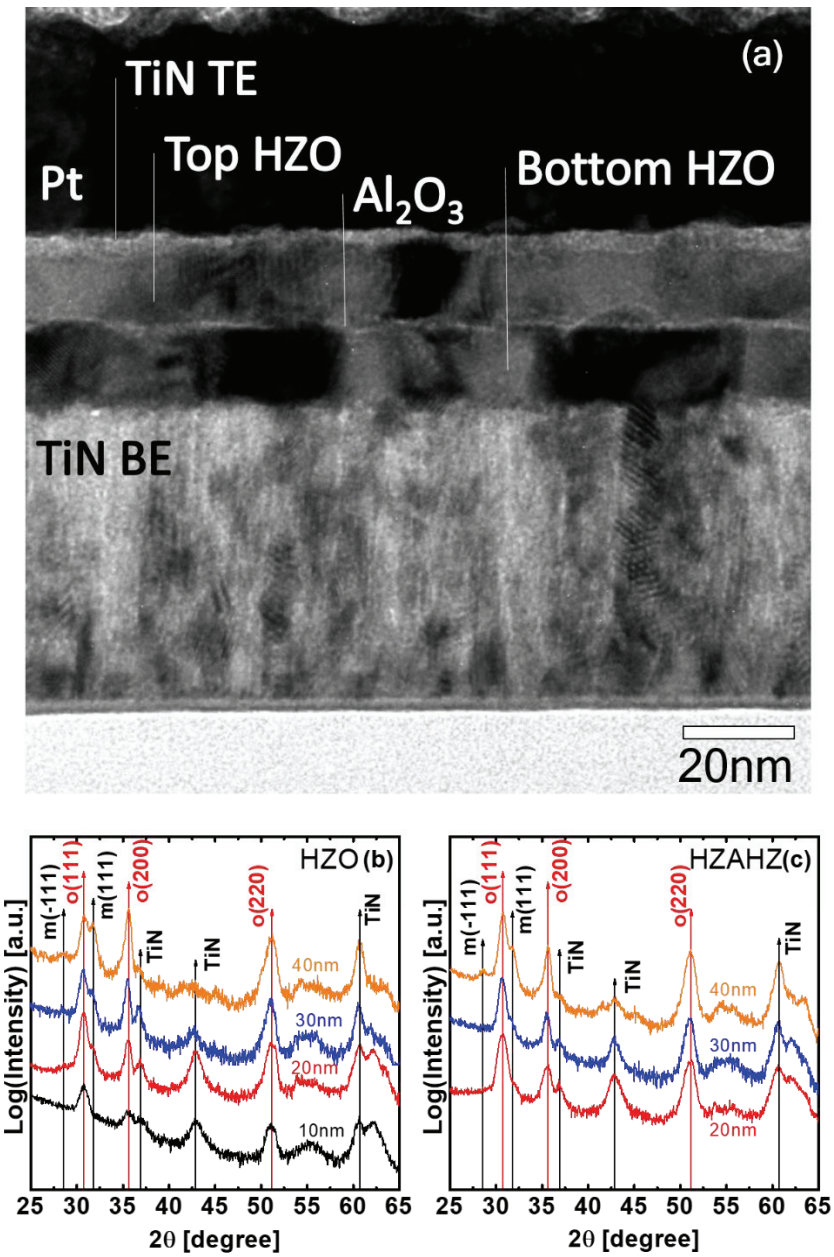

Figure 3. 1. (a) Cross-sectional transmission electron microscope image of the Pt/TiN/$Hf_{0.5}Zr_{0.5}O_2$/Al_2O_3/$Hf_{0.5}Zr_{0.5}O_2$/TiN structure. Grazing incidence X-ray diffraction pattern of (b) the $Hf_{0.5}Zr_{0.5}O_2$ films and (c) the $Hf_{0.5}Zr_{0.5}O_2$/Al_2O_3/$Hf_{0.5}Zr_{0.5}O_2$ films with various thicknesses.

Figure 3. 2(a) shows the variations in the relative ratio of the area of o(111)/{o(111) + m(111)}, which were estimated from the 2θ range of 27-33° of GIXRD, where the diffraction peaks of m(111) and o(111) are clearly distinguished, for the HZO and HZAHZ films as a function of their total t_f. o(111) indicates the 111 diffraction peak from the o-phase (111) plane. The details of the quantitative analysis of the o-phase portion were reported elsewhere. [24] The relative ratio o(111) diffraction peak in HZO film was ~94% when the t_f was ~10nm, and it decreased to ~ 82, ~ 70 and ~64% when t_f increased to ~20, ~30, and ~40nm, respectively. On the other hand, the relative ratio of o(111) diffraction peak of HZAHZ film was ~94% when the t_f was 20nm, and decreased to ~84%, and ~78% when t_f increased to ~30, and ~40nm, respectively, which are generally larger than that without the interlayer at similar t_f. Next, the average grain size (D_{avg}) of the two types of the films were examined from the plan-view SEM images (figure 3.3). Figure 3. 2(b) shows the variation in the D_{avg} of the HZO and HZAHZ films as function of t_f. The D_{avg} of the HZO films was ~14.2nm at the t_f of ~10nm, and increased to ~25.5, ~34.3, and ~43.1nm when t_f increased to ~20, ~30, and ~40nm, respectively. In contrast, D_{avg} of the HZAHZ films was ~14.4nm at the t_f of ~20nm, and increased to only ~20.3, and ~26.4nm when t_f increased to ~30, and ~40nm, respectively. This suggests that the Al_2O_3 interlayer interrupts the continuous grain growth of bottom HZO films as shown in figure 3. 1(a), and the D_{avg} of HZAHZ films could be remained at small values that could suppress the

transition to the stable m-phase. Next, the relative crystallographic orientations of the top and bottom HZO grains in HZAHZ films were examined by HRTEM and fast-Fourier transformation (FFT) of the lattice image to confirm that the physically separated grains are real crystallographically separate entity. Figure 3. 2(c) shows the HRTEM image of the ~30nm-thick FE HZAHZ film. The polycrystalline nature of the top and bottom HZO layers could be confirmed from the lattice fringes with different orientations in the figure. Two inset figures are FFT image of top (upper inset) and bottom (bottom inset) HZO layers of the portion of HRTEM image indicated by arrows. The FFT patterns generally match with the o-phase, and the diffraction spots from (111)-planes of the o-phase are marked by yellow circles in both FFT images. The o(111) d-spacing values calculated from those spots were 2.93 and 2.94 Å, respectively, which are similar values achieved from the GIXRD in this work and previous studies (table 3. 1). [3, 25-27] The directions of diffraction spots from two FFT images are significantly different from each other, suggesting that two grains in the top and bottom portions of the film had different crystallographic orientations although they are of commonly o-phase. This reveals that the insertion of 1-nm-thick Al_2O_3 layer effectively suppressed the continuous growth of the polycrystalline HZO grains and accompanying transition to the m-phase at total film thicknesses > ~ 20nm. Next, the FE properties of these films are reported.

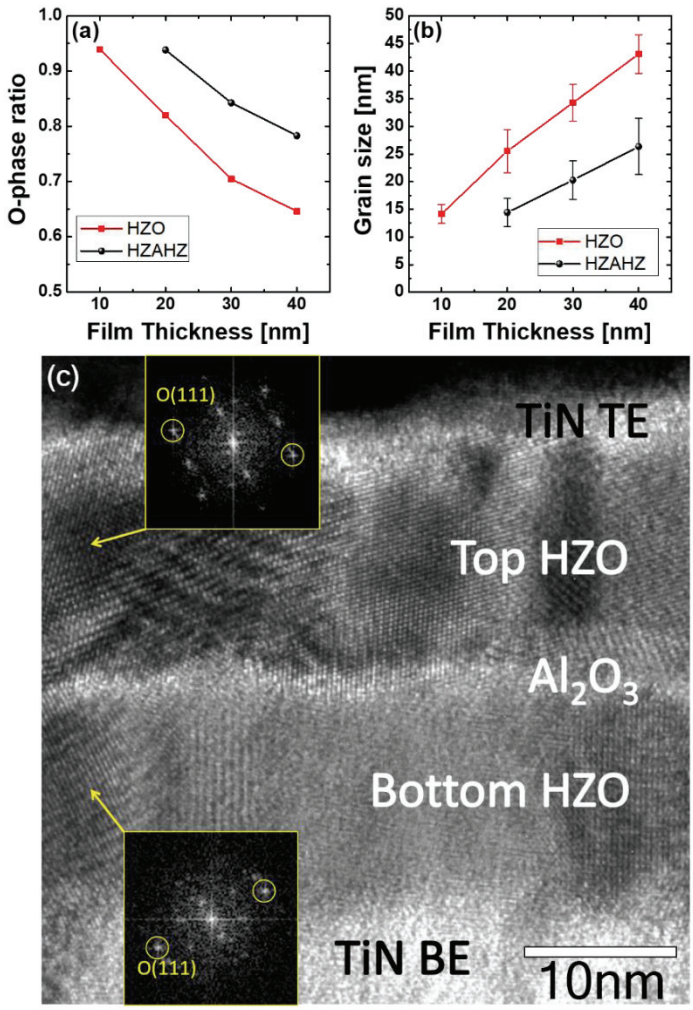

Figure 3. 2. (a) Variations in the relative ratio of the o(111)/{o(111) + m(111)}, and (b) those in the average grain size (with error bars whose magnitudes refer to the standard deviation of the average grain sizes from measurements) of $Hf_{0.5}Zr_{0.5}O_2$ films and $Hf_{0.5}Zr_{0.5}O_2/Al_2O_3/Hf_{0.5}Zr_{0.5}O_2$ films. (c) Cross-sectional high resolution transmission electron microscopy image of the 30nm-thick $Hf_{0.5}Zr_{0.5}O_2/Al_2O_3/Hf_{0.5}Zr_{0.5}O_2$ film. Two in-set figures are fast Fourier transformation image at the $Hf_{0.5}Zr_{0.5}O_2$ layers on and under the Al_2O_3 interlayer.

Table 3. 1. d-spacing values from (111)-planes of orthorhombic phase of HfO_2, ZrO_2 and $Hf_{0.5}Zr_{0.5}O_2$ films from various studies.

Authors	**This work**		**1995 JCPDS**	**Muller et al**	**Lowther et al**		**Kisi et al**
Methods	**XRD**	**HR-TEM**	XRD	XRD	Ab initio simulation		Neutron diffraction
Elements	**$Hf_{0.5}Zr_{0.5}O_2$**		HfO_2	$Hf_{0.5}Zr_{0.5}O_2$	HfO_2	ZrO_2	ZrO_2
(111) d-spacing (Å)	**2.91**	**2.94**	2.94	2.94	2.98	2.96	2.96

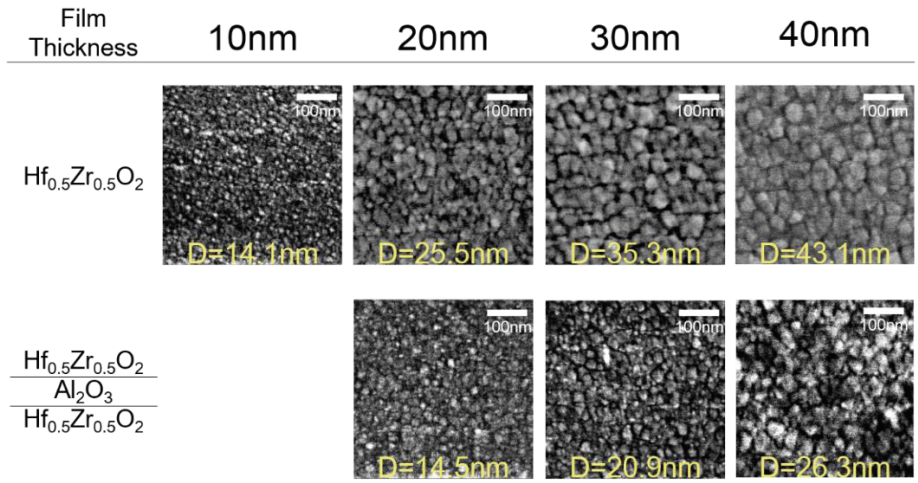

Figure 3. 3. The plan-view scanning electron microscope images of $Hf_{0.5}Zr_{0.5}O_2$ films and $Hf_{0.5}Zr_{0.5}O_2/Al_2O_3/ Hf_{0.5}Zr_{0.5}O_2$ films with various thickness. (D is the average grain size)

Figures 3. 4(a) and (b) show the P-E hysteresis loops of the HZO and HZAHZ films, respectively, with different t_f values. The P-E hysteresis loops from the initial measurement were presented, since the P-E characteristics of HZAHZ films were degraded during electric field cycling, which would be discussed in more detail in the later part of this letter and supplementary material. For the case of HZO films, the thinnest film (10 nm) shows a $2P_r$ value of 30.7 $\mu C/cm^2$, but it decreased to almost negligible value (~2.1 $\mu C/cm^2$) at a t_f of 40 nm, which is comparable to the previous report. [18] This is believed to be due to the fast transition of the phase of the HZO film from the FE o-phase (thinner film) to non-FE m-phase (thicker film). In contrast, the HZAHZ film maintained the reasonably high $2P_r$ value (~22.7$\mu C/cm^2$) up to the total thickness of 40 nm, thanks to the suppression of the grain growth and accompanying transition to m-phase. Surprisingly, $2P_r$ values of the 40 and 20nm-thick HZAHZ film (22.7 and 31.5 $\mu C/cm^2$) were almost equivalent with those of 20 and 10nm-thick HZO films (20.6 and 30.7 $\mu C/cm^2$). This means that the upper and lower HZO layers in HZAHZ films involves almost identical FE performances for the given thickness. However, the coercive field (E_c) of the HZAHZ film is generally higher than that of HZO film (0.98MV/cm vs. 1.37MV/cm). If two identical FE films simply stacked without any other adverse effects, their E_c must be invariant. Such increase in the E_c could be understood from the role of the thin Al_2O_3 layer as the tunneling barrier. [28] To further confirm the differences in the P-E hysteresis curves of HZO and HZAHZ capacitors, the transient

switching currents of the samples were also analyzed.

For the measurement, the pulse pattern generator and digital oscilloscope, whose internal resistances are all 50 Ω, were serially connected to our ferroelectric capacitor. The schematic of the measurement setup can be seen in figure 3. 5(a). The double remanent polarization ($2P_r$) values with increasing applied voltage of the 10nm-thick HZO and 20nm-thick HZAHZ films measured by pulse switching measurement system are shown in figure 3. S2b. Both films had similar saturated $2P_r$ values, which was consistent with P-E hysteresis in figure 3. 4. Figures 3. 5(c) and (d) show the transient switching current-time curves using various pulse heights. The pulse width was fixed at 20 μs, which was long enough for complete polarization switching. In the initial stage of pulse switching, the capacitor charging process occurred until the voltage across ferroelectric capacitor reached coercive value. After that, the linear regions could be observed both for switching current-time curves of HZO and HZAHZ films. Dashed lines were added to clearly show these regions. In this region, the transient switching current could be formulated as:

$$I_{SW}(t) = I_{SW}^{o} e^{-\frac{t-t_0}{R_L C_i}} \quad (t_0 \leq t \leq t_{sw}) \tag{3. 1}$$

, where t_0, t_{sw}, R_L, and C_i are the time when ferroelectric film starts to switch, the time when the switching process is completed, total resistance of measurement circuit and sample, and interfacial capacitance, respectively. The

total resistance is the summation of the internal resistance of pulse/pattern generator (50 Ω) and digital oscilloscope (50 Ω), parasitic resistance, and contact resistance. It should be noted that the ferroelectric layer does not work as a resistor or capacitor in this equation. When t is t_0, the switching current can be formulated as:

$$I_{SW}^{0} = \frac{V_{appl} - V_c}{R_L} \quad (3.\ 2)$$

, where V_{appl} and V_c are applied voltage and coercive voltage of ferroelectric layer, respectively. Therefore, I_{sw}^{0} – V_{appl} graph can be plotted from $I_{sw}(t_0)$ values of transient switching current-time curves with various pulse heights, and figure 3. 5(e) shows the results. From the slope and x-axis intercept of I_{sw}^{0}-V_{appl} curves, R_L and V_c can be calculated. Based on the calculated R_L values, C_i can be finally calculated from the slope of linear region in $\ln(I_{sw})$-t curve. With these steps, the R_L and C_i values of 10nm-thick HZO and 20nm-thick HZAHZ capacitors were calculated. The R_L of 10nm-thick HZO and 20nm-thick HZAHZ capacitors were ~137 and ~155 Ω, and their difference was ~18 Ω, which was similar to the resistance of 1nm-thick Al_2O_3 layer in our previous report (~15 Ω). [28] On the other hand, the C_i of both samples were even larger than 30 nF, meaning that the Al_2O_3 layer did not work as a series capacitor. If Al_2O_3 layer was a series capacitor, the C_i value of HZAHZ capacitor should be smaller than its theoretical capacitance (~8nF, assuming relative dielectric

constant of 9 and 1nm thickness of Al_2O_3), but it was not the case. From these results, it could be concluded that the Al_2O_3 layer works as a series resistor during ferroelectric switching. Moreover, the large coercive field of HZAHZ capacitor might not results from the wide distribution of switching current peak.

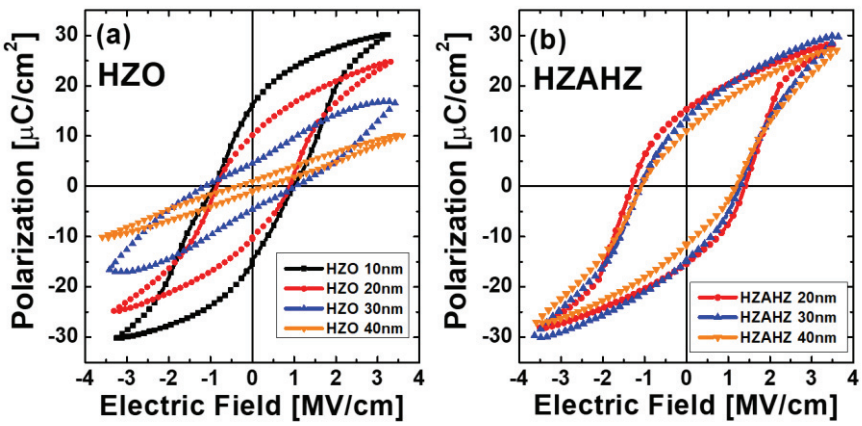

Figure 3. 4. Polarization-electric field curves of (a) the $Hf_{0.5}Zr_{0.5}O_2$ films and (b) $Hf_{0.5}Zr_{0.5}O_2/Al_2O_3/Hf_{0.5}Zr_{0.5}O_2$ films with various thicknesses.

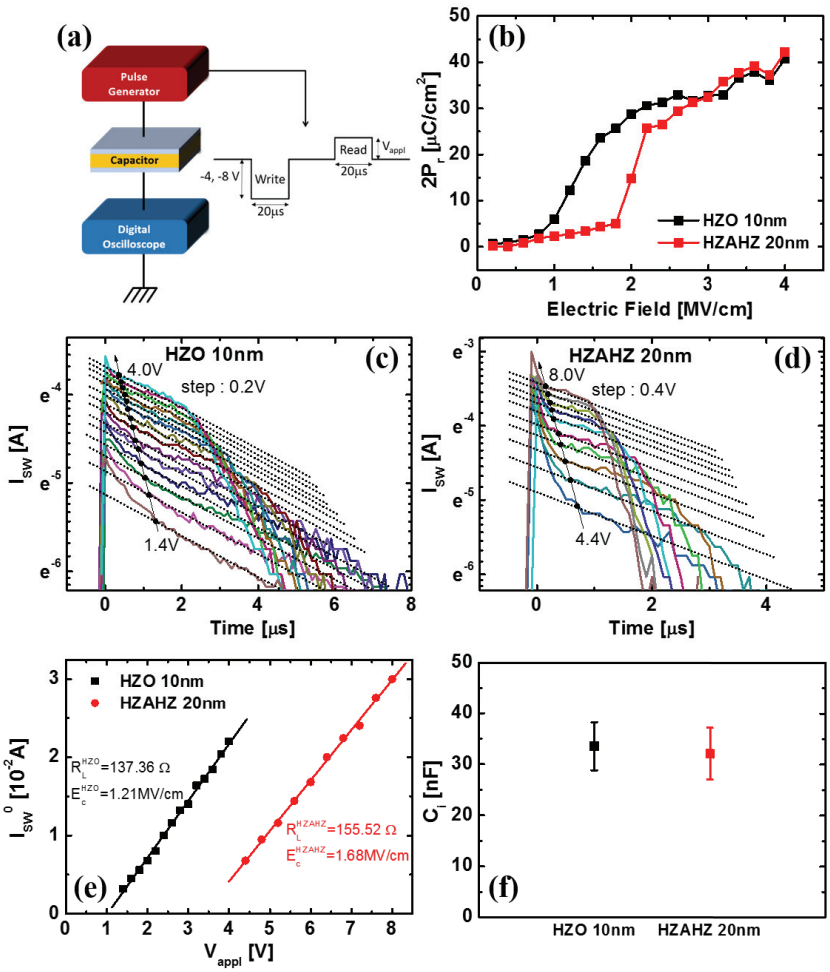

Figure 3. 5. (a) Schematic diagram of the measurement system using a pulse generator and digital oscilloscope (left panel), and shape of input pulse by the pulse generator (right panel). (b) Double remanent polarization-electrical field hysteresis loop measured by pulse switching technique. Transient switching current hysteresis of (c) the 10nm-thick $Hf_{0.5}Zr_{0.5}O_2$ film and (d) the 20nm-thick $Hf_{0.5}Zr_{0.5}O_2/Al_2O_3/Hf_{0.5}Zr_{0.5}O_2$ film, respectively. (e) The initial domain switching current as a function of the applied voltage hysteresis and the extracted resistance and (f) the extracted interfacial capacitance of the 10nm-thick $Hf_{0.5}Zr_{0.5}O_2$ film and the 20nm-thick $Hf_{0.5}Zr_{0.5}O_2/Al_2O_3/Hf_{0.5}Zr_{0.5}O_2$ film.

The saturated $2P_r$ and E_c values from P-E hysteresis curve were also verified by pulse switching measurement, which were consistent with that from P-E hysteresis measurements. The role of Al_2O_3 layer as a series resistor during ferroelectric switching could be clearly confirmed by transient switching current analysis. The total resistance (R_L) and interfacial capacitance (C_i) of Al_2O_3 interlayer can be calculated from the linear region of ln(switching current) – time curves, and the effect of Al_2O_3 layer on R_L and C_i could be examined by comparing those of 10nm-thick HZO and 20nm-thick HZAHZ films. From the analysis, calculated R_L of 20nm-thick HZAHZ film was larger than that of 10nm-thick HZO film by ~18 Ω, which is similar to the resistance of 1nm-thick Al_2O_3 film in the previous report (~15 Ω). [28] However, C_i values of 10nm-thick HZO film and 20nm-thick HZAHZ film are ~33nF and ~32nF, respectively. Since these values are much larger than the theoretical capacitance of 1nm-thick Al_2O_3 (~8nF with ε_r of 9), the Al_2O_3 layer did not work as a series capacitor. Thus, these results suggest that the Al_2O_3 interlayer works as a series resistor during domain switching, not as a dielectric layer. The thinness of the Al_2O_3 layer allows fluent carrier transport across the layer, which does not interfere with the polarization of the HZAHZ film across the entire film thickness. If the Al_2O_3 layer played role as an insulating paraelectric layer, the P-E hysteresis loop must become more with slanted shape and P_r should have been decreased. Therefore, the electrical role of Al_2O_3 in the HZAHZ stacked film is a series resistor, which increases the apparent E_c. [28]

One of the problems in the electrical performances of the HZO films is their exceptionally high E_c (~ 1MV/cm) which is higher than that of conventional FE materials by almost one order of magnitude. This requires application electric field with a magnitude of several MV/cm to observe fully saturated P-E hysteresis loops, which is generally too severe to safely measure the reliability the HZO FE films, such as fatigue resistance. In fact, the authors reported a fatigue test results of several HZO films recently, [29] but the genuine fatigue property could not be accurately estimated due to the involvement of sudden dielectric break down after certain number of switching cycles, although initial fatigue performance was quite impressive. Both HZO and HZAHZ samples could endure up to ~10^6 cycles with the pulse height of 2.5 MV/cm and frequency of 100 kHz. However, the P_r of HZAHZ films further decreased with increasing number of field cycling compared to that of HZO films. It is believed that Al_2O_3 interlayer can make charge trap sites in HZO layer, which degraded the endurance of HZAHZ films. (Figure 3. 6) However, the 10^6 cycle of field cycling might not be an intrinsic endurance limitation of HZAHZ capacitor, which could be improved by optimizing fabrication process. Therefore, suppressing the leakage current is another critical issue for the HZO film for both the property estimation and stable operation of the integrated FE devices.

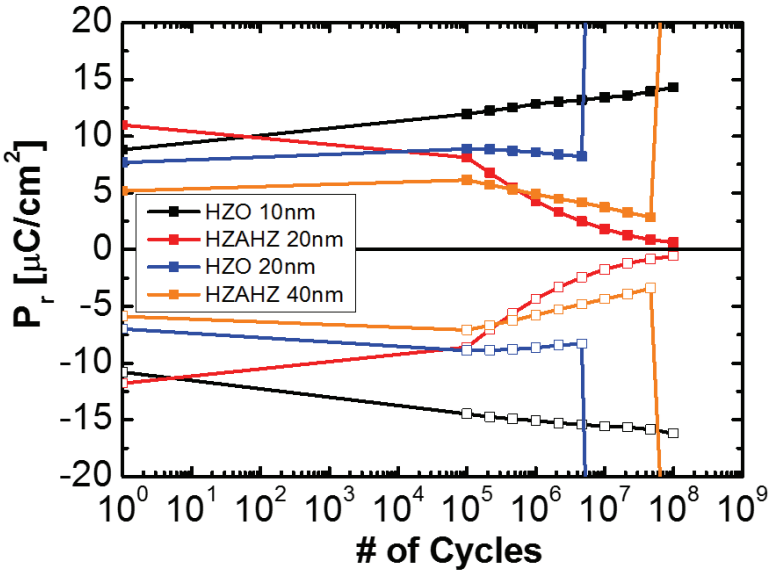

Figure 3. 6. Endurance properties of $Hf_{0.5}Zr_{0.5}O_2$ films and $Hf_{0.5}Zr_{0.5}O_2/Al_2O_3/Hf_{0.5}Zr_{0.5}O_2$ films with various thickness.

Figures 3. 7(a) and (b) show the J – E curves of the HZO and HZAHZ films with the various t_f values. While the J level of the thicker (> 30 nm) HZO films were low enough up to 2 MV/cm for both bias polarities, that of the thinner HZO film was largely degraded due to the involvement of possible defects and surface roughness. However, for the HZAHZ films, the J level is highly low with almost no change with the film thickness. It is notable that the J level of 20-nm-thick HZAHZ film is lower than that of single layer HZO layer with the identical thickness by several orders of magnitude over wide field region. As aforementioned, this is not due to the insulating property of the thin Al_2O_3 layer since it plays a role as the series resistor via the probable involvement of tunneling mechanism. The interruption of straight grain boundaries across the film thickness, which could play a role as the local leakage current path, [30] could be-critical reason for such improvement in the J-E performance. Further details for the leakage current conduction mechanism, and evaluation of the reliability performance based on this improvement will be reported in subsequent works.

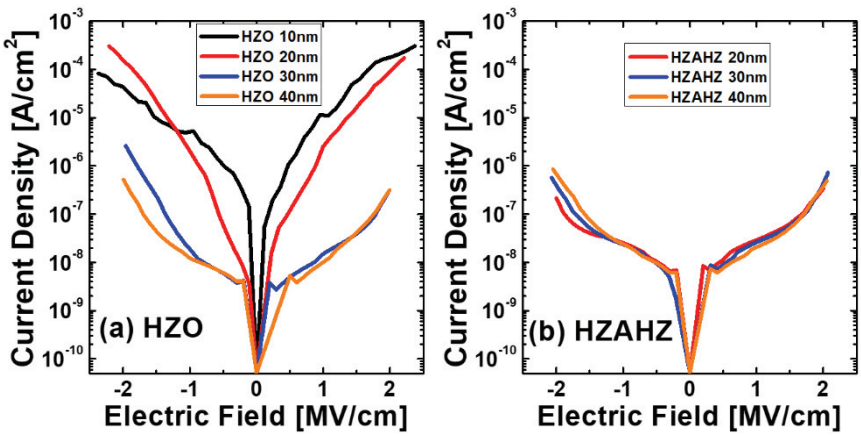

Figure 3. 7. The current density-electric field curves of (a) the $Hf_{0.5}Zr_{0.5}O_2$ films and (b) $Hf_{0.5}Zr_{0.5}O_2/Al_2O_3/Hf_{0.5}Zr_{0.5}O_2$ films with various thicknesses.

3.4. Conclusion

In conclusion, the problem of degrading ferroelectric performance of the HZO films with increasing t_f, which could be ascribed to the increased portion of non-ferroelectric m-phase at higher t_f could be resolved by interposing the Al_2O_3 interlayer at the middle position of HZO film. The Al_2O_3 interlayer interrupted the continuous grain growth HZO film, which was accompanied with the decrease in the average grain size. Therefore, the higher portion of ferroelectric o-phase could be retained up to the film thickness of 40 nm. The two portions of the HZO films at upper and lower position appear to have identical ferroelectric performances even though the lower portion was grown on TiN BE while the upper portion was grown on the inserted thin Al_2O_3 layer. This implies that the repetition of even higher number of stacking might be possible without degrading the ferroelectric performance, which is under investigation. The insertion of thin Al_2O_3 layer was also highly effective to largely decrease the leakage current, which will greatly facilitate the stable operation of integrated device as well as the precise evaluation of the reliability of this ferroelectric layer.

3.5. References

[1] T. S. Böscke, J. Müller, D. Bräuhaus, U. Schröder, and U. Böttger, Appl. Phys. Lett. **99**, 102903 (2011).

[2] S. Mueller, J. Mueller, A. Singh, S. Riedel, J. Sundqvist, U. Schroeder, and T. Mikolajick, Adv. Funct. Mater. **22**, 2412 (2012).

[3] J. Müller, T. S. Böscke, U. Schröder, S. Mueller, D. Bräuhaus, U. Böttger, L. Frey, and T. Mikolajick, Nano Lett. **12**, 4318 (2012).

[4] J. Müller, U. Schröder, T. S. Böscke, I. Müller, U. Böttger, L. Wilde, J. Sundqvist, M. Lemberger, P. Kücher, T. Mikolajick, and L. Frey, J. Appl. Phys. **110**, 114113 (2011).

[5] S. Mueller, C. Adelmann, A. Singh, S. Van Elshocht, U. Schroeder, and T. Mikolajick, ECS J. Solid St. Sci. and Technol. **1**, N123 (2012).

[6] T. Schenk, S. Mueller, U. Schröder, R. Materlik, A. Kersch, M. Popovici, C. Adelmann, S. Van Elshocht, and T. Mikolajick, 2013 European Solid-State Device Research Conference, ESSDERC 2013, Bucharest, 16-20 September 2013, p. 260.

[7] J. Muller, T. S. Boscke, S. Muller, E. Yurchuk, P. Polakowski, J. Paul, D. Martin, T. Schenk, K. Khullar, A. Kersch, W. Weinreich, S. Riedel, K. Seidel, A. Kumar, T. M. Arruda, S. V. Kalinin, T. Schlosser, R. Boschke, R. van Bentum, U. Schroder, and T. Mikolajick, 2013 Electron Devices Meeting, Washington, DC, 9-11 December 2013, p. 10.8.1

[8] T. Watanabe, S. Hoffmann-Eifert, F. Peter, S. Mi, C. Jia, C. S. Hwang and

R. Waser, J. Electrochem. Soc. **152**, G262 (2007).

[9] T. Watanabe, S. Hoffmann-Eifert, C. S. Hwang, and R. Waser, J. Electrochem. Soc. **155**, D715 (2008).

[10] T. Watanabe, S. Hoffmann-Eifert, S. Mi, C. Jia, R. Waser, and C. S. Hwang, , J. Appl. Phys. **101**, 014114 (2007).

[11] International Technology Roadmap for Semiconductors (ITRS) 2013 http://www.itrs.net/Links/2013ITRS/

[12] E. Bersch, S. Rangan, and R. A. Bartynski, E. Garfunkel, and E. Vescovo, Physical Review B, **78**, 085114 (2008)

[13] S. K. Pandey, A. R. James, R. Raman, S. N. Chatterjee, A. Goyal, C. Prakash, and T. C. Goel, Physica B, **369**, 135 (2005)

[14] S. Sakai, and R. Ilangovan, IEEE Electr. Device L. **25**, 369 (2004).

[15] M. H. Park, H. J. Kim, Y. J. Kim, W. Lee, H. K. Kim, and C. S. Hwang, Appl. Phys. Lett. **102**, 112914 (2013).

[16] M. H. Park, H. J. Kim, Y. J. Kim, T. Moon, and C. S. Hwang, Appl. Phys. Lett. **104**, 072901 (2014).

[17] W. D. Nix and B. M. Clemens, J. Mater. Res. **14**, 3467 (1999).

[18] M. H. Park, H. J. Kim, Y. J. Kim, W. Lee, T. Moon, K. D. Kim, and C. S. Hwang, Appl. Phys. Lett. **105**, 072902 (2014).

[19] E. Yurchuk, J. Müller, S. Knebel, J. Sundqvist, A. P. Graham, T. Melde, U. Schröder, and T. Mikolajick, Thin Sold Films, **533**, 88 (2013)

[20] M. W. Pitcher, S. V. Ushakov, A. Navrotsky, B. F. Woodfield, G. Li, J.

Boerio-Goates, and B. M. Tissue, J. Am. Ceram. Soc. **88**, 160 (2005)

[21] M. Shandalov, and P. C. Mclntyre, J. Appl. Phys. **106**, 084322 (2009).

[22] H. J. Cho, Y. D. Kim, D. S. Park, E. Lee, C. H. Park, J. S. Jang, K. B. Lee, H. W. Kim, Y. J. Ki, I. K. Han, and Y. W. Song, Solid-State Electronics, **51**, 1529 (2007)

[23] C. V. Thompson, Annu. Rev. Mater. Sci., **20**, 245 (1990)

[24] M. H. Park, H. J. Kim, Y. J. Kim, W. Lee, T. Moon, and C. S. Hwang, Appl. Phys. Lett. **102**, 242905 (2013).

[25] J. E. Lowther, J. K. Dewhurst, J. M. Leger, and J. Haines, Phys. Rev. B **60**, 14485 (1999).

[26] E. H. Kisi and C. J. Howard, J. Am. Ceram. Soc. **72**, 1757 (1989)

[27] E. H. Kisi, J. Am. Ceram. Soc. **81**, 741 (1998)

[28] A. Q. Jiang, H. J. Lee, G. H. Kim, and C. S. Hwang, Adv. Mater. **21**, 2870 (2009)

[29] M. H. Park, H. J. Kim, Y. J. Kim, W. Jeon, T. Moon, and C. S. Hwang, Phys. Status Solidi-R, DOI: 10.1002/pssr.201409017.

[30] K. McKenna, A. Shluger, V. Iglesias, M. Porti, M. Nafría, M. Lanza, and G. Bersuker, Microelectronic Engineering **88**, 1272 (2011)

4. A study on the wake-up effect of ferroelectric $Hf_{0.5}Zr_{0.5}O_2$ films by pulse-switching measurement

4.1. Introduction

Since the first report on the emergence of (unexpected) ferroelectricity in a doped-HfO_2 film in 2011, [1] motivations for the deeper understanding of this phenomenon occurred [2-6] and the active research in this field for its practical application to semiconductor and energy related devices has been triggered. [7-9] It is now generally being accepted that the emergence of unexpected ferroelectricity in this material system is due to the formation of non-centrosymmetrical orthorhombic phase (o-phase) of which space group is $Pca2_1$. This phase is not thermodynamically stable at usual processing conditions (several hundred degrees Celsius and near atmospheric pressure). The thin film fabrication processes, therefore, appear to induce various (asymmetric) stresses and grain size effects, [10, 11] which stabilize the ferroelectric (FE) o-phase over the other phases, such as monoclinic (m-phase) or tetragonal (t-phase) phases.

HfO_2–ZrO_2 (HZO) solid solution system is one of the very promising FE materials due to its wide composition range (Hf:Zr ratio) and lower

processing temperature (400 – 700 °C) for the emergence of these functional properties compared with other doped-HfO_2, such as Si-doped HfO_2, which requires precise control of Si concentration (~4%) and high processing temperature (~1000°C). Even more interesting aspect of HZO material is that it shows wide range of electrical properties (and crystal structure too) depending on Hf:Zr ratio; when it is ~0.9:0.1, ~0.5:0.5, and ~0.1:0.9, the film showed dielectric, ferroelectric, and anti-ferroelectric (AFE) properties, respectively. [12] The composition boundaries between these different properties are not clear, which could be further modified by detailed processing conditions.

Recovering the usual dielectric property with increasing Hf concentration in HZO film is understandable considering the well-known high-k dielectric property of HfO_2. However, emergence of AFE property in Zr-rich composition and unclear composition boundary with the mostly FE-like 0.5:0.5 HZO impose a certain conceptual difficulty on the understanding of the origin of these unexpected FE-AFE behaviors in this material system. This difficulty is becoming even worse when identifying the fact that the microstructures of HZO films showing feasible FE or AFE properties are not single crystalline or even a single phase; they generally have small grain size with random orientation and often contain non-FE or non-AFE phases. These factors hinder the straightforward application of several theoretical works based on the first-principles

calculation. The involvement of so called “wake-up” effect in many of these films add more difficulties since the FE and AFE properties vary with the number of FE or AFE switching cycles. It has been reported that the FE properties of many doped-HfO_2 thin films, including $Hf_{0.5}Zr_{0.5}O_2$ film, became more evident as the cycle number increases, before they eventually become frustrated due to the fatigue effect. [13-16] This suggests that some of the FE domains are pinned by defects or traps within the film or at the electrodes interface, which are typically TiN, at a pristine state, and repeated electrical cycles make the domains unpinned. In this work, the authors systematically examined the FE property change with electrical cycling (wake-up effect) using standard polarization-electric field (P-E) hysteresis curve measurements and pulse-switching (PS) technique. The former is useful to examine the evolution of FE – AFE properties with increasing cycling number while the latter can give the detailed quantitative information on the evolution of HZO/TiN contact property, coercive field (E_c), and possibly involved interfacial capacitance (C_i).

In general, the involvement of C_i is more complicated to understand. The presence of C_i in FE thin films has been identified in many experiments, [17-20] and is now quite well understood for standard FE materials with an epitaxial structure, such as $SrRuO_3/BaTiO_3/SrRuO_3$, based on the imperfect interfacial charge screening model using atomic scale simulations. [21] However, it is

quite evident that such standard approach can hardly be applicable in polycrystalline microstructure with relative random orientation of the FE grains, which would be the case for TiN/HZO/TiN. It has to be noted that such small grain size with relatively random orientations is the prerequisite for achieving FE and AFE properties, otherwise they will regain the stable m-phase with well-known high-k property. The possible involvement of physical interfacial layer by the oxidation of TiN, i. e. TiO_x ($x \sim 2$), cannot be completely disregarded although its formation must be highly suppressed in well-performing HfO_2-based FE films. In addition, the involvement of intrinsic low-k layer at the interface due to the incomplete screening of FE bound charges by the free carriers in TiN must be considered to correctly interpret the electrical properties. Nevertheless, the comprehensive understanding in this field is still lacking, especially in conjunction with the wake-up effect. Therefore, in this work, pulse switching technique, which is useful to examine the evolution of various physical parameters with the switching cycles, in addition to the standard polarization – electric field technique, was adopted. The evolutions of physical interface properties are discussed in detail in conjunction with the depinning of the pinned domains and the possible field-induced phase transition between the FE and AFE phases.

4.2. Experimental

The 9nm-thick HZO films were deposited on a 50-nm-thick TiN bottom electrode (BE) formed on a SiO_2/Si substrate via thermal ALD at a substrate temperature of 280 °C using $Hf[N(C_2H_5)CH_3]_4$ (TEMAH), $Zr[N(C_2H_5)CH_3]_4$ (TEMAZ), and ozone (170 g/cm^3) as the precursor of Hf, Zr, and oxygen source, respectively. The TiN BE was deposited via DC reactive sputtering. The growth per cycle of HfO_2 and ZrO_2 was almost identical (~0.12 nm/cycle), so the HZO films with a 0.5:0.5 Hf:Zr ratio could be deposited using a 1:1 HfO_2:ZrO_2 ALD cycle ratio.

For electrical characterization, a Pt(30nm-thickness)/TiN(5nm-thickness) top electrode (TE) was deposited via DC sputtering through a shadow mask with a 400 μm hole diameter (TiN contacted the HZO film). After the TE deposition, post-metallization-annealing was performed for 30 seconds at 500 °C in a N_2 atmosphere using rapid thermal annealing for the film crystallization. The composition and the film thickness of the HZO films were examined via X-ray fluorescence (Quant'X, Thermo SCIENTIFIC) and ellipsometry (L-116d, Gaertner), respectively. The cross-sectional images of HZO film were obtained by high-resolution transmission electron microscopy (HRTEM, JEM-2100F, JEOL). The focused ion beam (Helios 650, NanoLab) in the NCIRF of Seoul National University was used to prepare the sample for HRTEM analysis. The crystal structure of the HZO films was analyzed using an X-ray diffractometer (X'pert Pro, Panalytical) via grazing-angle incidence X-ray diffraction

(GIXRD, incidence angle = 0.5°). For electrical characterization, the polarization - electric field (P-E) characteristics were measured using a ferroelectric tester (TF Analyzer 2000, Aixacct Systems) in virtual mode. Triangular bipolar pulses with a 1 kHz frequency were applied to the TE with the BE grounded. The dielectric constant-electric field (ε_r-E) characteristics were measured using an impedance analyzer (4194A, Hewlett-Packard, at the AC bias frequency of 10 kHz and amplitude of 50 mV). For the pulse switching measurements, rectangular positive or negative pulses with a pulse width of 10μs and rising/falling time of 2ns, were supplied by a pulse generator (81110A, Agilent) with an internal resistance of 50 Ω. The switching current response from the HZO film was monitored using an oscilloscope (TDS684Dm Tektronix) with an internal resistance of 50 Ω.

4.3. Results and Discussions

Figure 4. 1(a) shows the cross-sectional TEM image of the Pt/TiN/$Hf_{0.5}Zr_{0.5}O_2$/TiN capacitor on a SiO_2/Si substrate. The deposition of uniform and flat HZO films with clean interfaces could be confirmed. From the HRTEM image shown in figure 4. 1(b), the polycrystalline nature of HZO films could be confirmed from the lattice fringes with different directions in different areas. The crystal structure of the HZO films might be o-phase, which were examined via fast Fourier transformation of the lattice fringes. However, it was challenging to clearly distinguish the o-phase from t-phase (d-spacing value of o-phase (111) plane and t-phase (101) plane are 2.94 and 2.97 Å, respectively) due to their structural similarity. Figure 4. 1(c) shows the GIXRD spectra in 2θ range of 25°-50° for the $Hf_{0.5}Zr_{0.5}O_2$ film. The diffraction peaks from the (111), and (200) planes of the o-phase (or t-phase) HZO could be clearly observed in the diffraction patterns. According to the Joint Committee on Powder Diffraction Standards, 2θ of the (111) plane of the o-phase and (101) plane of the t-phase are 30.35° and 30.09°, respectively, indicating the challenge for making clear identification of GIXRD peaks. Similar difficulty is encountered when identifying the peak near 2θ value of ~36°. Therefore, the diffraction peaks near 2θ values of ~31° and 36° are assigned to be the mixture of o-phase (111) and t-phase (101), and o-phase (200) and t-phase (110), respectively. In fact, the coexistence of

these two phases has important implication for the electrical characteristics of the films as discussed below.

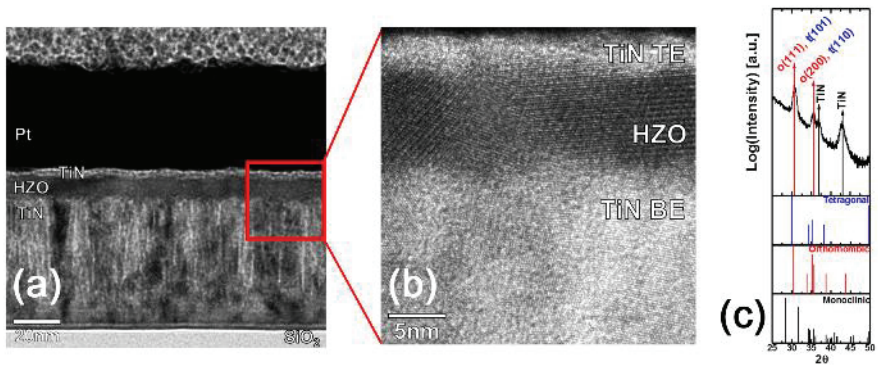

Figure 4. 1. (a) Cross-sectional low magnitude transmission electron microscope image and (b) Cross-sectional high resolution transmission electron microscopy image of the Pt/TiN/$Hf_{0.5}Zr_{0.5}O_2$/TiN structure. (c) Grazing incidence X-ray diffraction pattern of the $Hf_{0.5}Zr_{0.5}O_2$ films.

Figures 4. 2(a) shows the change in the P-E hysteresis loops with an increase in the number of electrical switching cycles of the $Hf_{0.5}Zr_{0.5}O_2$. For these experiments, the film samples were field-cycled using the pulse generator with a field strength of ± 3.8 MV/cm and 10μs duration, and the P-E hysteresis loops were obtained by an FE tester after the intended number of cycling was performed. When the $Hf_{0.5}Zr_{0.5}O_2$ film is in the pristine state, shape of the P-E hysteresis loop was slanted including bumps especially in the left portion of the curve, which might be induced by the inclusion of charged defects, non-FE phase, and AFE-like phase. However, after the cycling by only 10^2 times, the film showed an almost complete FE-like P-E curves, and further increase in the cycle number makes the P-E curve more square-like, i. e. FE-property improved. Inset figure shows the increase in the $2P_r$ value with increasing the cycle number. It can be understood that the $2P_r$ of the $Hf_{0.5}Zr_{0.5}O_2$ film increased from 30.2 $\mu C/cm^2$ at the pristine state to 43.4 $\mu C/cm^2$ after the 10^5 cycles. $2P_r$ of > ~40 $\mu C/cm^2$ has not been reported for the HZO film yet, and is a highly promising value for FE memory application. Such increase in $2P_r$ and general disappearance of the AFE-like distortions in the P-E curves with increasing the cycle number indicate the followings could have occurred. The pristine film appears to have pinned domains, indicated by the smaller $2P_r$ value, some of which are anti-parallel with each other, thereby induces the AFE-like distortions of the P-E loop. These domain

pinning could be induced by the presence of charged point defects such as oxygen vacancies, or even non-FE phases such as t-phase $Hf_{0.5}Zr_{0.5}O_2$. [22] Therefore, the field cycling is believed to induce the depinning the pinned domains, combined with the local phase transition from non-FE phase to FE phase. It has been identified from the careful fitting of the GIXRD patterns that field cycled $Hf_{0.5}Zr_{0.5}O_2$ which apparently is FE-like still contains non-negligible t-phase. Confirming the possible transition of some of the non-FE phase, t-phase, into FE o-phase during the field cycling by an in-situ type experiment, such as focused X-ray analysis using synchrotron source on field cycling device would be an interesting topic for future research. This work provides an indirect proof for the change of the non-FE phases into FE phase by the field cycling using the pulse switching technique as shown later.

Figure 4. 2(b) shows the ε_r-E characteristics with different number of electrical switching cycles within the same film. It shows the butterfly-like feature, a typical characteristic of FE materials, at the pristine state. The ε_r value of the film over the ~2 MV/cm electrical field where the FE switching effect is excluded, was ~33.0 when the film was at the pristine state, and it gradually decreased with electrical switching cycles. Finally, the ε_r value reached to ~30.5 at the 10^5 cycles. From the changes in P-E and ε_r-E characteristics during electrical switching cycles, it could be conjectured that the phase transition from t- to o-phase had occurred.

Lomenzo et al. and Park et al. also suggested the phase transformation from t- to o-phase based on the simultaneous increase in P_r and decrease in ε_r during field cycling in Si-doped HfO_2 thin film [23] and HZO thin film. [24] Also, the intersection points of the butterfly curve are shifted toward the positive bias with increasing switching cycles, which implies that the internal field of the HZO film increases simultaneously. It has been reported that the distribution of oxygen vacancies within the HZO film could be affected by the pulsed wake-up cycling. [16] As the internal field is significantly related with charged defects, the internal field increases during the wake-up process. In addition, the peaks of dielectric constant near E_c decrease with increasing number of switching cycles. Although the low-frequency dielectric constants of the FE-phase HZO along the parallel and perpendicular direction to the P_r direction have not been solidified yet, experimental and theoretical results for the conventional FE material, such as $BaTiO_3$ and $Pb(Zr,Ti)O_3$ (PZT), reasonably illustrate that the dielectric constant is lower along the P_r-direction. [25, 26] Therefore, the ε_r-E characteristics of the film with increasing cycle number correspond to the ε_r-E characteristics of typical FE materials with field cycling, meaning that the obtained $Hf_{0.5}Zr_{0.5}O_2$ film was mostly FE, and it becomes more uniformly “poled” along the field direction during the cycling.

The change in FE domain switching kinetics with cycling is further examined by adopting the PS experiments as shown in Figs. 4. 3. For this experiment, the films were pre-poled to the opposite direction to the switching pulse direction and domain switching current (I_{sw}) was estimated as a function of time with different magnitude of applied field, for the differently cycled films.

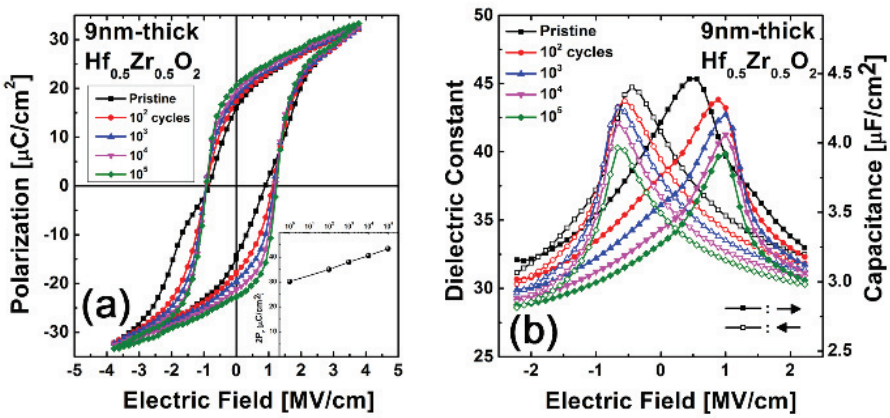

Figure 4. 2. (a) Polarization - electrical field hysteresis and (b) Dielectric constant - electrical field characteristics of the 9nm-thick $Hf_{0.5}Zr_{0.5}O_2$ film with an increase in the number of electrical switching cycles, respectively.

Figure 4. 3(a) shows the schematic diagram for pulse application with time. For these experiments, 10μs pulses were adopted, which is long enough to induce sufficient FE switching even at the lowest field (2.2MV/cm). The switching charges for both negative to positive switching (up → down) and positive to negative (down → up) switching were estimated for different electrical cycling numbers. Figures 4. 3(b) - (d) show the switching current transient for the pristine, after cycling for 10^2 and 10^5 times, respectively. According to the polarization reversal theory in FE film mediated by the reverse domain nucleation and growth, of which detailed functional form can be varied depending on the specific circumstance (Komogolov-Avrami-Ishibashi kinetic model or nucleation limited switching model), the I_{sw} can be described by Eq. (4. 1) at a given electric field.

$$I_{SW}(t) = I_{SW}^{o} e^{-\frac{t-t_0}{R_L C_i}} \quad (t_0 \leq t \leq t_{SW}) \tag{4. 1}$$

, where t_0, t_{sw}, R_L, and C_i are the time when ferroelectric film starts switching, the time when the switching process is completed, the total resistance of measurement circuit and sample, and the interfacial capacitance, respectively. The R_L is the summation of the internal resistance of pulse/pattern generator (R_W) and digital oscilloscope (R_O), parasitic resistance (R_P), and contact resistance (R_C). The summation of

R_W, R_O and R_P is estimated to be ~104 Ω in this experiment. This representation basically assumes that the FE capacitor has a non-FE interfacial capacitance (C_i) which is invariant during the field application time, so capacitive charging current flows with a time constant, $R_L C_i$, while a constant switching current flows into the FE layer during the switching time period. This means that the FE layer itself behaves like a resistor during the FE switching. [27] Therefore, if there is no interfacial capacitance involved ($C_i \sim \infty$) a constant I_{sw} must be achieved during switching, which is generally not the case. The observed I_{sw} vs. time curves at different field in Figs. 4. 3(b) - (d) show an abrupt increase in current at the beginning of pulse application, which corresponds to the capacitive charging of overall capacitor structure, followed by a rapid decrease in I_{sw} with time as the charging completes. At $t = t_0$, indicated by the black arrow within the figures, which is the time when the film starts switching, $I_{sw}(t)$ aligns with Eq. (4. 1) and follows the linear behavior of the semi-log plot (dotted lines). According to Eq. (4. 1), the I^0_{sw}, which is the current at the moment when FE switching starts, is given as Eq. (4. 2).

$$I_{SW}^0 = \frac{(E_a - E_c) t_f}{R_L} \tag{4. 2}$$

, where E_a is an applied field and t_f is a thickness of the film. This means that at the moment of the FE film switching, E_c, a portion of E_a, is applied

to the FE layer while the rest portion of the E_a is applied over R_L. Therefore, for different cycling conditions, R_L and E_c can be calculated from the slope and the intercept of abscissa by taking I^0_{sw} at each E_a and plotting the value as a function of E_a (Figs. 4. 3(e) - (g)). Since R_L value is achieved from Eq. (4. 2), C_i can also be calculated from the slopes of the fitting graphs of I_{sw} at each E_a (dashed lines in Figs. 4. 4(e) - (g)), which showed a common value at different E_a's for the given cycle number. It has to be noted that the calculated E_c value corresponds to the genuine coercive field value of the FE layer without involving any additional term that could be induced from the series resistance and C_i, which is not how E_c is obtained from the P-E hysteresis loops.

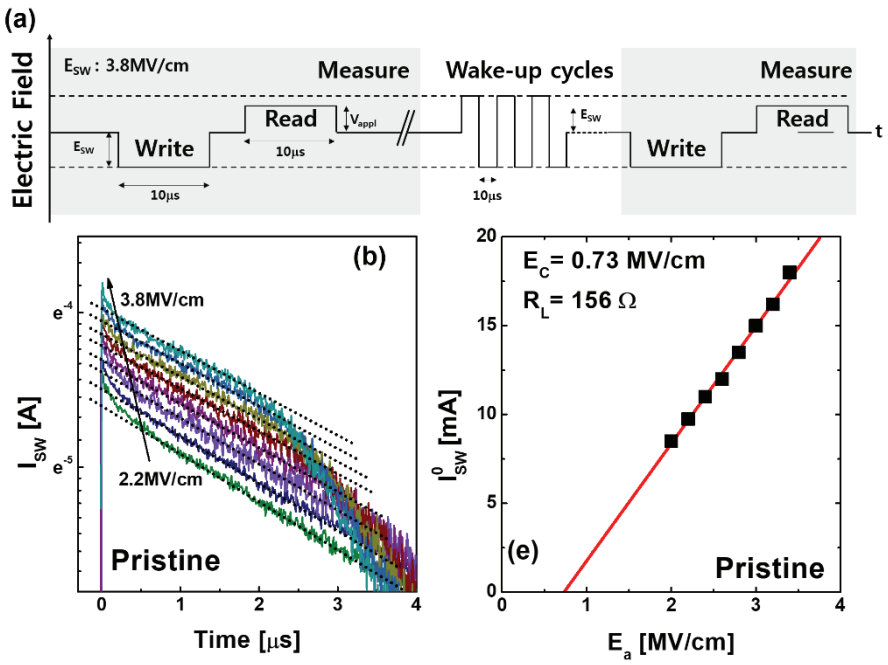
(a)
Electric Field
E_SW : 3.8MV/cm
Measure
Wake-up cycles
Measure
Read
V_appl
E_SW
Write
10μs
10μs
10μs
E_SW
Write
Read
t
(b)
3.8MV/cm
2.2MV/cm
Pristine
I_SW [A]
e^-4
e^-5
Time [μs]
E_C= 0.73 MV/cm
R_L= 156 Ω
(e)
Pristine
I^0_SW [mA]
E_a [MV/cm]

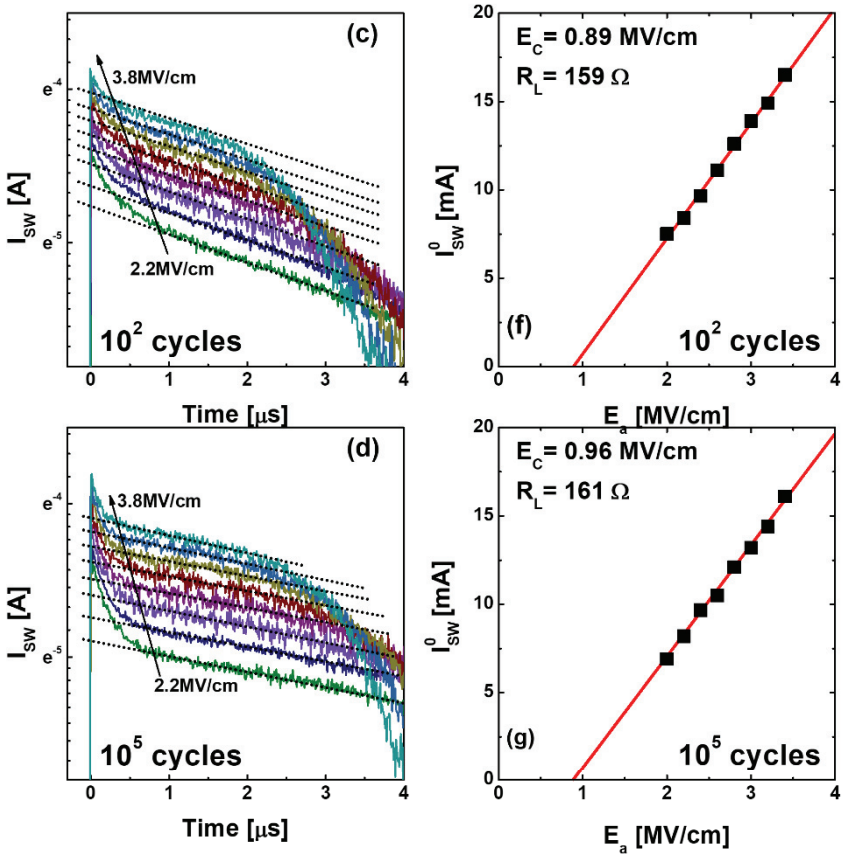

Figure 4. 3. (a) The schematic diagram for pulse application with time. The domain switching current transient - time curves of the $Hf_{0.5}Zr_{0.5}O_2$ film with various applied electrical fields, (b) at the pristine state, (c) after the 10^2 electrical switching cycles and (d) after the 10^5 electrical switching cycles, respectively. The initial domain switching current as a function of the electric field and extracted genuine coercive field and resistance of the same film, (e) at the pristine state, (f) after the 10^2 electrical switching cycles and (g) after the 10^5 electrical switching cycles, respectively.

From the integration of I_{sw} with time, the $2P_r$ value can be estimated as a function of time, where the charges due to the reversible capacitive charging are excluded by including the discharging peak at the moment of pulse termination into the current integration. Figure 4. 4(a) summarizes the results for negative to positive switching (open symbols) and positive to negative switching (closed symbols). While the former shows a generally slightly higher switching charge, possibly due to the involvement of a small imprint effect, both data show a common trend with increasing cycle number. At the pristine state, the film shows a quite gradual switching, i. e. $2P_r$ varies over a wide field region, with the smallest saturation $2P_r$ value. With increasing cycle number, the switching became more and more abrupt with higher saturation $2P_r$ value, which is in accordance with the results in figure 4. 2(a).

To confirm the reliability of the PS technique, change in the C_i as a function of a cell area at the pristine film is plotted in Fig. 4. 4(b). As the data points, although not sufficiently many, are fitted well with a straight line, it is believed that the PS technique gives reliable results. The intercept at the y-axis of the fitted line corresponds to the parasitic capacitance of the PS measurement system, which was ~ 2.2 nF. The parasitic capacitance is induced by the probe station, pulse generator and oscilloscope in the experimental set-up. Hence, C_i is subtracted by the value (~ 2.2 nF) of the parasitic capacitance, which is connected on circuit in parallel, for the future calculations.

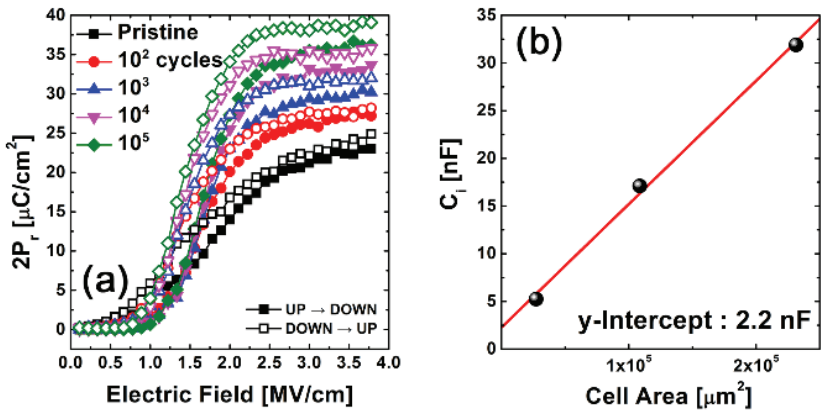

Figure 4. 4. (a) Double remanent polarization - electric field curves measured by pulse-switching technique. (b) The change in the interfacial capacitance as function of cell area at the pristine state of the $Hf_{0.5}Zr_{0.5}O_2$ film.

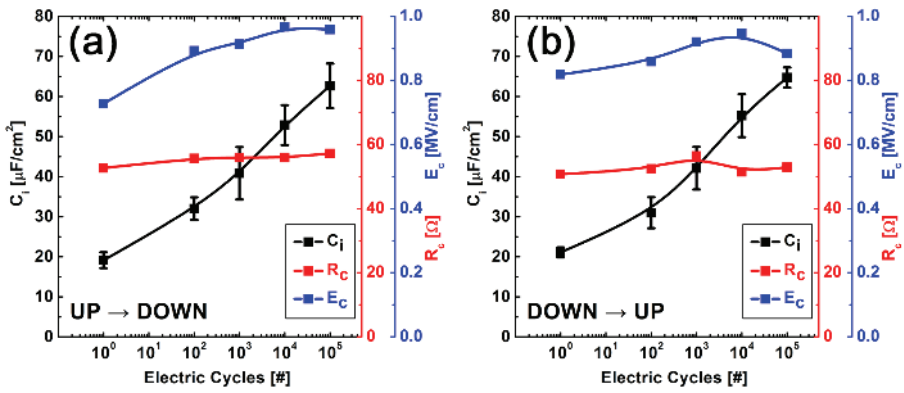

Figure 4. 5. Summary of the estimated variation of interfacial capacitance, coercive field, and contact resistance for (a) positive-to-negative and (b) negative-to-positive pulse-switching measurement, respectively.

Figures 4. 5(a) and (b) show the summary of the estimated variation of C_i, E_c and R_c for positive-to-negative and negative-to-positive PS, respectively, as a function of cycle number. R_c does not show any notable variations suggesting that the electrical contact between the TiN electrode and HZO film does not vary with field cycling. However, E_c shows clear increase from ~0.8 MV/cm at pristine state to ~0.95 MV/cm after 10^5 cycles with increasing cycle number. These values are generally smaller than the value estimated from the P-E hysteresis curves in Fig. 4. 2(a), where the $+E_c$ and $-E_c$ are ~1.2 MV/cm and ~0.9 MV/cm. This is because the voltage drop across the series components (R_L and C_i) is involved when obtaining the E_c from the P-E curves.

The increase in E_c with cycle number indicates that the following critical change has occurred in the FE property of the film. If the field cycling merely induces the depinning of the pinned domains while the amount of the FE domains exhibiting FE performance remains invariant, E_c should have been decreased. Therefore, the increase in E_c suggests that the amount of actively contributing FE domains with slightly higher local E_c values actually increases with cycle number. This is consistent with the increase in the $2P_r$ values with the cycle number, and also consistent with the idea that some of the originally non-FE phases in the pristine film could be changed into the FE phase by the sufficiently high field cycling.

The E_c of such transformed FE phase could be slightly higher than that of the originally FE phase.

Change in C_i is also consistent with the idea of changing the non-FE phase into the FE phase with cycling. While the accurate nature of the C_i, generally estimated from such PS measurements, is not very well understood yet, it might be closely related with the presence of an interfacial dielectric layer and/or an intrinsic dead-layer. Although it is an indirect method to characterize the C_i parameters of the non-FE parts from the whole measurement circuit which includes FE parts, this method can be feasibly used for identifying the nanoscale changes within the FE thin films. It has been reported that the critical nuclei size of a few nm level could be examined during the initial stage of polarization switching using similar PS technique, signifying the usefulness of this technique to evaluate the nanoscale structural change. [27] Since the dielectric constants of the FE HZO and the non-FE HZO phases are not very much different (~30 for o-phase and ~35-40 for t-phase), compared with the cases involving the conventional FE material, such as PZT, the large increase in C_i value during the cycling (from ~19 $\mu F/cm^2$ at pristine state to ~62 $\mu F/cm^2$ after 10^5 cycles) may correspond to the decrease in the thickness of the interfacial non-FE phase. Since there are two interfaces that contribute to the estimated C_i, the actual capacitance of one interface must be twice the estimated values (38 – 124 $\mu F/cm^2$). It must be

reasonable to assume that these non-FE phases are present mostly at the interface region with the electrodes. At this region, after the nucleation stage when the film grows, the phase transition from t-phase (non-FE phase) to the o-phase is restricted due to surface energy effect. It can be concluded that the field cycling changes the interfacial non-FE phases into FE phase. This is consistent with the idea of increasing the FE domain volume with slightly higher E_c mentioned above. As can be understood from the continuously increasing $2P_r$ value with increasing cycle number up to 10^5 in Figure 4. 4(a), there could be further increase in the FE performance at even higher cycle number. However, further increase in cycle number induced the fatigue effect and was excluded from the data. Hence, it is believed that there is not much room left for further improvement from the maximum value of C_i at 10^5 cycles. It can be understood that the low C_i value at low cycle number is due to the involvement of both physical non-FE phase at the interface and intrinsic dead-layer effect. While the capacitance of intrinsic dead-layer in TiN/HZO interface has not been estimated yet, values for the idealized perovskite/metal interfaces, such as $PbTiO_3$/Pt and $PbTiO_3$/$SrRuO_3$, can be referenced to qualitatively estimate C_i values. They were calculated to be ~79 $\mu F/cm^2$ and ~58 $\mu F/cm^2$, respectively, for one interface from the first principles calculation. [22] The relatively low electrical conductivity (lower carrier concentration) of an oxide electrode ($SrRuO_3$) compared

with pure metal (Pt) generally induced less efficient screening of the polarization charge of the ferroelectric or dielectrics layer in contact, and thus, the C_i value is lower. Because TiN has a resistivity (~220 μΩcm) closer to that of $SrRuO_3$ (~100 – 200 μΩcm) than Pt (~10 μΩcm), electrode polarization must be rather significant, which would render the smaller C_i. Therefore, the estimated 124 μF/cm^2 (per one HZO/TiN interface) after the 10^5 cycling appears quite unusual, because this value must have come from two contributions, if any, from both electrode polarization and interfacial dielectric layer. Nevertheless, a specific form of $BaTiO_3$/Pt interface (Ba – Pt bond formation) is reported to have an interfacial capacitance density as high as ~2,700 μF/cm^2 implying the validity of having a C_i value > 100μF/cm^2. [21] In fact, Kim et al. and Jiang et al. also performed similar PS measurement on the Pt/PZT/Pt capacitor [28] and Pt/Al_2O_3/PZT/Ir capacitor. [29] They acquired similar $2C_i$ value of ~160 μF/cm^2 and ~130 μF/cm^2, respectively. Further theoretical work is necessary in this field.

According to the above mentioned model, the C_i^{-1}, which is the inverse interfacial capacitance, is given as Eq. (4. 3).

$$\frac{1}{C_i} = \frac{1}{C_{int,top}} + \frac{2}{C_{non-FE}} + \frac{1}{C_{int,btm}} \qquad (4.\ 3)$$

, where $C_{int,top}$ and $C_{int,btm}$ are intrinsic dead-layer capacitance at the top and bottom interface, respectively, and C_{non-FE} is a physical non-FE phase capacitance. It should be noted that the $C_{int,top}$ and the $C_{int,btm}$ are intrinsic values of the electrode, which must be remained invariant during the field cycling. The contribution from charged defects at the interfaces is linked with the C_{non-FE}. Because $C_{int,top}$ and $C_{int,btm}$ are not known for TiN, C_{non-FE} cannot be calculated from the estimated C_i values at pristine state and after 10^5 cycles. Nevertheless, the difference between the two estimated values can be used to approximate the change in C_{non-FE} when the $C_{int,top}$ and $C_{int,btm}$ are assumed to be identical and not affected by the wake-up effect, which is a reasonable assumption. When the dielectric constant of the non-FE layer was taken as 40 (t-phase), an approximate thickness decrease of 1.1 nm was calculated for two interfaces by the 10^5 electrical switching cycles. This can be a negligible value in conventional FE capacitor, where the FE thickness is usually higher than ~100nm. However, in this HZO case, the total film thickness is only 9 nm, which means that ~ 12% of the whole thickness was non-FE phase at the pristine state. Considering that the $2P_r$ value increased from ~30μC/cm^2 to ~43 μC/cm^2 after 10^5 cycles (in P-E characteristics), which corresponds to ~43% increase from the initial value, the ~12% transition from the t-phase into the o-phase during the cycling cannot solely explain the $2P_r$ enhancement. Therefore, it is believed that there was significant contribution from the

depinning of the pinned FE domains during the wake-up cycling. It might be possible that the domain pinning of the original FE phase (o-phase) has been caused by the presence of the non-FE phase (t-phase). The field cycling may induce the transition from the t-phase to o-phase and eliminate the pinning effect, which enable the FE domains to switch more efficiently.

4.4. Conclusion

In conclusion, the wake-up behaviors of $Hf_{0.5}Zr_{0.5}O_2$ with increasing electric field cycling number were examined by the P-E hysteresis loop, ε_r-E curves, and pulse switching tests. $Hf_{0.5}Zr_{0.5}O_2$ film shows mostly the FE-like behavior from the pristine state, where the slight AFE-like distortion could be ascribed to the anti-parallel distribution of some of the FE domains and the AFE phase. The field cycling of only 100 cycles almost completely removed such anti-parallel pinned domains. Further increase in the field cycling number more effectively poled the domains making the P_r largely increase. The field cycling also transformed the non-FE phases, mostly at the electrode interface, to FE-phase, which could be inferred from the increase in the interfacial capacitance. These results indicate that the physical state of the FE-phases in the HZO film is quite different from the conventional FE thin films, such as PZT, in a sense that it is the outcome of variously oriented domains, possibly including anti-parallel orientation. The field cycling plays a role as the poling in conventional FE materials, but the high field-induced non-FE t-phase to FE o-phase transition could also contribute to the effective poling (depinning of pinned FE domains).

4.5. References

[1] T. S. Böscke, J. Müller, D. Bräuhaus, U. Schröder, U. Böttger, *Appl. Phys. Lett.*, **99**, 102903 (2011).

[2] M. H. Park, H. J. Kim, Y. J. Kim, T. Moon, C. S. Hwang, *Appl. Phys. Lett.*, **104**, 072901 (2014).

[3] M. H. Park, Y. H. Lee, Kim, H. J. Kim, Y. J. Kim, T. Moon, K. D. Kim, J. Müller, A. Kersch, U. Schröder, T. Mikolajick, C. S. Hwang, *Adv. Mater.*, **27**, 1811–1831 (2015).

[4] R. Materlik, C. Künneth, A. Kersch, *J. Appl. Phys.*, **117**, 134109 (2015).

[5] X. Sang, E. D. Grimley, T. Schenk, U. Schröder, J. M. LeBeau, *Appl. Phys. Lett.*, 2015, **106**, 162905 (2015).

[6] T. D. Huan, V. Sharma, G. A. Rossetti Jr., R. Ramprasad, *Phys. Rev. B*, 2014, **90**, 064111 (2014).

[7] M. H. Park, H. J. Kim, Y. J. Kim, T. Moon, K. D. Kim, C. S. Hwang, *Phys. Status Solidi Rapid Res. Lett.*, **8**, 857–861 (2014).

[8] M. H. Park, H. J. Kim, Y. J. Kim, T. Moon, K. D. Kim, C. S. Hwang, *Adv. Energy Mater.*, **4**, 1400610 (2014).

[9] M. H. Park, H. J. Kim, Y. J. Kim, T. Moon, K. D. Kim, C. S. Hwang, *Nano Energy*, **12**, 131–140 (2015).

[10] M. H. Park, H. J. Kim, Y. J. Kim, W. Lee, T. Moon, K. D. Kim, C. S. Hwang, *Appl. Phys. Lett.*, **105**, 072902 (2014).

[11] H. J. Kim, M. H. Park, Y. J. Kim, Y. H. Lee, W. Jeon, T. Gwon, T. Moon, K. D. Kim, C. S. Hwang, *Appl. Phys. Lett.*, **105**, 192903 (2014).

[12] J. Müller, T. S. Böscke, U. Schröder, S. Müller. D. Bräuhaus, U. Böttger, L. Frey, T. Mikolajick, *Nano Lett.*, **12**, 4318−4323 (2012).

[13] D. Zhou, J. Xu, Q. Li, Y. Guan, F. Cao, X. Dong, J. Müller, T. Schenk, U. Schröder, *Appl. Phys. Lett.*, **103**, 192904 (2013).

[14] D. Martin, J. Müller, T. Schenk, T. M. Arruda, A. Kumar, E. Strelcov, E. Yurchuk, S. Müller, D. Pohl, U. Schröder, S. V. Kalinin, T. Mikolajick, *Adv. Mater.*, **26** , 8198–8202 (2014).

[15] T. Schenk, U. Schröder, M. Pešić, M. Popovici, Y.V. Pershin, T. Mikolajick, *ACS Appl. Mater. Interfaces*, **6**, 19744–19751 (2014).

[16] M. H. Park, H. J. Kim, Y. J. Kim, T. Moon, K. D. Kim, Y. H. Lee, S. D. Hyun, C. S. Hwang, *J. Mater. Chem. C*, **3**, 6291—6300 (2015).

[17] C. T. Black, J. J. Welser, *IEEE Transactions on Electron Devices*, **46**, 776-780 (1999).

[18] M. Grossmann, O. Lohse, D. Bolten, U. Böttger, T. Schneller, R. Waser, *Appl. Phys. Lett.*, **80**, 1427 (2002).

[19] C. S. Hwang, *J. Appl. Phys.*, **92**, 432 (2002).

[20] R. Plonka, R. Dittmann, N. A. Pertsev, E. Vasco, R. Waser, *Appl. Phys. Lett.*, **86**, 202908 (2005).

[21] M. Stengel, D. Vanderbilt, N. A. Spaldin, *Nat. Mater.*, **8**, 392 – 397 (2009).

[22] M. Dawber, J. F. Scott, *Appl. Phys. Lett.*, **76**, 1060 (2000).

[23] P. D. Lomenzo, Q. Takmeel, C. Zhou, C. M. Fancher, E. Lambers, N. G. Rudawski, J. L. Jones, S. Moghaddam, T. Nishida, *J. Appl. Phys.*, **117**, 134105 (2015).

[24] M. H. Park, H. J. Kim, Y. J. Kim, Y. H. Lee, T. Moon, K. D. Kim, S. D. Hyun, C. S. Hwang, *Appl. Phys. Lett.*, **107**, 192907 (2015).

[25] B. Jaffe, W. R. Cook Jr., H. Jaffe, *Piezoelectric Ceramics*, Academic Press, London, (1971).

[26] M. Kohli, P. Muralt, *Ferroelectrics,* **225**, 155 (1999).

[27] A. Q. Jiang, H. J. Lee, C. S. Hwang, T. A. Tang, *Phys. Rev. B*, **80**, 024119 (2009).

[28] G. H. Kim, H. J Lee, A. Q. Jiang, M. H. Park, C. S. Hwang, *J. Appl. Phys.*, **105**, 044106 (2009)

[29] A. Q. Jiang, H. J. Lee, G. H. Kim, C. S. Hwang, *Adv. Mater.*, **21**, 2870–2875 (2009).

5. Two-step polarization switching mediated by nonpolar intermediate phase in $Hf_{0.4}Zr_{0.6}O_2$ thin films

5.1. Introduction

The ferroelectricity in doped HfO_2-based ferroelectric thin films, including $Hf_{0.5}Zr_{0.5}O_2$ thin film, was first reported in 2011. [1, 2] This unexpected ferroelectricity is now elucidated to originate from the formation of $Pca2_1$ orthorhombic phase (o-phase) which has not been carefully considered when the materials were extensively studied for their application as high-k gate dielectrics for field effect transistors or capacitor dielectrics in dynamic random access memory. [3-6] By controlling the Zr contents, $Hf_{1-x}Zr_xO_2$ (HZO) thin films showed dielectric (x=0), ferroelectric (x~0.5), and antiferroelectric (x~0.7) properties, which are due to the involvement of various polymorphs such as monoclinic (m-phase, space group: $P2_1/c$, dielectric), o-phase (space group: $Pca2_1$, ferroelectric), and tetragonal (t-phase, space group: $P4_2/nmc$, antiferroelectric) phases. [7] While the dielectric and ferroelectric phases have attracted a great deal of attention for the aforementioned applications, including ferroelectric field effect transistors, the antiferroelectric phases have gained interests only very

recently due to their high potential for solid-state energy-related applications. [8-11] Classical understanding on the emergence of antiferroelectricity is based on the anti-parallel alignment of polarizations within the lattice, which has been proved in conventional antiferroelectrics, such as $PbZrO_3$. [12-14] The anti-parallel polarizations can be switched to align under the external bias with sufficiently high field, which is accompanied with the two branches of ferroelectric-like hysteresis loops at both large positive and negative bias regions in their polarization – electric field (P-E) curves. Similar arguments can be applied to the HZO system, and recent theoretical calculations based on the first principles elucidated that ZrO_2 in t-phase could be antiferroelectric. [15] This means that these antiferroelectic properties must result from the field-induced phase transition between t- and o-phases, provided that the free energy difference between the t- and o-phase is sufficiently small to be overcome by applying electric field of a few MV/cm magnitudes. [15] Owing to the temperature dependence of this field-induced phase transition, the giant pyroelectric energy harvesting and electrocaloric effect could be observed in Zr-rich antiferroelectric HZO thin films. [15, 16] The ferroelectricity and antiferroelectricity in HZO and doped HfO_2 thin films were comprehensively reviewed in 2015. [3] For theoretical understanding, Materlik et al. [17] systematically examined the stability of the various

polymorphisms in HZO thin films based on the computational calculations using the density functional theory. This report showed that the relative energy of the t-phase compared to that of the o-phase decreased with increasing Zr content from 0.5 to 1.0, [17] which was consistent with the experimental observation on the transition from the ferroelectric phase to the antiferroelectric phase with increasing Zr content. [7] From the report, it could be also understood that the transition temperature of HZO thin films between the t- and o-phases is not far from room temperature. [17] In the o-phase unit cell, the permanent dipoles formed by the displacement of four among eight oxygen ions relative to the cations are with the same directions, making it ferroelectric. [1, 17] However, in the t-phase unit cell, four among eight oxygen ions move slightly upward from their neutral position in eight tetrahedral sites within the cubic fluorite phase, whereas the others move downward with the equivalent magnitude resulting in zero net polarization in a unit cell. [1, 17] It should be noted that the magnitude of the displacements of oxygen ions in t-phase is much smaller compared to that of the o-phase. [17] Therefore, there is an important difference between the antiferroelectric structure of a perovskite-based material, such as $PbZrO_3$, and Zr-rich HZO, which is more like a (super) structure of distorted fluorite lattice. In the former case, the magnitude of permanent dipoles in the lattice is almost identical to that of the ferroelectric counterpart, such as $PbTiO_3$.

Hence, the nonpolar structure is actually due to the antiparallel arrangement of the permanent dipoles within the structure and appearance of the double hysteresis loops under the application of high field is due to the alignment of all the permanent dipoles into one direction. [12-14] However, for the latter case, the theoretical calculation showed that the magnitude of permanent dipoles in the t-phase (super) structure is much smaller than that of the o-phase ferroelectric structure, albeit the dipoles are also antiparallel making it a nonpolar phase. Therefore, under the application of high field, the appearance of the antiferroelectric-like double hysteresis loop might be due to both field-induced dipole formation and its alignment with the field direction. In this work, the t-phase is regarded as either nonpolar or antiferroelectric, but two terms are not precisely discerned.

The temperature-dependent phase transition of polar materials is one of the most extensively studied topics in solid state physics, but the most researches have been focused on the perovskite structure materials. [18-20] In many multi-cation polar materials, the transition temperature could be changed by controlling the cation composition, since the relative free energy of their polymorphs is affected by the cation ratio. [18-20] The changes in P-E curves of HZO films with varying Zr contents also showed that the relative free energy and resulting transition temperatures of HZO films could be changed by controlling Zr contents. [7, 17] The phase

transition in polar materials are generally categorized into two different types; the first order and the second order. For the case of the former, the remanent polarization (P_r) disappears abruptly at a certain temperature (Curie temperature, T_c), whereas the P_r decreases continuously with increasing temperature and finally becomes zero for the case of the latter. [21] It is generally known that the abrupt polarization disappearance during the first order phase transition originates from the involvement of the nonpolar (NP) phase. [21]

The conventional polarization switching in ferroelectric thin film systems, where the ferroelectric bound charge is well compensated by free carriers in metal electrodes, can be explained by the nucleation and growth of reverse domains. [21] However, as shown in this report, the reversible switching of the polarization near phase transition can be mediated by the involvement of NP phase during the switching process, which is in a stark contrast to the ferroelectrics far below the transition temperature. Especially, the P-E hysteresis loop of the specific HZO film with a Hf:Zr ratio of 0.4:0.6 showed an intermediate shape between the typical ferroelectric and antiferroelectric, which is called “broken hysteresis loop”, and such peculiar behaviour could be understood from the involvement of the NP phase. [21]

5.2. Experimental

HZO films were deposited on a TiN substrate, which also plays a role as the bottom electrode (BE) for electrical tests, using thermal atomic layer deposition at a substrate temperature of 280 °C using $Hf[N(C_2H_5)CH_3]_4$ (TEMA-Hf), $Zr[N(C_2H_5)CH_3]_4$ (TEMA-Zr), and ozone (200 g m^{-3} of concentration) as the Hf-precursor, Zr-precursor, and oxygen source, respectively. The growth per cycle of HfO_2 and ZrO_2 is almost identical (~0.11nm/cycle), so the composition of the HZO films can be controlled by changing the ALD cycle ratio for HfO_2 and ZrO_2. 9-nm-thick $Hf_{0.4}Zr_{0.6}O_2$ film could be deposited using an ALD cycle ratio for HfO_2:ZrO_2 of 4:6. In order to electrically characterize the HZO films, Pt(30nm)/TiN(5nm) top electrode (TE) was deposited using direct current sputtering through a shadow mask whose hole diameter is 300 m (TiN contacts with the HZO film). After the TE deposition, post-metallization-annealing was performed for 30s at 500°C in N_2 atmosphere under 100torr pressure using rapid thermal annealing for the crystallization of the films. The composition and the thickness of the HZO films were examined using X-ray fluorescence (Quant'X, Thermo SCIENTIFIC) and spectroscopic ellipsometry (ESM-300, J.A. Woolam), respectively. The crystal structure of the HZO films were examined using a grazing-angle incidence X-ray diffractometer (X'pert pro, Panalytical), and the X-ray

diffraction pattern of the $Hf_{0.4}Zr_{0.6}O_2$ film was reported in previous works. [11, 16] The P-E characteristics were measured using a ferroelectric tester (TF analyzer 2000, Aixacct systems). For the pulse switching measurements, rectangular positive or negative pulses with a pulse width of 10 μs and rising/falling time of 2ns, were supplied by a pulse generator (81110A, Agilent) with an internal resistance of 50 Ω. The switching current response from the HZO film was monitored using an oscilloscope (TDS684Dm Tektronix) with an internal resistance of 50 Ω. For all the electric characterizations, TE was biased while BE was grounded during the measurements.

5.3. Results and Discussions

5. 3. 1. Theoretical model for phase transitions

Figures 5. 1(a) and (b) show the schematic energy-polarization (U-P) and P-E curves based on the simple mathematical model for the first order phase transition of a polar material. [21] The P-E curves were derived from the U-P curves by noting that electric field is given as a differentiation of U with respect to P. It should be noted that these theoretical P-E curves could be different from the experimentally measured P-E curves since the theory did not take the kinetic barrier into account for polarization switching, which actually plays critical role in an experiment. [21] Especially, the negative slope regions in the P-E curves correspond to the negative capacitance behaviour of the material, which is of course unrealistic in general experiments. [21] Therefore, the nucleation and growth of reverse domains with opposite polarization generally occur during polarization switching of these polar materials, which is accompanied with a sudden change in the polarization state as indicated by the vertical dash lines in Fig. 5. 1(b). [21] These transitions mediated by the reverse domain nucleation and growth also involve kinetic limitations, which makes the experimental P-E curves of general slanted shapes and hysteretic behaviours as shown in Fig. 5. 1(c). In the figure, three HZO films show a typical ferroelectric, broken hysteresis loop, and antiferroelectic hysteresis behaviour for 0.5:0.5, 0.4:0.6, and

0.3:0.7 of Hf:Zr ratio, respectively. The four transition temperatures (T_0, T_c, T_1, and T_2) exist for the case of the first order phase transition, [21] and the dotted lines in Fig. 5. 1(a) correspond to the U-P curves at the four critical temperatures. T_0 is the Curie-Weiss temperature over which the NP phase starts to exist as a metastable state with respect to the stable ferroelectric phase. When the temperature is lower than T_0, only two potential wells are present in U-P curve (black curve in Fig. 5. 1(a)), and the single loop can be observed during the P-E measurement (black curve in Fig. 5. 1(b)), which is the characteristics of ferroelectric materials. At $T = T_0$, one more potential well emerges in U-P curves near P=0 (corresponding to the NP phase, red dash curve in Fig. 5. 1(a)). When the temperature is between T_0 and T_c, the minimum energy state still corresponds to the polar state, and the P-E curve appears to be similar to the single ferroelectric hysteresis curve (blue curves in Figs. 5. 1(a) and (b)) with lower coercive field (E_c). At T_c, the free energy of the ferroelectric phase and the NP phase becomes identical (red dash curve in Fig. 5. 1(a)), hence the polar phase becomes metastable for $T_c<T<T_1$ (dark green dash and lines in Figs. 5. 1(a) and (b)). Because of this characteristic feature of U-P curve, the P-E curve becomes to show a ferroelectric-like hysteresis but its detailed shape can be appropriately described as the “broken hysteresis loop”. [21] In this temperature region, the NP phase corresponds to the global minimum, whereas the two polar

states correspond to the local minimum. There are energy barriers between the local minima of the polar phase and the NP phase, which makes part of the polar material to be retained even when the external field disappears, once the material is fully (pre-) polarized into one direction with sufficiently high external field. Therefore, the broken hysteresis state contains certain non-negligible P_r and E_c, whereas, the genuine antiferroelectric material becomes to be composed of equal portions of anti-parallel polarized lattices when E = 0, and, thus, the P_r = 0 and E_c = 0, which is the case of $T > T_1$. This type of broken hysteresis loop was experimentally observed from the $Hf_{0.4}Zr_{0.6}O_2$ thin film at room temperature as shown in Fig. 5. 1(c). With further increase in temperature, T_1 is reached, which is the limiting temperature of polar phase at which the barrier between the polar phase and the NP phase disappears, and the polar phase loses metastability at zero electric field (dark blue dash curve in Fig. 5. 1(a)). Under this circumstance, the polar phase can exist only under a certain magnitude of external electric field, so the double hysteresis with field-induced phase transition can be observed within this temperature range (magenta dash and magenta line curves in Figs. 5. 1(a) and (b)). When T increases to T_2, the polar phase cannot be induced even under an external electric field (green curve in Fig. 5. 1(a)). Thus, only paraelectric properties can be observed above T_2 (green curve in Fig. 5. 1(b)).

Figure 5. 1(c) shows the experimental P-E curves of the HZO films with various Hf:Zr ratios which are reproduced from the previous reports. [5, 11, 16, 22, 23] With the Hf:Zr ratios of 0.5:0.5 and 0.3:0.7, the characteristic single and double loops, which refer to ferroelectric and field-induced ferroelectric (or antiferroelectric) properties, can be observed. While the graphs in Figs. 5. 1(a) and (b) represent the transition between different states with varying temperature for a given polar material, the data in Fig. 5. 1(c) reveals that similar transition can be induced by varying the Hf:Zr ratio at room temperature. The different shapes of hysteresis curves imply that the $Hf_{0.5}Zr_{0.5}O_2$ thin films match well with the $T<T_c$ case whereas the $Hf_{0.3}Zr_{0.7}O_2$ thin films match with the $T_1<T<T_2$ case. It is uncertain, however, whether the $Hf_{0.5}Zr_{0.5}O_2$ film actually corresponds to $T<T_0$ or $T_0<T<T_c$ case, since ferroelectric single P-E hysteresis can be observed for both cases. As expected from the previous theoretical work, [17] the transition temperatures are believed to decrease with increasing Zr contents. For the case of the $Hf_{0.4}Zr_{0.6}O_2$ films, the broken hysteresis could be observed, which might be induced by the involvement of the intermediate NP phase, and the most probable crystallographic phase for the NP phase is a t-phase. Based on its P-E characteristics, the $Hf_{0.4}Zr_{0.6}O_2$ thin film corresponds to the $T_c<T<T_1$ case. From the observed double and broken hysteresis loops, the phase transition in HZO thin films is believed to be the first-order. However,

the abrupt disappearance of polarization with increasing temperature might be hardly observed due to the polycrystalline nature and surface-energy-dependent polymorphism in HZO films, which induce distributions in physical parameters, such as E_c. Hence, the first-order-like rather than the first order would be a better description in this case. [17]

Although the shape of the P-E hysteresis of $Hf_{0.4}Zr_{0.6}O_2$ film and its composition dependent variations seem to be qualitatively matched with the classical first order phase transition theory, the broken hysteresis can result from other origin such as the mixture of two ferroelectrics with two different E_c values. If there are two kinds of ferroelectrics with different E_c values, the single hysteresis with smaller P_r will be observed with the external field between two E_c values. With further increasing electric field above higher E_c value, the broken hysteresis will be observed. Therefore, the P-E characteristics with various electric field were measured, and the results are included in figure 5. 2(a). As seen in figure 5. 2(a), the single hysteresis under relatively low electric field could not be observed under the low field. The temperature dependent P-E hysteresis was also measured, and the results are shown in figure 5. 2(b). Since the E_c of ferroelectrics generally does not increase with increasing temperature, the E_c values in P-E curves might not increase with increasing temperature. For the case of the broken hysteresis, on the other hand, the transition

electric field for tetragonal-to-orthorhombic phase would increase with increasing temperature according to the classical first order phase transition theory since the energy difference between the tetragonal and orthorhombic phase would increase with increasing temperature. As seen in figure 5. 2(b), the electric field required for phase transition increases with increasing temperature, which also validates the argument based on the first order phase transition theory. Furthermore, the temperature dependent variations in $2P_r$ values can be seen in figure 5. 2(c). The decrease in $2P_r$ values with increasing temperature could be clearly observed, meaning that the temperature further increases to T_1 within this temperature range. Based on the above mentioned evidences, it is believed that the possibility of the mixture of ferroelectrics with two different coercive fields can be disregarded.

As previously mentioned, the polarization switching in a typical ferroelectric film can be represented by the nucleation and growth of reverse domains upon the bias application of which direction is opposite to the previous poling bias. This is because there are only two stable polarization states with opposite polarity. However, in case of the antiferroelectric or broken hysteresis loops, there is one more (meta) stable state of NP phase, which may mediate the polarization switching. From the P-E curve of the $Hf_{0.4}Zr_{0.6}O_2$ film (dark green curve) in Fig. 5. 1(c), the two step polarization switching of (1) ferroelectric with $-P_r$ (UP)

which was initially poled with a negative bias (bottom panel of Fig. 1d) to mostly NP phase (second top panel) and (2) mostly NP phase with a small opposite bias (second top panel) to ferroelectric with $+P_r$ (DOWN) state (top panel) can be observed. It should be noted that the first step starts with the decrease of negative bias so UP and NP phase are mixed at zero electric field (second bottom panel). During such transition, it could be noted that a certain portion of initial polarization ($-P_r$) could be retained even at E = 0 due to the presence of energy barrier between the $-P_r$ state and NP state, although the stable phase is the NP state. Therefore, the P = 0 state must be acquired at a slightly positive field, explaining the presence of non-zero E_c in this case. It should be noted that this material with two-step polarization switching of broken hysteresis totally differs from the field-induced phase transition in antiferroelectrics. For antiferroelectric materials, they should stay in nonpolar phase with no external field, so their P_r value should be always zero even with prepoling pulses. These considerations can explain quite well the emergence of broken hysteresis loop qualitatively. Nevertheless, the time constant of the P-E measurement is quite long (order of μsec), meaning that it can hardly examine the kinetics of dynamic polarization switching. To the authors' knowledge, the dynamic polarization switching of polar material films with broken hysteresis loop have rarely been reported, although the two step polarization switching with the involvement of intermediate NP

state could be intriguing. This might be due to the fact that the broken hysteresis loop can be observed only in a highly limited temperature range near T_c of the first order transition materials. [24] Merz reported the changes in the P-E curves of single crystalline $BaTiO_3$ near phase transition, and reported the broken hysteresis at 108.2°C. [24] However, the shape of the P-E curves changed into antiferroelectric double hysteresis at 109.1 °C, meaning that the temperature ranges for broken hysteresis is narrower than ~1 °C. Therefore, the switching kinetics of the $Hf_{0.4}Zr_{0.6}O_2$ film were further examined using a pulse-switching (PS) measurement technique, which has been applied to other conventional ferroelectric materials. [25-28] The PS technique is useful to achieve not only the understanding on the dynamic evolution behaviour of the polar phase but also the insights on the interposed passive components, such as interfacial capacitance (C_i), which is generally interpreted as the presence of non-ferroelectric phase in any arbitrary ferroelectric/electrode system. In this study, the estimation of C_i with PS time provides critical information on the evolution of the NP phase from one polarization state and its evolution to the opposite polarization state as shown in the next section.

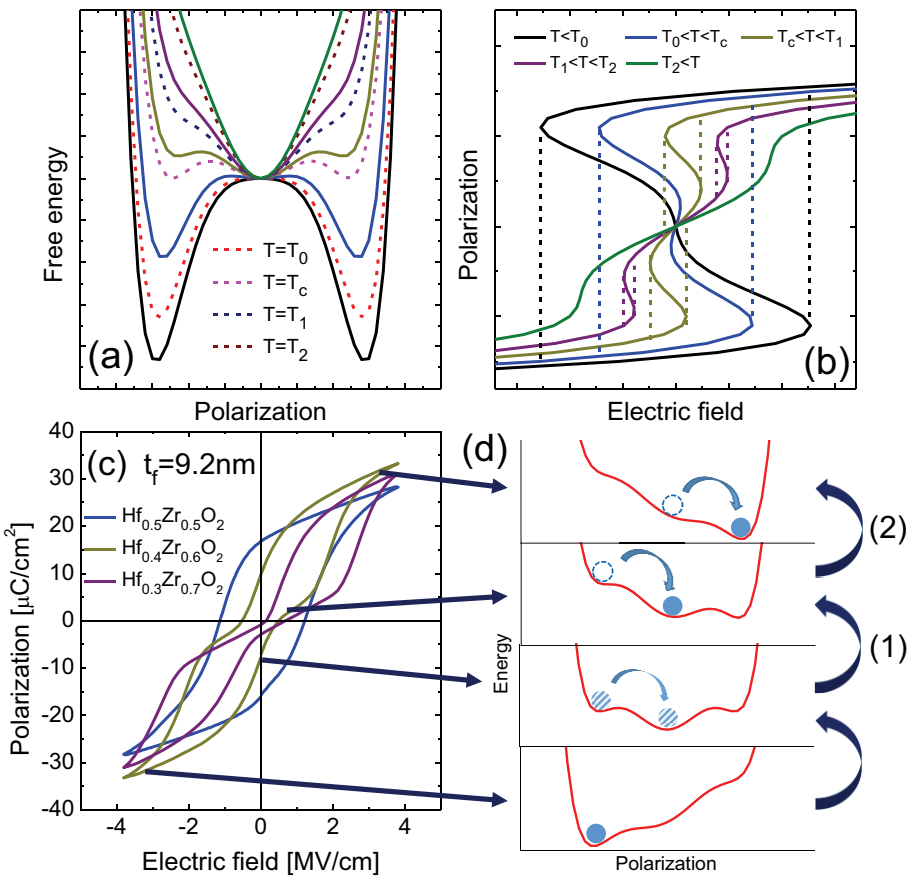

Figure 5. 1. The schematic (a) free energy-polarization and (b) polarization-electric field curves of first order phase transition at various temperatures. (c) The polarization-electric field hysteresis curves of $Hf_{1-x}Zr_xO_2$ films with various Zr contents (x=0.5, 0.6, 0.7). (d) The schematic diagram for two step polarization switching with the involvement of intermediate nonpolar phase. (t_f: film thickness)

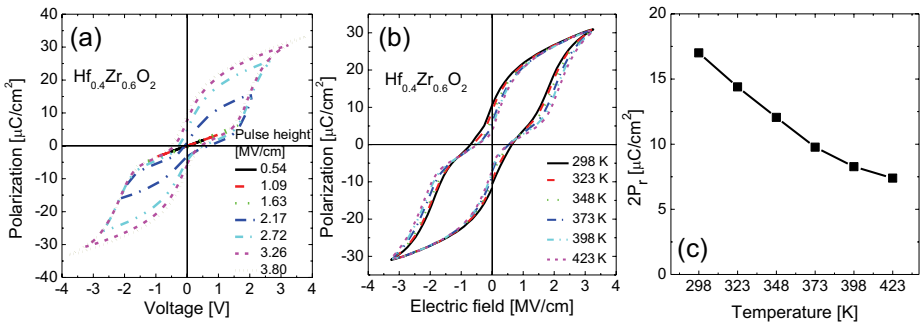

Figure 5. 2. (a) Polarization-electric field curves of $Hf_{0.4}Zr_{0.6}O_2$ films with various pulse height (0.54 to 3.80 MV/cm), (b) Polarization-electric field curves of $Hf_{0.4}Zr_{0.6}O_2$ films at various temperature, and (c) the variations in double remanent polarization ($2P_r$) with changing temperatures.

5. 3. 2. Pulse switching measurement for dynamic evolution of polar and non-polar phases

For the pulse measurement, the pulse generator and the digital oscilloscope were serially connected with the $Hf_{0.4}Zr_{0.6}O_2$ capacitor. The pulse generator generates rectangular electric pulses for pre-poling and switching of the $Hf_{0.4}Zr_{0.6}O_2$ capacitors, while the switching current responses were monitored by a digital oscilloscope. Before the switching pulse was applied, the $Hf_{0.4}Zr_{0.6}O_2$ capacitors were pre-poled either upward or downward using the rectangular electric pulse with the -3.8 or 3.8 MV/cm height and the 10 μs width. After the pre-poling, the switching pulses with the 10 μs width and various field strength (3.3 – 3.9 MV/cm) of opposite polarity were applied to the $Hf_{0.4}Zr_{0.6}O_2$ capacitor. Figures 5. 3(a) and (b) show the switching current responses for UP→DOWN and DOWN→UP polarization switching. As seen in Figs. 5. 3(a) and (b), the two (slanted) plateau regions, which were the characteristic sign of ferroelectric switching current, could be observed. [25-28] For the case of UP→DOWN polarization switching, the first and the second plateau regions might be relevant to the UP→NP switching and NP→DOWN switching, respectively, which is not the case of general ferroelectric capacitors. For general ferroelectric capacitors, a single plateau switching current region is generally observed, which could be attributed to the reverse domain nucleation and growth. [26] In case of polar materials

containing the NP phase, such as $Hf_{0.4}Zr_{0.6}O_2$ film, the nucleation and growth (both in vertical and lateral directions) of the NP phase within the pre-poled ferroelectric phase is energetically more favourable compared with the nucleation and growth of domains with anti-parallel polarization considering the electrostatic boundary conditions at the polar phase/NP phase and polar phase/anti-parallel polar phase interface.

The switching current responses (I_{SW}) during the polarization switching can be fitted using the following equation (5. 1). [25]

$$\boldsymbol{I_{SW}} = \frac{\boldsymbol{V_a - V_c}}{\boldsymbol{R_L}} \exp\left(\frac{\boldsymbol{t - t_0}}{\boldsymbol{R_L C_i}}\right) \quad (5.\ 1)$$

, where V_a, V_c, R_L, C_i, t, and t_0 are applied voltage, coercive voltage, total load resistance, interfacial capacitance, time, and the time when polarization switching starts, respectively. [25] The $(V_a\text{-}V_c)/R_L$ value refers to the initial switching current (I_{sw}^0) which is the switching current value when the polarization switching of ferroelectric films starts. The detailed description of the pulse measurement system can be found in previous works. [25-28] The R_L is the summation of all resistors in the measurement circuit, including the resistance of a pulse generator (R_{PG}), the resistance of an oscilloscope (R_{OSC}), parasitic resistance (R_P), and contact resistance (R_C). [25-28] From the pulse measurement with short circuited configuration and no capacitor sample connected, the sum of

R_{PG}, R_{OSC}, and R_P was estimated to be 104 Ω. [29] C_i is the summation of interfacial capacitance and parasitic capacitance of the measurement circuit, but the parasitic capacitance could be ignored based on the previous work, where the parasitic capacitance was revealed to be smaller than C_i by one order of magnitude. [29]

Figures 5. 3(c) and (d) show the change of I_{SW}^0 as a function of pulse height for the two plateau regions, region I (~0.0-0.5 μs) and region II (~0.7-3.0 μs) for UP→DOWN and DOWN→UP polarization switching, respectively. Here, the t_0 was taken from crossing point between the upward arrows and experimental data in Figs. 5. 3(a) and (b), which was the point where the experimental data deviated from the best-linear-fitted graphs (dotted lines) based on the equation (5. 1). From the slope and x-intercept of the best-linear-fitted graphs, the R_L and E_c values (V_c/film thickness) could be estimated. For the case of UP→DOWN polarization switching, the (R_L, E_c) values of region I and region II were (157 Ω, 0.52 MV/cm) and (173 Ω, 2.11 MV/cm), respectively. The estimated E_c value from region II was slightly smaller than that (2.52 MV/cm) from the static P-E measurement in Fig. 5. 1(c). It should be noted that the E_c values in P-E loops were estimated from the field value at which the largest slope in the P-E loop could be observed, not from the cross point of the P-E curve with the field axis (x-axis). In general, the E_c value estimated through pulse measurement refers to the intrinsic E_c when the switching

frequency is infinitely low, whereas the E_c value from the P-E hysteresis encompasses the contribution from the voltage drop across the parasitic components. [30] Although there were finite differences from the values estimated from UP→DOWN and DOWN→UP polarization switching, the difference was generally small, suggesting that the polarization switching is symmetrical with respect to the bias polarity. This is consistent with the symmetrical configuration of a capacitor structure, TiN/HZO/TiN. The C_i values were also calculated from the slopes of the best-linear-fitted lines and known R_L values for regions I and II. The estimated C_i values for region I and II were 11.1 and 24.7 $\mu F/cm^2$, respectively, for the case of UP→DOWN polarization. The similar C_i values (11.1 and 25.3 $\mu F/cm^2$ for region I and II, respectively) were also calculated for DOWN→UP polarization switching. The C_i value from region II was ~2.2 times larger than that from region I, whereas the difference in R_L values was less than 10%. Generally, the C_i value is strongly related with the non-switching region of ferroelectric films, such as interfacial dead layers. Therefore, the largely different C_i values in regions I and II indicate that there is an intricate factor, which could be different for the two switching regions. This could be interpreted with two switching regions represent spatially different regions across the capacitor area of which polar nature of the bulk as well as interfacial properties is different. However, it is rather unusual to assume that there

are two distinctive regions with such distinctive polar natures despite the presence of highly uniform film microstructure grown by an atomic layer deposition method. Therefore, the two-step ferroelectric switching is hypothesized to be mediated by the intermediate NP phase as shown in Fig. 5. 4.

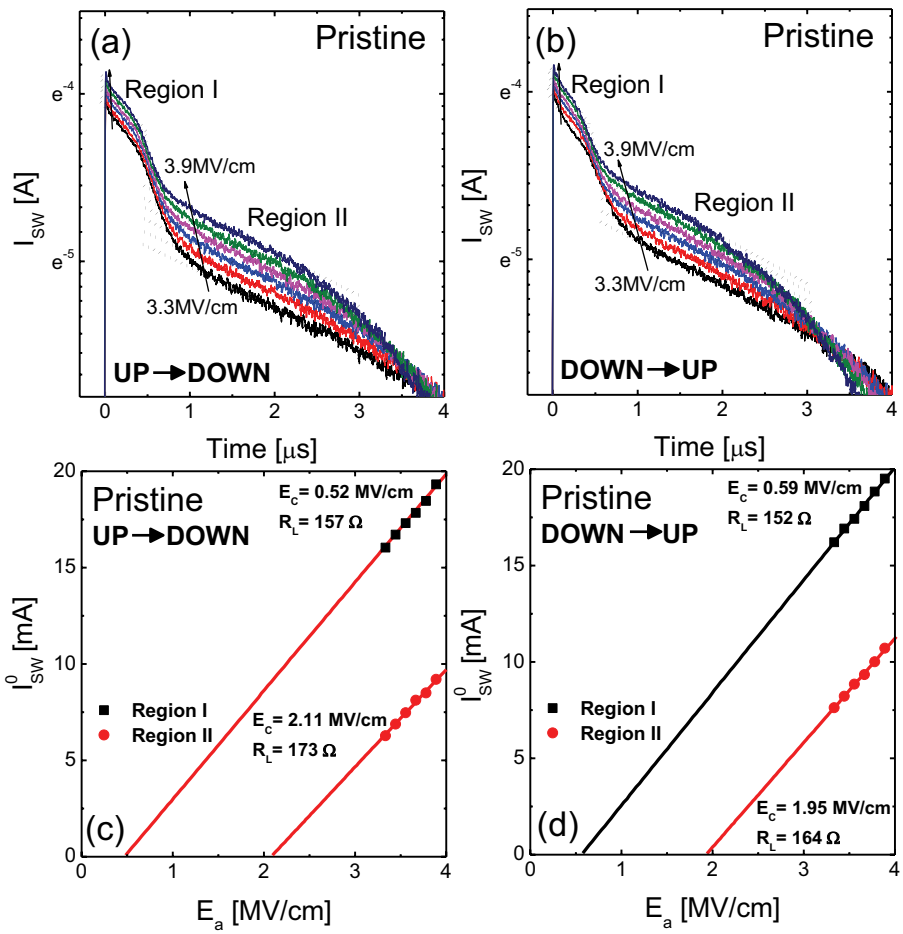

Figure 5. 3. The switching current response-time curves of $Hf_{0.4}Zr_{0.6}O_2$ films under (a) positive and (b) negative switching electric pulse with various field strengths (3.3-3.8 MV/cm). The changes in initial switching current with varying pulse field strengths and their linear fitting under (a) positive and (b) negative switching electric pulse. (I_{SW}: switching current, I_{SW}^0: initial switching current, E_c: coercive field, R_L: total resistance, and E_a: applied electric field)

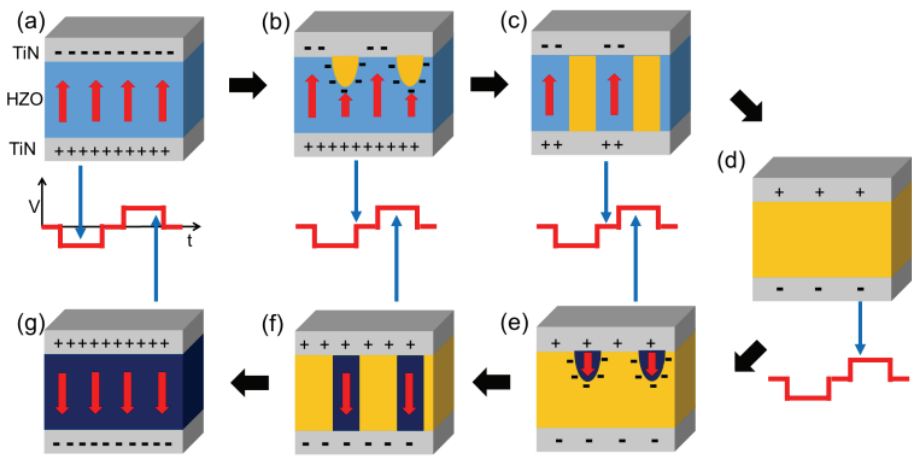

Figure 5. 4. The schematic diagram for the two step polarization switching of $Hf_{0.4}Zr_{0.6}O_2$ films. (a) Upward pre-polarized state, (b) nucleation and (c) growth of nonpolar tetragonal phase upon the removal of pre-poling field, (d) nonpolar state, (e) nucleation and (f) growth of downward polarized sate, and (g) downward switched state upon the application of switching field.

Figure 5. 4 shows the schematic diagram for the two-step polarization switching (UP→DOWN) with the involvement of the intermediate NP phase. Under the high negative field, the polarization in $Hf_{0.4}Zr_{0.6}O_2$ film might be uniformly upward (pre-poling, Fig. 5. 4(a)). This state corresponds to initially negatively poled state in Fig. 5. 1(c) or Fig. 5. 3(a). With decreasing negative electric field in P-E or at the termination of the negative pre-poling pulse in a PS measurement, the nucleation (Fig. 5. 4(b)) and growth (Fig. 5. 4(c)) of the NP, which could be the t-phase, have occurred. Under the condition of E = 0, the polar state of the sample would be correspondent to Fig. 5. 4(c) and a certain part of UP polarization is retained, because there is finite energy barrier between the polar state and the NP state although the NP state is energetically stable. During the nucleation process, the electrons are assumed to be injected from the TE to boundary region between the NP and UP polarization (Fig. 5. 4(b)) to minimize the electrostatic energy at the NP/polar phase interface, and the vertical growth of nuclei would occur extremely fast due to the relatively large boundary energy. [26] When the NP domains reach the opposite electrode (BE), the carried negative charges are neutralized by the positive charges at the BE. As a result, when the external bias is terminated, the $Hf_{0.4}Zr_{0.6}O_2$ film contains mixed UP and NP regions as shown in Fig. 5. 4(c). Now, when the opposite bias is applied either in P-E sweep or PS measurement, the domain wall motion would occur and

the material would possess entirely NP phase as shown in Fig. 5. 4(d). This step, i. e. Figs. 5. 4(c)-(d), may correspond to the change occurring in region I in Fig. 5. 3(a). Jiang et al. showed that during the polarization switching, the ferroelectric domains could be regarded as a resistor because a constant voltage (V_c) is applied across the layer irrespective of V_a, and the finite slope in the I_{sw} – t curve in their plateau region is due to the involvement of C_i. In other words, the switching current transient can be interpreted as the charging behaviour of C-R series connection. [25] Therefore, the estimated C_i refers to the portion of UP region in Fig. 5. 4(c) because that region is responsible for the first switching transient. When this first switching transient is completed, the actual switching to the opposite polarization will start from the NP phase to DOWN ferroelectric phase via similar nucleation and growth processes of DOWN domains within the NP phase as shown in Figs. 5. 4(e) - (g). It can be easily understood that, in this case, the entire volume of the material, which was now NP, switches to DOWN ferroelectric phase, so the involved C_i represents the entire surface area of the capacitor. This is related with the region II in Fig. 5. 3(a). This finding indicates that the C_i values estimated from regions I and II can be quantitatively compared with the change in polarization values related with the changes associated with Figs. 5. 4(c) - (d) and Figs. 5. 4(d) – (g). It can be noted that the polarization change associated with Figs. 5. 4(c) – (d) is annihilation of

remaining UP polarization, which must be identical to the negative P_r in Fig. 5. 1(c) (~10μC/cm^2). On the other hand, the polarization change associated with Figs. 5. 4(d) – (g) corresponds to the positive saturation polarization, which is ~30 μC/cm^2 in Fig. 5. 1(c). However, this value contains contribution from the dipolar displacement of the dielectric portion of the thin film, which seems to be ~5 μC/cm^2 from the comparison with the P-E curve from $Hf_{0.5}Zr_{0.5}O_2$. Therefore, the polarization charges involved in regions I and II are ~10 and ~25 μC/cm^2. It is interesting to note that the ratio between these two values, 2.5, is quite similar to the ratio of the estimated C_i values, 2.2. This clearly indicates that the material is uniform across the entire electrode area, and involved interfacial layers are also uniform, in terms of its thickness and dielectric constant. The authors have reported that the interfacial layer is most probably composed of the t-phase with an approximate thickness of ~1nm. [29] Similar analysis applied to the DOWN→UP switching tests also produced an identical conclusion. These findings also imply that the hypothesis on the involvement of intermediate NP phase during the polarization switching in this film is reasonable.

Next, the wake-up effect of $Hf_{0.4}Zr_{0.6}O_2$ film was examined. In HZO and doped HfO_2 ferroelectric thin films, the increase in P_r and E_c values is observed with increasing number of electric field cycling. [31-33] This phenomenon is called the wake-up effect and several mechanisms have

been suggested as the origin behind it. Zhou et al. suggested that the wake-up effect originates from the depinning of domains due to the reduction of the defect concentration near TiN electrode. [31] Martin et al. suggested that the wake-up effect comes from the phase transition from m- to o-phase based on transmission electron microscope study. [32] Lomenzo et al. suggested the t-to-o phase transition as the origin of the wake-up effect based on the concurrent increase in P_r and decrease in dielectric constant. [33] The authors also examined the wake-up effect in thin $Hf_{0.5}Zr_{0.5}O_2$ films (thinner than 8nm), and reported that the wake-up effect results from the t-to-o phase transition within such ultrathin films. [34] In addition, the change in C_i of $Hf_{0.5}Zr_{0.5}O_2$ thin films was also examined using a PS measurement, and it was found that the C_i increased with increasing field cycling number which could be ascribed to the t-to-o phase transition of the interfacial layer. [29] Even though several studies focused on the wake-up effect of ferroelectric $Hf_{0.5}Zr_{0.5}O_2$ and doped HfO_2 films, the evolution of broken hysteresis loop and two-step switching current response from pulse switching measurement has not been examined.

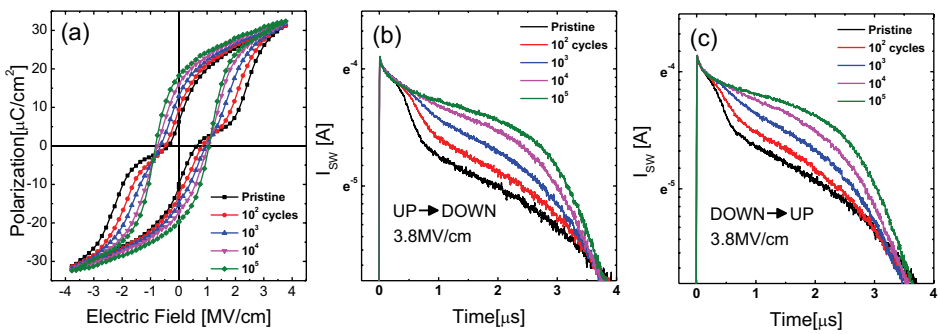

Figure 5. 5. (a) Double remanent polarization - electric field curves measured after various number of pulse application for wake-up. The switching current response (I_{SW}) – time curves of (b) UP→DOWN and (c) DOWN→UP switching. The magnitude of electric pulse strength was fixed at 3.8 MV/cm.

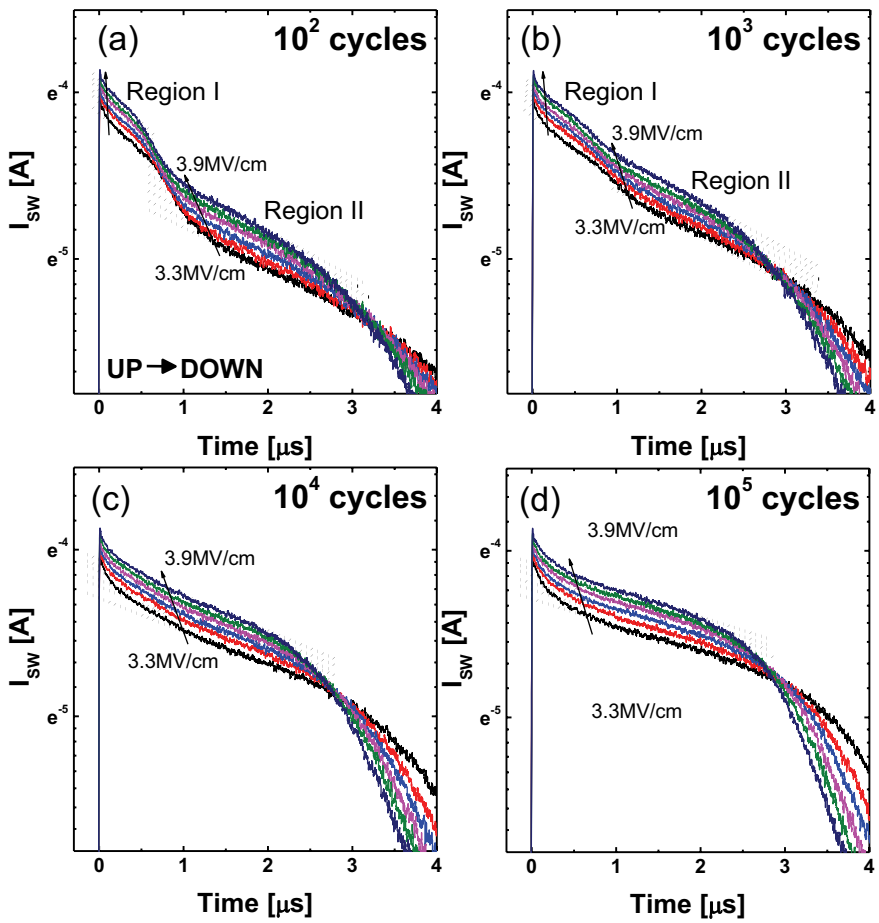

Figure 5. 6. The switching current response (I_{SW}) – time curves measured with positive electric pulse (UP → DOWN) strength of 3.3-3.8 MV/cm after electric field cycling of (a) 10^2, (b) 10^3, (c) 10^4, and (d) 10^5 times.

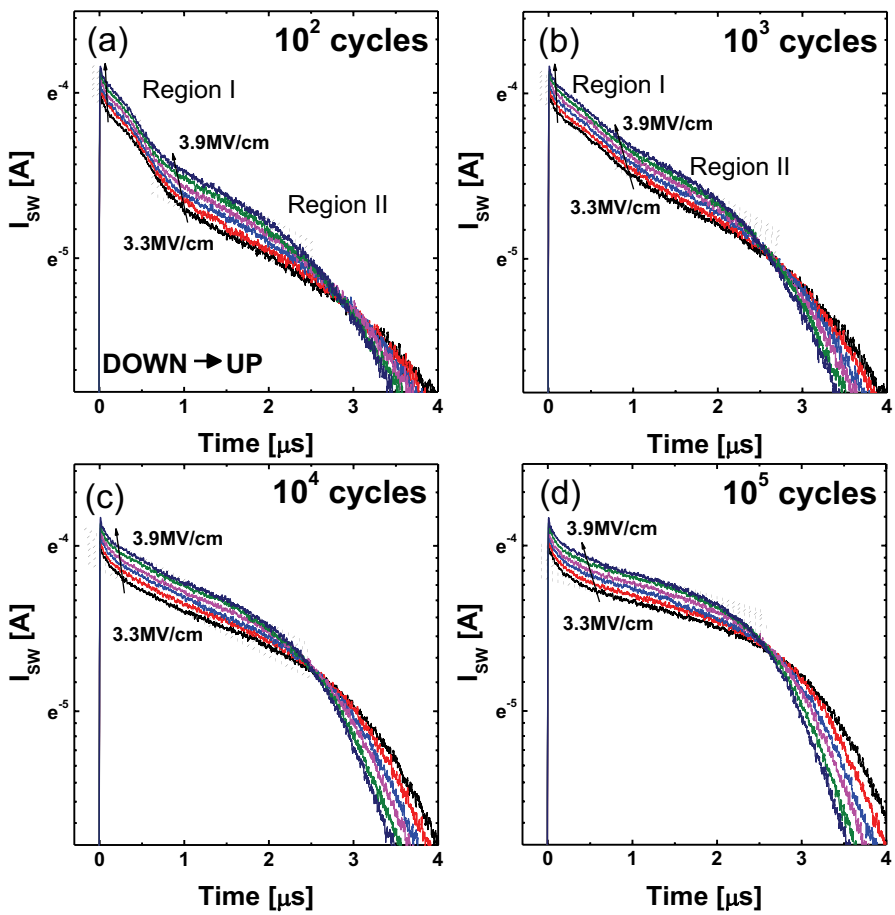

Figure 5. 7. The switching current response (I_{SW}) – time curves measured with negative electric pulse (DOWN → UP) strength of 3.3-3.8 MV/cm after electric field cycling of (a) 10^2, (b) 10^3, (c) 10^4, and (d) 10^5 times.

For the PS measurement, the positive and negative square electric pulses of 3.8 MV/cm height and 10 μs width were applied, prior to the P-E or pulse measurement. Figures 5. 5(a) – (c) show the P-E curves and switching current responses for UP→DOWN and DOWN→UP switching, respectively, of the $Hf_{0.4}Zr_{0.6}O_2$ film in a pristine state and after 10^2, 10^3, 10^4, and 10^5 times of electrical pulses. As seen in Fig. 5. 5(a), the intermediate hump region became narrower with increasing number of field cycling, which almost disappeared after 10^3 times of electric field cycling. After 10^3 times of field cycling, the ferroelectric single loop could be observed. The similar tendency could be observed in I_{sw}-t curves for UP→DOWN and DOWN→UP switching in Figs. 5. 5(b) and (c). The electric pulse height of the PS measurement was fixed at 3.8 MV/cm. After 10^3 times of electric field cycling, the two-step polarization switching could not be observed both of UP→DOWN and DOWN-UP switching, and the time transient feature became to be of a single plateau region, which is a typical characteristic of ferroelectric thin films. This means that the mostly antiferroelectric structure of the $Hf_{0.4}Zr_{0.6}O_2$ film changes to ferroelectric one upon the repeated electric cycling with such high field. This also means that the involvement of the NP t-phase during the polarization reversal becomes negligible with increasing field cycling. If free energy of the ferroelectric phase is much larger than the NP t-phase, such transition would hardly be happened. It has been theoretically

elucidated that the free energy difference between the ferroelectric o- and NP t-phase is quite small (<5 J/cm^3), so it might be possible to transform the material from the NP to a polar phase if there is redistribution of defects. [17] Since the electric field strength for this wake-up experiment is relatively high (a few MV/cm level), the charged defects might redistribute during the polarization switching. [35] It should be noted that the magnitude of the electric field used in this experiment is similar with the HfO_2-based resistive random access memories based on the field-induced migration of oxygen vacancies. [36]

From the switching current responses measured at various pulse height of 3.3-3.9 MV/cm, the variations in C_i, R_c, and E_c values as a function of switching cycle number were also calculated. I_{sw} – t data for these tests are included in Figs. 5. 6 and 5. 7 for samples after cycling for 10^2, 10^3, 10^4, and 10^5 times for UP→DOWN and DOWN→UP switching, respectively. The estimated C_i, R_c, and E_c values are summarized in Figs. 5. 8(a) and (b) for UP→DOWN and DOWN→UP switching. Up to the electric field cycling number of 10^3, the switching current transient showed a two-step behaviour, which is consistent with the data in Fig. 5. 3, and the C_i and R_c values did not vary significantly. Here, these values were extracted from the first plateau region of the switching responses up to 10^3 cycling number, while the values after that cycle number were extracted from the single plateau region. When the cycling number

became higher than 10^3, C_i and E_c values significantly increased. On the other hand, the magnitude of E_c from DOWN→UP switching was larger than that from UP→DOWN switching after 10^5 times of electric field cycling by 0.4 MV/cm. This might be due to the presence of the internal field in $Hf_{0.4}Zr_{0.6}O_2$ capacitor and the similar tendency could be observed in the P-E curves in Fig. 5. 5(a). Such significant increases in C_i and E_c after field cycling were also observed in ferroelectric $Hf_{0.5}Zr_{0.5}O_2$ films, but in that case the C_i and E_c values increased continuously with the cycle numbers, while its P_r value increased abruptly only after 10^2 cycles. In ferroelectric $Hf_{0.5}Zr_{0.5}O_2$ film, it was elucidated that the increase in C_i and E_c could be ascribed to the decrease in the non-ferroelectric interfacial layer thickness, i. e. the interfacial t-phase is transformed to o-phase by the electrical cycling. [29, 33] It should be noted that the C_i values before and after the wake-up occurs between $Hf_{0.5}Zr_{0.5}O_2$ (~20–25 μF/cm^2 for pristine and ~60 μF/cm^2 after wake-up) and $Hf_{0.4}Zr_{0.6}O_2$ (~11 μF/cm^2 for pristine and ~46 μF/cm^2 after wake-up) films have finite differences. Especially for the case of the pristine sample, the C_i value of $Hf_{0.4}Zr_{0.6}O_2$ film was smaller than the half of C_i value of the $Hf_{0.5}Zr_{0.5}O_2$ film. This difference could be understood based on the difference in the area of switching region. As previously mentioned, before positive switching pulse is applied, the $Hf_{0.4}Zr_{0.6}O_2$ film contains mixed UP and NP states, whereas the $Hf_{0.5}Zr_{0.5}O_2$ film is mostly UP polarized. As a result, only 40-

50% of the total area of the $Hf_{0.4}Zr_{0.6}O_2$ film might switch from UP to NP state, whereas whole area of the $Hf_{0.5}Zr_{0.5}O_2$ might switch from UP to DOWN state. By assuming that the qualities of electrode/ $Hf_{0.5}Zr_{0.5}O_2$ and electrode/ $Hf_{0.4}Zr_{0.6}O_2$ interfaces are almost equivalent, the differences between C_i values in pristine $Hf_{0.4}Zr_{0.6}O_2$ and $Hf_{0.5}Zr_{0.5}O_2$ films could be reasonably understood from the difference in the area that actually contribute to switching. The increase in C_i value of $Hf_{0.4}Zr_{0.6}O_2$ film during the electric field cycling might be also partly explained by the change in switching area. However, the ~2 times increase in switching area, as discussed in Figs. 5. 3 and 5. 4, itself cannot explain the >~4 times increase in C_i value by the wake-up. Therefore, it is believed that the t-to-o phase transition observed in $Hf_{0.5}Zr_{0.5}O_2$ also occurred in $Hf_{0.4}Zr_{0.6}O_2$ films, which might be induced by the decreasing portion of non-switching interfacial layer. [29]

The disappearance of the two-step switching behaviour in the $Hf_{0.4}Zr_{0.6}O_2$ film after 10^3 switching cycle suggests that the polarization switching in this film does not involve the NP phase anymore; it became ferroelectric-like involving the nucleation and growth of domains with reversed polarization. This could be understood based on the t-to-o phase transition mechanism for the wake-up effect. In ferroelectric films, a smaller P_r, than the saturation polarization, P_s, is generally achieved by the depolarization field effect when applied field is removed. Such depolarization effect

arises mostly from the interfacial dead layer, which prohibits the complete screening of ferroelectric bound charges by compensation charges in metal electrodes, and charged point defects, such as oxygen vacancies, which pin the local ferroelectric polarization into a certain direction. There are other contributions to this decrease in P_r such as mechanical strain or dielectric displacement components. Upon the removal of the external field, the depolarization effect can induce two possible configurations of domains with polarization other than the (pre-polarized) matrix phase; reverse domain as in typical ferroelectrics and NP phase domain as in this $Hf_{0.4}Zr_{0.6}O_2$ film before the wake-up. Compared to ferroelectric $Hf_{0.5}Zr_{0.5}O_2$, the relative energy of the t-phase compared to that of the o-phase is relatively lower in $Hf_{0.4}Zr_{0.6}O_2$, so it is more probable to induce the NP t-phase when the field is removed as shown in Figs. 5. 4(b) and (c). T_c of $Hf_{0.4}Zr_{0.6}O_2$ film might be lower than room temperature, so the free energy of the t-phase must be lower than the o-phase. It should be noted that T_c is the temperature at which the free energy of the ferroelectric and the NP phase become identical. As a result, there might be no driving force for the reverse domain nucleation with o-phase structure in the $Hf_{0.4}Zr_{0.6}O_2$ film. For the case of the $Hf_{0.5}Zr_{0.5}O_2$ film, on the other hand, the free energy of o-phase must be lower than that of the t-phase, since its T_c is higher than room temperature. After electric field cycling more than 10^3 times, however, it can be understood that most

of the interfacial layer disappears, as can be understood from the significantly increased C_i value, and many of the point defects can be healed out by the thermal energy assisted (Joule heating by the leakage current) field migration. This means that the driving force for the NP domain formation is greatly reduced when the external field is removed. Upon the application of reversed bias, domains with reversed polarization would be directly nucleated and grown as in the case of ferroelectric film. It might be argued that the NP phase can still be nucleated and grown upon the reverse bias application, but the small energy difference between the NP t-phase and polar o-phase can be easily overcompensated by the electrostatic energy under the reverse bias application, and the direct transition to the opposite polarization could be induced. Before the wake-up cycling, some parts of the (pre-) polarized region need to be depolarized by the depolarization effect, which might not be sufficiently high to overcompensate the t- and o-phase energy difference, and NP phase is already formed when the pre-poling field is removed.

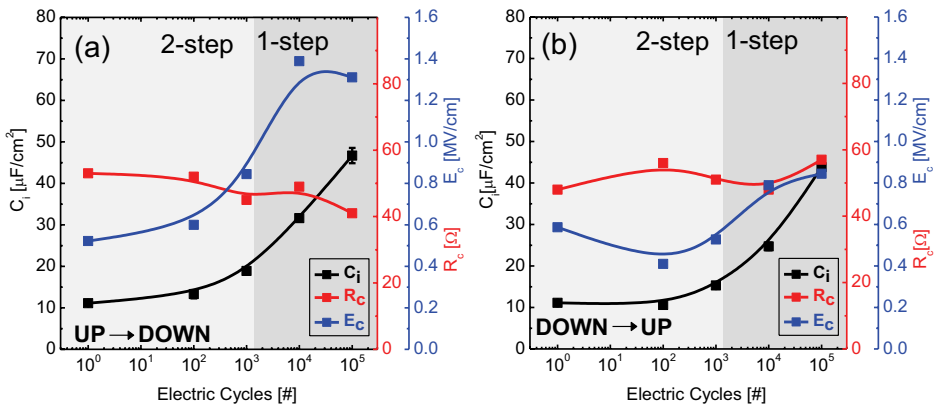

Figure 5. 8. The changes in interfacial capacitance (C_i), contact resistance (R_c), and coercive electric field (E_c) estimated from the switching current responses as a function of electric field cycling numbers for (a) DOWN → UP and (b) UP → DOWN switching, respectively.

5.4. Conclusion

In conclusion, the broken hysteresis loop in P-E test and two-step polarization switching in pulse switching measurement from $Hf_{0.4}Zr_{0.6}O_2$ films were systematically examined based on the first-order-like phase transition theory. The broken hysteresis $Hf_{0.4}Zr_{0.6}O_2$ film could be understood based on the classical theory on the first order phase transition, where the NP phase is involved during the transition from one polarization state to the opposite polarization state. The expected two-step (UP→NP (region I) and NP→DOWN (region II)) polarization switching could be also confirmed by dynamic pulse switching measurement. The relatively smaller C_i values extracted from the region I compared to that from the region II could be understood as the area ratio between retained UP polarization portion at zero bias and complete capacitor area. The broken hysteresis loop and two plateau region in switching current response-time curves changed to a single hysteresis and a single plateau region, respectively, after the electric field cycling of 10^3 times. The C_i and E_c values were almost invariant before electric field cycling of 10^3 times, whereas they significantly increased after the electric field cycling of 10^3 times. The increase in C_i and E_c values could be understood from the t-to-o phase transition as in the case of the $Hf_{0.5}Zr_{0.5}O_2$ film in addition to the increase in the area of thin film portion to the switching. Their

retardation up to switching cycles of 10^3 could be attributed to the relatively low free energy of t-phase compared to o-phase in $Hf_{0.4}Zr_{0.6}O_2$ film.

5.5. References

[1] T. S. Böscke, J. Müller, D. Bräuhaus, U. Schröder, U. Böttger, *Appl. Phys. Lett.*, **99**, 102903 (2011).

[2] J. Müller, T. S. Böscke, D. Bräuhaus, U. Schröder, U. Böttger, J. Sundqvist, P. Kücher, T. Mikolajick, L. Frey, *Appl. Phys. Lett.*, **99**, 112901 (2011).

[3] M. H. Park, Y. H. Lee, Kim, H. J. Kim, Y. J. Kim, T. Moon, K. D. Kim, J. Müller, A. Kersch, U. Schröder, T. Mikolajick, C. S. Hwang, *Adv. Mater.*, **27**, 1811–1831 (2015).

[4] X. Sang, E. D. Grimley, T. Schenk, U. Schröder, J. M. LeBeau, *Appl. Phys. Lett.*, **106**, 162905 (2015).

[5] M. H. Park, H. J. Kim, Y. J. Kim, T. Moon, C. S. Hwang, *Appl. Phys. Lett.*, **104**, 072901 (2014).

[6] T. Shimizu, K. Katayama, T. Kiguchi, A. Akama, T. J. Konno, H. Funakubo, *Appl. Phys. Lett,.* **107**, 032910 (2015).

[7] J. Müller, T. S. Böscke, U. Schröder, S. Müller. D. Bräuhaus, U. Böttger, L. Frey, T. Mikolajick, *Nano Lett.*, **12**, 4318−4323 (2012).

[8] G. Sebald, E. Lefeuvre, D. Guyomar, *IEEE T. Ultrason. Ferr.*, **55**, 538-551 (2008).

[9] A. S. Mischenko, Q. Zhang, J. F. Scott, R. W. Whatmore, N. D. Mathur, *Science*, **311**, 1270-1271 (2006).

[10] R. W. Whatmore, *J. Electroceram.*, **13**, 139-147 (2004).

[11] M. H. Park, H. J. Kim, Y. J. Kim, T. Moon, K. D. Kim, C. S. Hwang, *Adv. Energy Mater.*, **4**, 1400610 (2014).

[12] C. Kittel, *Phys. Rev.*, **82**, 729-732 (1951).

[13] E. Sawaguchi, H. Maniwa, S. Hoshino, *Phys. Rev.*, **83**, 1078 (1951).

[14] F. Jona, G. Shirane, F. Mazzi, R. Pepinsky, *Phys. Rev.* **105**, 849-856 (1957).

[15] S. E. Reyes-Lillo. K. F. Garrity, K. M. Rabe, *Phys. Rev. B*, **90**, 140103 (2014).

[16] M. H. Park, H. J. Kim, Y. J. Kim, T. Moon, K. D. Kim, C. S. Hwang, *Nano Energy*, **12**, 131–140 (2015).

[17] R. Materlik, C. Künneth, A. Kersch, *J. Appl. Phys.*, **117**, 134109 (2015).

[18] V. V. Lemanov, E. P. Smirnova, P. P. Syrnikov, E. A. Tarakanov, *Phys. Rev. B*, **54**, 3151 (1996).

[19] Y. Guo, K. Kakimoto, H. Ohsato, *Appl. Phys. Lett.,* **85**, 4121 (2004).

[20] L. Bellaiche, A. Garcia, D. Vanderbilt, *Phys. Rev. Lett.*, **84**, 5427-5430 (2000).

[21] M. E. Lines, A. M. Glass, *Principles and applications of ferroelectrics and related materials*, Oxford University Press. (1977).

[22] M. H. Park, H. J. Kim, Y. J. Kim, W. Lee, T. Moon, C. S. Hwang, *Appl. Phys. Lett.*, **102**, 242905 (2013).

[23] M. H. Park, H. J. Kim, Y. J. Kim, W. Lee, H. K. Kim, C. S. Hwang, *Appl. Phys. Lett.*, **102**, 112914 (2013).

[24] W. J. Merz, *Phys. Rev.,* **91**, 513-517 (1953).

[25] A. Q. Jiang, H. J. Lee, G. H. Kim, C. S. Hwang, *Adv. Mater.*, **21**, 2870-2875 (2009).

[26] A. Q. Jiang, H. J. Lee, C. S. Hwang, T.-A. Tang, *Phys. Rev. B*, 80, 024119 (2009).

[27] H. J. Lee, G. H. Kim, M. H. Park, A.-Q Jiang, C. S. Hwang, *Appl. Phys. Lett.*, **96**, 212902 (2010).

[28] H. J. Lee, M. H. Park, G. H. Kim, J. Y. Seok, Y. J. Kim, C. S. Hwang, A. Q. Jiang, *J. Appl. Phys.*, **109**, 114113 (2011).

[29] H. J. Kim, M. H. Park, Y. J. Kim, Y. H. Lee, T. Moon, K. D. Kim, S. D. Hyun, C. S. Hwang, *Nanoscale*, **8**, 1383-1389 (2016).

[30] A. Q. Jiang, D. W. Zhang, *Thin Solid Films*, **545**, 145-148 (2013).

[31] D. Zhou, J. Xu, Q. Li, Y. Guan, F. Cao, X. Dong, J. Müller, U. Schröder, *Appl. Phys. Lett.*, **103**, 192904 (2013).

[32] D. Martin, J. Müller, T. Schenk, T. M. Arruda, A. Kumar, E. Strelcov, E. Yurchuk, S. Müller, D. Pohl, U. Schröder, S. V. Kalinin, T. Mikolajick, *Adv. Mater.* **26**, 8198 (2014).

[33] P. D. Lomenzo, Q. Takmeel, C. Zhou, C. M. Fancher, E. Lambers, N. G. Rudawski, J. L. Jones, S. Moghaddam, T. Nishida, *J. Appl. Phys.*, **117**, 134105 (2015).

[34] M. H. Park, H. J. Kim, Y. J. Kim, Y. H. Lee, T. Moon, K. D. Kim, S. D. Hyun, C. S. Hwang, *Appl. Phys. Lett.*, **107**, 192907 (2015).

[35] M. H. Park, H. J. Kim, Y. J. Kim, T. Moon, K. D. Kim, Y. H. Lee, S. D. Hyun, C. S. Hwang, *J. Mater. Chem. C*, **3**, 6291—6300 (2015).

[36] J.-W. Yoon, J. H. Yoon, J.-H. Lee, C. S. Hwang, *Nanoscale*, **6**, 6668-6678 (2014).

6. $Hf_{1-x}Zr_xO_2$ films for capacitive layers in dynamic random access memory

6.1. Introduction

With ever increasing data to be stored and processed, the dramatic advance in memory technology has been a working horse which has successfully supplied the demand. It was possible since scaling down of memory size has been a master key which enables high speed, high density, and low cost. It was same for the dynamic random access memory (DRAM) which works as a primary memory in-memory architecture. The feature size of the DRAM is now scaled down to < 30 nm, and extending the scaling trend according to well-known Moore's law is becoming more challenging due to various difficulties. Generally, DRAM consists of 1 transistor and 1 capacitor, and scaling down of the capacitor is believed to be much more challenging compared to that of the transistor. In fact, DRAM might depend mostly on the performance (high capacitance density with extremely low leakage current and low loss factors) of the capacitor among the various semiconductor-related microelectronic devices. [1] The specific technical difficulties in memory devices including DRAM was extensively reviewed by Hwang. [2]

To extend the scaling trend in conventional DRAM, new materials with high dielectric constant (ε_r) for the capacitive layer is highly required. However, to

find a perfect candidate with high ε_r and extremely low leakage current has not been an easy task, since the electrical bandgap and ε_r are generally inversely proportional. [1] Therefore, the selection of electrode materials or dopants, as well as selection of capacitive layer materials, is also highly important to achieve significant capacitance density with sufficiently low leakage current. Currently, $ZrO_2/Al_2O_3/ZrO_2$ (ZAZ) system is widely used in commercial DRAM, but ZAZ should meet its physical limit shortly. Therefore, extremely high ε_r materials, such as rutile TiO_2 ($\varepsilon_r \sim 100$) and perovskite $SrTiO_3$ ($\varepsilon_r \sim 490$) are intensively studied as next-generation capacitive layer materials. [3, 4] For their utilization, however, special conditions, such as special electrode materials and dopants, are needed. For the formation of Rutile TiO_2, Ru or RuO_2 electrode are needed to suppress the formation of Anatase phase. [5] Moreover, Al doping is required to reduce the leakage current by increasing Schottky barrier height. [6] The deposition of perovskite $SrTiO_3$ using thermal atomic layer deposition (ALD) is a rather challenging task due to their complex growth chemistry which originates from the different reactivity of Sr- and Ti-precursors. [7] Furthermore, the adoption of Ru, RuO_2, or $SrRuO_3$ electrode is also required for Perovskite $SrTiO_3$ films. Although these two candidates showed highly promising properties with very low equivalent oxide thickness (t_{ox}), they also have many difficulties in the fabrication process. Therefore, if the scaling trend can be extended with new high ε_r materials with conventional

standard materials and process, it would be highly beneficial for the scaling down of DRAM shortly.

The utilization of morphotropic phase boundary (MPB) might be another viable solution to find out new high ε_r materials since MPBs in many materials system showed unexpected extraordinary properties deviated from the general relation between ε_r and bandgap. [8] Especially for the case of MPB between nonpolar and polar phase, high ε_r can be achieved by controlling the free energy difference between the two phases. [9] However, the utilization of MPB as a capacitive layer in DRAM has been considered not so promising, since most researches have been concentrated on perovskite structure materials within a single crystal or epitaxial film form. [8] The adoption of special electrode materials (such as $SrRuO_3$) for epitaxial film growth might not be a practical solution for commercial devices. Even worse, their ε_r decreased abruptly with a decreasing film thickness in many cases, and the deposition of high-quality films on Si substrate is a highly challenging task. [7] Moreover, most of perovskite structured materials lack matured deposition techniques appropriate for a nanoscale 3-dimensional structure such as ALD. However, utilization of MPB in DRAM capacitors is still believed to be an attractive solution, if we can find out a new MPB in industry-friendly material systems with well-known physics and chemistry.

Ferroelectricity and antiferroelectricity in the solid solution of HfO_2 and ZrO_2 have been studied since its first report in 2011 and 2012. [10, 11] The

ferroelectricity with P_r larger than 17 $\mu C/cm^2$ could be observed with the Hf:Zr ratio of 0.5:0.5 and film thickness of ~10nm. [11] This unexpected ferroelectricity in thin $Hf_{0.5}Zr_{0.5}O_2$ films is now believed to originate from the formation of noncentrosymmetric orthorhombic phase (o-phase, space group: $Pca2_1$) which might be stabilized due to the combination of various factors such as asymmetric strain, surface energy, and doping. [12] The ferroelectric $Hf_{0.5}Zr_{0.5}O_2$ films are considered to be promising for the memory applications including 1 capacitor – 1 transistor-type ferroelectric random access memory (FeRAM) or 1 transistor-type ferroelectric field effect transistor (FeFET). The antiferroelectricity with the field-induced phase transition between o-phase and tetragonal phase (t-phase, space group: $P4_2/nmc$) could be observed within more Zr-rich composition compared to ferroelectricity. [11] It was suggested that the antiferroelectricity could be used for various energy-related applications, such as electrostatic energy storage, pyroelectric energy harvesting, electrocaloric cooling, and infrared sensing. [13-15]

Another highly interesting topic in HZO films should be an MPB of o- and t-phase in thin $Hf_{1-x}Zr_xO_2$ (HZO) films. In the authors' previous works, $Hf_{0.3}Zr_{0.7}O_2$ films showed the largest ε_r of ~45 at 0V with the film thickness of ~9.2 nm among the films with various Hf:Zr ratio and this value is also desirable when its relatively small film thickness and low leakage current are considered. [16] The MPB in HZO films seems highly attractive owing to their large bandgap (~5.5 eV), high Si-compatibility, and matured deposition

techniques. [9] In fact, HfO_2 has been used as a gate oxide material since its first adoption in Penryn chip by Intel company, and ZrO_2 is currently used as a capacitive layer in commercial DRAM. [1] Moreover, TiN, which is currently a standard electrode material in DRAM, can be used as electrode material. [2] Another promising feature of HZO capacitor is that the interfacial capacitance of TiN/HZO interface is relatively high (~1200 fF μm^{-2}), which should be beneficial for scaling of capacitive layers. [17] The authors recently examined the interfacial capacitance of TiN/HZO interface from pulse switching measurement, and came to know the relatively high interfacial capacitance. [17]

However, the utilization of MPB in HZO films might not be a simple task, since the polymorphism in HZO thin films is strongly affected by size effect. [18] Therefore, the scaling of HZO capacitors using MPB composition cannot be achieved by simply decreasing film thickness within the fixed Hf:Zr atomic ratio. According to the previous works, the film thickness and grain size also affect the complicated polymorphism in thin HZO films, meaning that the composition of MPB might be strongly affected by film thickness. [19] In this study, therefore, the competition of various phases in HZO films would be systemically examined based on the authors' previous works, and the effect of film thickness on the MPB would be systemically studied firstly. Based on this understanding, the strategy to scale down the HZO film utilizing the thickness-dependent MPB would be presented.

6.2. Experimental

HZO films were deposited on a TiN-electroded SiO_2/Si substrate via thermal ALD at a 280°C substrate temperature, using $Hf[N(C_2H_5)CH_3]_4$, $Zr[N(C_2H_5)CH_3]_4$, and ozone as the Hf precursor, Zr precursor, and oxygen source, respectively. The 50-nm-thick TiN electrodes were deposited on the SiO_2/Si substrates via DC reactive sputtering. The growth per cycle of HfO_2 and ZrO_2 were almost identical (~0.11 nm/cycle). Thus, the Hf:Zr atomic ratio could be controlled easily by changing the ratio of the ALD cycles for the HfO2 and ZrO_2. For the electrical characterization, a Pt(30nm)/TiN(5nm) top electrode was deposited via DC sputtering through a shadow mask with a 300μm hole diameter (TiN contacted the HZO film). After the TE deposition, post-metallization annealing was performed for 30 s at 500°C in an N_2 atmosphere using rapid thermal annealing, to crystallize the films. The composition and tf of the HZO films were examined via X-ray fluorescence (Quant'X, Thermo SCIENTIFIC) and ellipsometry (L-116d, Gaertner), respectively. For the electrical characterization, the P-E, J-E, and C-V characteristics were measured using a ferroelectric tester (TF Analyzer 2000, Aixacct Systems, at a 1 kHz frequency), a pA METER/DC voltage source (4140B, HP, with hold time of 1.0 s) and an impedance analyser (4194A, HP, at the AC bias frequency of 10 kHz). The crystal structure of the HZO films was analyzed using an X-ray diffractometer (X'pert Pro, Panalytical), via GIXRD with an incidence angle of 0.5°.

6.3. Results and Discussions

Figure 6. 1 shows the schematic phase diagram based on the experimental results in the authors' previous and present works. [12] The HZO films were deposited using thermal ALD at 280°C on TiN bottom electrode and annealed at 500°C in the N_2 atmosphere for 10-30 seconds. It should be noted that the phase can be different for different film deposition and annealing conditions. For all compositions, the m-phase is formed in relatively thick films, since the m-phase is a stable phase both for HfO_2 and ZrO_2. However, o- and t-phase could be observed in relatively thin films when the formation of stable m-phase is prevented by the size effect. [18] The broken loop in the phase diagram refers to the films of which polarization-electric field (P-E) curves show broken hysteresis loop, and the broken loop originates from the two-step polarization switching due to the involvement of the intermediate nonpolar structure, t-phase in HZO films. [9] The broken hysteresis is evidence which shows that the free energy difference of o- and t-phase is tiny. The largest ε_r of MPB can be achieved with a slightly more Zr-rich composition compared to the broken loop states. In the authors' another work, the phase transition in $Hf_{0.5}Zr_{0.5}O_2$ films with decreasing film thickness occurred at ~7 nm. [18] However, the thickness-dependent o-to-t phase transition in HfO_2 films have not been reported yet, this might be because the film thickness is too small to be characterized either electrically or physically. Olsen et al. and Polakowski et al.

reported the ferroelectricity in pure HfO_2 films, but these results were from the mixture of o- and monoclinic phase (m-phase, space group: $P2_1/c$). [20] Materlik et al. theoretically examined the complicated competition between various polymorphs in polycrystalline HfO_2, ZrO_2, and $Hf_{0.5}Zr_{0.5}O_2$ films with columnar grain structure. [21] In this report, the HfO_2 and $Hf_{0.5}Zr_{0.5}O_2$ film can exist in o-phase within the thickness range of 3-5 and 8-16 nm, respectively. [21] According to their work, the Hf:Zr ratio for MPB within the film thickness of 8 nm is 0.5:0.5, and the Zr contents of MPB might decrease with decreasing film thickness. [21] This trend can be understood based on the combination of the effect of Zr contents on the surface energy and bulk energy difference between o- and t-phase. The bulk free energy of o-phase is lower than that of t-phase in HfO_2, whereas it is the opposite in ZrO_2. Therefore, the increase in Zr contents increases the relative free energy of o-phase compared to that of t-phase. As a result, the smaller film thickness is required to stabilize t-phase in more Hf-rich HZO films. [21] This theoretical calculation seems fairly consistent with the experimental results. [21] Based on these experimental and theoretical works, the MPB of o- and t-phase in HZO films were marked by red dotted line in Figure 1, and the scaling strategy of HZO capacitors along this line would be systematically examined.

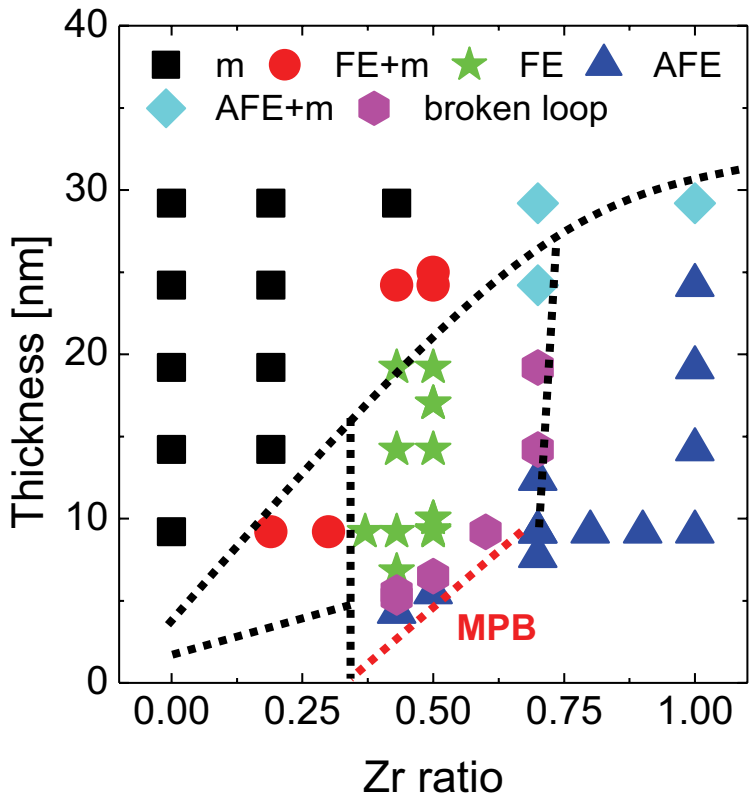

Figure 6. 1. The schematic phase diagram of $Hf_{1-x}Zr_xO_2$ films with various thickness and Zr contents.

In this experiment, rapid thermal annealing (RTA) was carried out at various temperatures (400, 500, 600 °C). Since crystallization is not easy when the thin film is thin, however, only the result of the RTA at 600 °C has been shown in figure 6. 2.. Crystallization was observed to occur well in the 5nm-thick thin film at 600 °C RTA. However, as seen from polarization curve, leakage currents were huge in some compositions. When the thickness of the films becomes thinner, it is highly likely to be vulnerable to leakage current or break down, so that it is impossible to increase the RTA temperature further. It can be seen that the phase transition from FE to AFE is observed as the ZrO_2 contents increases at the same film thickness. It is also observed that the AFE phase transition occurs as the film thickness becomes thinner in the same composition. For example, the peak of ε_r appears in the direction of the voltage sweep at the ε_r-E curve of the 0.5:0.5 contents thin film. From this peak location, it can be seen that the peak appears at the far side in the sweep direction in the 8nm-thick film, which is a typical feature of ferroelectricity. However, when the thickness of films becomes thinner, it can be seen that the location of the peak is gathered in the middle. Moreover, when the film thickness is 5 nm, the location of the peak is completely inverted with respect to each other. This means that the phase transition is entirely complete. Therefore, when the peak is all around 0V, the area with the highest ε_r is the MPB region.

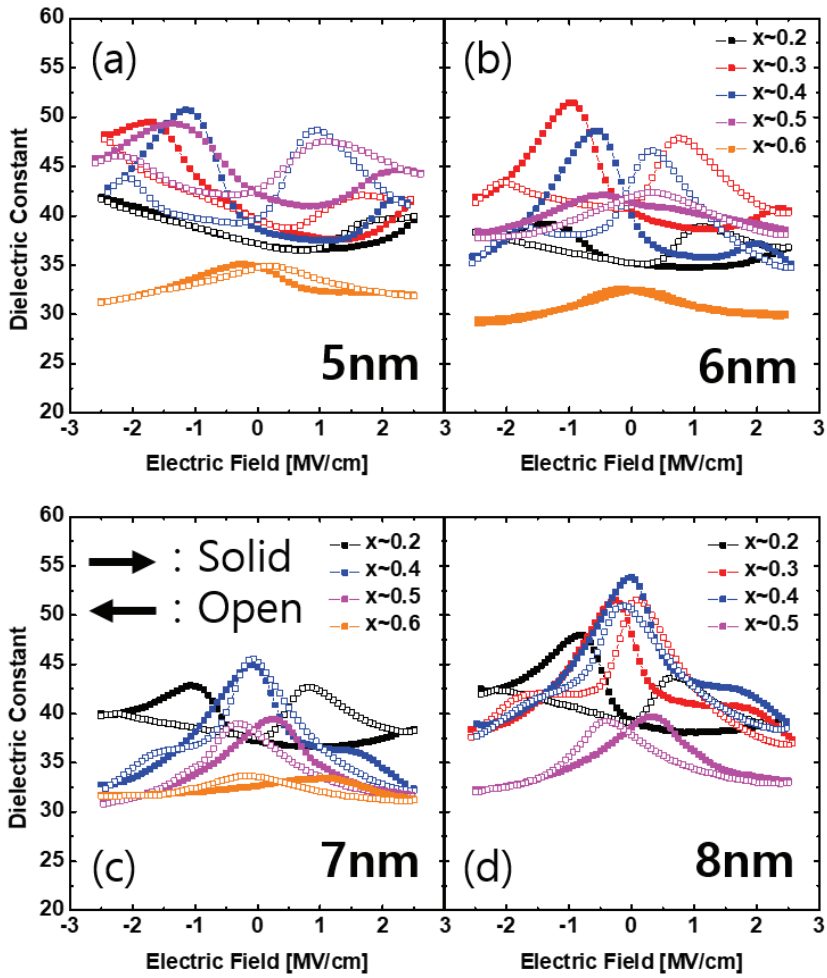

Figure 6. 2. The dielectric constant - electrical field characteristics of the (a) 5nm, (b) 6nm, (c) 7nm, (d) 8nm-thick $Hf_{1-x}Zr_xO_2$ films.

Figure 6. 3 shows the location of the ε_r peaks according to the applied field in the ε_r-E results shown figure 6. 2. First, solid dots are the result when the applied voltages are changed from negative to a positive direction, and open dots are the result when the applied voltages are changed from positive to the negative direction. When the ZrO_2 contents are more than 0.7, the location is not inverted because the AFE behavior is already observed from the 8nm-thick film. However, when the HfO_2 contents are larger than that, the locations appear to be inverted when the film thickness decreases. Therefore, MPB appears at a film thickness of about 7.1 nm, 6.7 nm, and 5.6 nm when the film compositions (Hf:Zr) are 0.4:0.6, 0.5:0.5 and 0.6:0.4, respectively. As contents of ZrO_2 decreases, the thickness of MPB decreases gradually. Therefore, to reduce the thickness of the appearing the MPB, it is necessary to increase the HfO_2 contents. However, since crystallization is difficult when the contents of HfO_2 is increased, and thickness of the film is thinner, an appropriate composition and thickness of HZO films should be chosen.

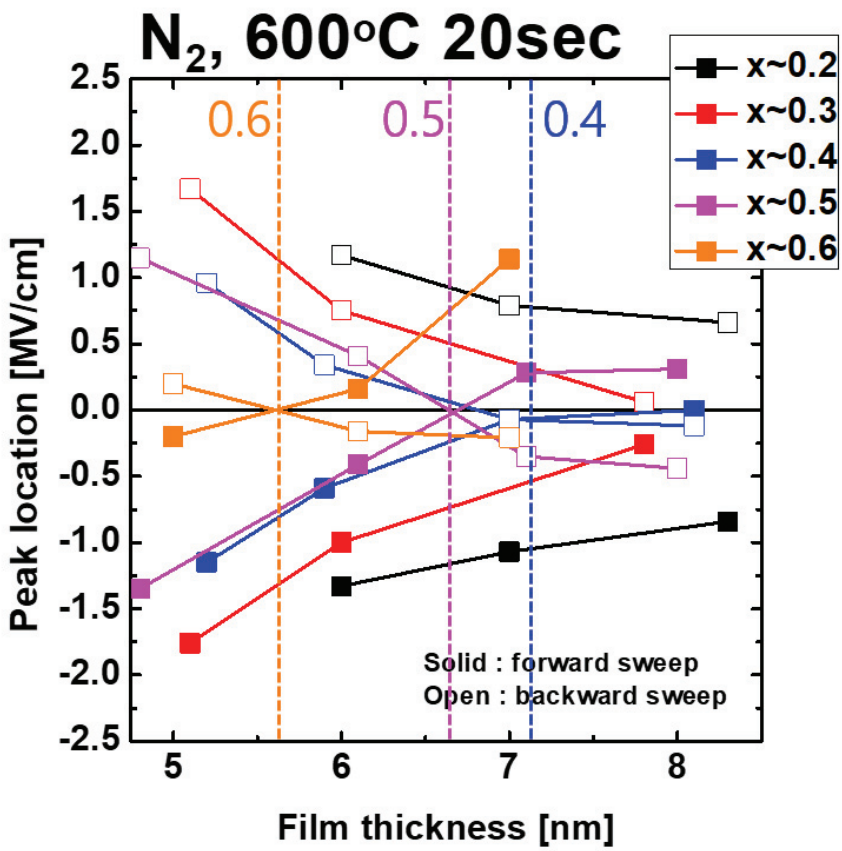

Figure 6. 3. The change in the peak location in ε_r-E curves for $Hf_{1-x}Zr_xO_2$, films with various thicknesses.

Figure 6. 4. shows the relations of leakage current characteristics and t_{ox}. The composition of the films with the lowest t_{ox} was 0.4:0.6. Among the best examples, the t_{ox} of a 7 nm-thick film by annealed on 500 ^{o}C is 0.60 nm, and the t_{ox} of an 8.1 nm-thick film by annealed on 600 ^{o}C is 0.59 nm. As seen from fig 6. 2., these films have high ε_r with overlapped peak locations in the ~ 0 V ranges. The 8.1 nm-thick film has a ε_r about ~55.

There is one innovative way to reduce t_{ox} of the films. To lower the t_{ox}, a thin physical thickness of the film is required, while retaining the ε_r. However, as noted above, it is difficult for these films to have a high ε_r because the location of the peaks of these films was separated. So when these films experience an appropriate wake-up field cycle, peaks can be placed in the center, which means that it could be induced the phase transition of HZO films by electric fields.

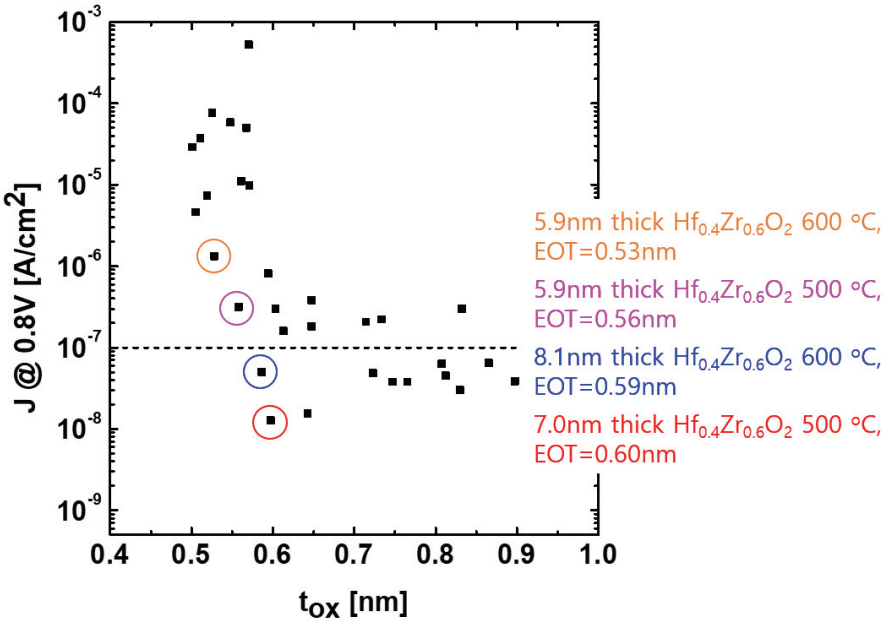

Figure 6. 4. Relationship between the current density (J) at an applied voltage of 0.8V and equivalent oxide thickness for $Hf_{1-x}Zr_xO_2$ films.

Figure 6. 5(a) shows the P-E curves of the 5.9 nm-thick $Hf_{0.4}Zr_{0.6}O_2$ film in a pristine state and after wake-up field cycles. The wake-up field cycles were conducted by repetitive electric field of 10^7 times with a pulse height of 3.5 MV/cm and a pulse width of 10 μs. At the initial state, the film appears AFE characteristics with double hysteresis loops. By sufficient wake-up cycles, however, the phase transition of the film could change the shape of P-E hysteresis curve into a broken loop. Figure 6. 5(b) shows ε_r–E curves of the film in a pristine state and after wake-up field cycles. In the pristine state, the curve shows two separate peaks at both side corners. After wake-up field cycles, these two separate peaks located in the center with high ε_r about ~50. Due to the high ε_r and thin physical thickness, the t_{ox} of the film dropped extremely low to 0.45 nm during the wake-up field cycle. However, as shown in Figure 6. 5(c), the leakage current increased by about an order. Another problem is the need to have a wake-up field cycles applied to each cell in advance because the voltage of the field cycles is much larger than the DRAM operating voltage range. However, it is believed that there is enough room to be improved by optimizing the fabrication processes.

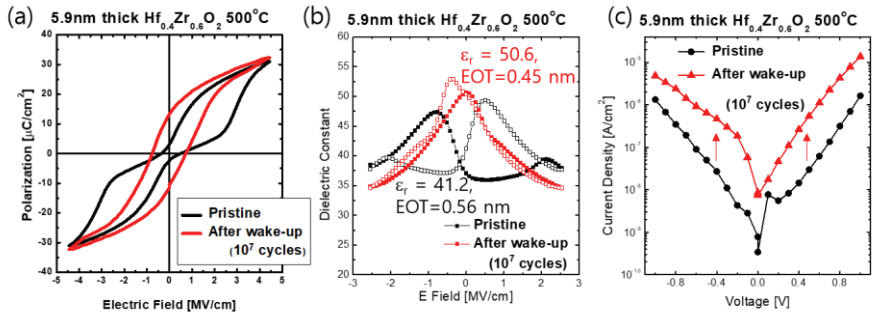

Figure 6. 5. (a) The polarization – electric field characteristics, (b) the dielectric constant – electric field characteristics and (c) the current density – applied voltage characteristics of 5.9 nm-thick $Hf_{0.4}Zr_{0.6}O_2$ thin films in pristine state and after wake-up fields, respectively.

As previously mentioned in the introduction, various materials to replace the state-of-the-art ZAZ capacitive layer have been extensively studied these days. Among the various candidates, the Al-doped TiO_2 and $SrTiO_3$ are believed to be the most promising. The ε_r and bandgap of rutile TiO_2 are ~100 and 3.0 eV, respectively. However, to suppress the formation of Anatase phase of which ε_r is only 35-40, special conditions, such as Ru or RuO_2 electrode, are required. Moreover, to decrease the relatively large leakage current, Al doping is essential to achieve the t_{ox} value smaller than 0.8 nm by decreasing leakage current density by increasing Schottky barrier height. Based on these optimizations, t_{ox} of ~0.37 nm could be achieved. The bulk ε_r (~490) of $SrTiO_3$ is even larger than that of Rutile TiO_2 with similar bandgap. However, the ε_r value decreases with decreasing film thickness, and Ru, RuO_2, $SrRuO_3$ electrode is required to achieve sufficiently low t_{ox} value with low leakage current. [6, 7] Moreover, the film growth of $SrTiO_3$ using ALD is a rather challenging task due to their complicated chemistry which originates from the different reactivity of Sr- and Ti-precursors. [7] Despite such difficulties, the minimum t_{ox} of 0.39 nm could be achieved for $SrTiO_3$. Compared to these materials, the t_{ox} value (~0.62nm) of TiN/HZO/TiN capacitors in the present study seems rather large. However, this value was achieved by using standard electrode material (TiN), and this is only a pioneering work. It is believed that the electrical properties of HZO capacitors might be improved by optimizing film deposition, electrode deposition, and annealing conditions. Al doping

might decrease the leakage current by increasing Schottky barrier height, similar with Al:TiO_2. The adoption of Ru or RuO_2 electrodes seems not so promising, but exploration on various electrode materials might be another option.

6.4. Conclusions

In conclusion, the schematic phase diagram of HZO films with various thickness and Hf:Zr ratio was presented based on the previous works, and the scaling strategy for DRAM capacitors using the MPB of o- and t-phase in HZO films was suggested. From the C-V characterizations, the extraordinary ε_r values could be observed in the MPB, and it could be confirmed that the composition of films changes with changing film thickness. The Zr contents for MPB decreased with decreasing film thickness owing to the relative decrease of the free energy of o-phase compared to that of t-phase. The minimum t_{ox} of 0.59 nm could be achieved for 8.1nm-thick $Hf_{0.4}Zr_{0.6}O_2$ films.

6.5. References

[1] G. He, Z. Sun, M. Liu, L. Zhang, in High-k Gate Dielectric for CMOS Technology (Ed. G. He, Z. Sun), Wiley-VCH, Weinheim, Germany, Ch. 1. (2012).

[2] C. S. Hwang, *Adv. Electron. Mater.* **6**, 1400056 (2015).

[3] C. S. Hwang, S. K. Kim, S. W. Lee, in Atomic Layer Deposition for Semiconductors (Ed. C. S. Hwang), Springer, New York, Ch. 4. (2013).

[4] S. K. Kim, S. W. Lee, J. H. Han, B. Lee, S. Han, C. S. Hwang, *Adv. Funct. Mater.* **20**, 2989 (2010).

[5] S. K. Kim, K. M. Kim, W. D. Kim, C. S. Hwang, *Appl. Phys. Lett.* **18**, 4112 (2004).

[6] S. K. Kim, G. J. Choi, S. Y. Lee, M. Seo, S. W. Lee, J. H. Han, H. S. Ahn, S. Han, C. S. Hwang, *Adv. Mater.* **20**, 1429 (2008).

[7] W. Lee, J. H. Han, W. Jeon, Y. W. Yoo, S. W. Lee, S. K. Kim, C. H. Ko, C. Lasalot-Matras, C. S. Hwang, *Chem. Mater.* **6**, 953 (2013).

[8] A. Rachakom, S. Jiansirisomboon, A. Watcharapasorn, *Ceramics International,* **39**, S139 (2013).

[9] M. H. Park, H. J. Kim, Y. H. Lee, Y. J. Kim, T. Moon, K. D. Kim, S. D. Hyun, C. S. Hwang, *Nanoscale,* **8**, 13898 (2016).

[10] J. Müller, T. S. Böscke, D. Bräuhaus, U. Schröder, U. Böttger, J. Sundqvist, P. Kücher, T. Mikolajick, L. Frey, *Appl. Phys. Lett.* **99**, 112901 (2011).

[11] J. Müller, T. S. Böscke, U. Schröder, S. Mueller, D. Brauhaus, U. Böttger, L. Frey, T. Mikolajick, *Nano Lett.* **12**, 4318–4323 (2012)

[12] M. H. Park, Y. H. Lee, H. J. Kim, T. Schenk, W. Lee, K. D. Kim, F. P. G. Fengler, T. Mikolajick, U. Schoeder, C. S. Hwang, *Nanoscale,* **9**, 9973-9986 (2017).

[13] M. H. Park, H. J. Kim, Y. J. Kim, T. Moon, K. D. Kim, C. S. Hwang, *Adv. Energy Mater.* **16**, 1400610 (2014).

[14] M. H. Park, H. J. Kim, Y. J. Kim, T. Moon, K. D. Kim, C. S. Hwang, *Nano Energy,* **12**, 131-140, (2015)

[15] M. H. Park, H. J. Kim, Y. J. Kim, T. Moon, K. D. Kim, Y. H. Lee, S. D. Hyun, C. S. Hwang, *Adv. Mater.* **28**, 7956-7961 (2016).

[16] M. H. Park, H. J. Kim, Y. J. Kim, W. Jeon, T. Moon, C. S. Hwang, *Physica Status Solidi R.R.L.* **6**, 532-535 (2014).

[17] H. J. Kim, M. H. Park, Y. J. Kim, T. Moon, K. D. Kim, S. D. Hyun, C. S. Hwang, *Nanoscale,* **8**, 1383 (2016).

[18] M. H. Park, H. J. Kim, Y. J. Kim, Y. H. Lee, T. Moon, K. D. Kim, S. D. Hyun, C. S. Hwang, *Appl. Phys. Lett.* **107**, 192907 (2015).

[19] H. J. Kim, M. H. Park, Y. J. Kim, Y. H. Lee, W. Jeon, T. Gwon, T. Moon, K. D. Kim, C. S. Hwang, Appl. *Appl. Phys. Lett.* **105**, 192903 (2014).

[20] P. Polakowski, J. Müller, *Appl. Phys. Lett.* **106**, 232905 (2015).

[21] R. Materlik, C. Künneth, and A. Kersch, *J. Appl. Phys.* **117**, 134109 (2015).

7. Conclusion

In this dissertation, the internal structure of $Hf_{1-x}Zr_xO_2$ thin films was examined based on their grain size, crystallographic structure, and micro-structures. The ferroelectricity could be seen only for the case of $Hf_{1-x}Zr_xO_2$ films thinner than 20 nm. For the case of HfO_2, m-phase was easily formed with small grain size, whereas o-phase cannot be formed due to the large difference of crystal structure of t-phase and o-phase. The o-phase can be formed only in $Hf_{1-x}Zr_xO_2$ films because the formation of the m-phase is prevented and the difference of the crystal structure of the t-phase and the o-phase is small.

The problem of degrading the ferroelectric performance of the HZO films with increasing film thickness (t_f), which could be ascribed to the increased portion of non-ferroelectric m-phase at higher t_f could be resolved by interposing the Al_2O_3 interlayer in the middle portion of HZO film. The Al_2O_3 interlayer retarded the continuous grain growth HZO film, which was accompanied by the decrease in the average grain size. Therefore, the higher portion of ferroelectric o-phase could be retained up to the film thickness of 40 nm. Two portions of the HZO films at upper and lower position appear to have identical ferroelectric performances even though the lower portion was grown on TiN BE while the upper portion was grown on the inserted thin Al_2O_3 layer. This implies that the repetition of an even higher number of stacking is possible without degrading the ferroelectric performance. The insertion of the thin Al_2O_3

layer was also highly promising to mainly decrease the leakage current, which will significantly facilitate the stable operation of the integrated device as well as the precise evaluation of the reliability of this new ferroelectric layer.

As the next step, the wake-up behaviors of $Hf_{0.5}Zr_{0.5}O_2$ with increasing electric field cycling number were examined by the P-E hysteresis loop, ε_r-E curves, and pulse switching tests. The $Hf_{0.5}Zr_{0.5}O_2$ film shows mostly the FE-like behavior from the pristine state, where the slight AFE-like distortion could be ascribed to the anti-parallel distribution of some of the FE domains and the AFE phase. The field cycling of only 100 cycles almost completely removed such anti-parallel pinned domains. Further increase in the field cycling number more effectively poled the domains making the P_r increase. The field cycling also transformed the non-FE phases, mostly at the electrode interface, to FE-phase, which could be inferred from the interfacial capacitance enhancement. These results indicate that the physical state of the FE-phases in the HZO film is entirely different from the conventional FE thin films, such as PZT, in a sense that it is the outcome of variously oriented domains, possibly including anti-parallel orientation. The field cycling plays a role as the poling in conventional FE materials, but the high field-induced non-FE t-phase to FE o-phase transition could also contribute to the effective poling (depinning of pinned FE domains).

In addition to that, the broken hysteresis loop in P-E test and two-step polarization switching in pulse switching measurement from $Hf_{0.4}Zr_{0.6}O_2$ films

were systematically examined based on the first-order-like phase transition theory. The broken hysteresis $Hf_{0.4}Zr_{0.6}O_2$ film could be understood based on the classical theory of the first order phase transition, where the NP phase is involved during the transition from one polarization state to the opposite polarization state. The broken hysteresis loop and two plateau region in switching current response-time curves changed to a single hysteresis and a single plateau region, respectively, after the electric field cycling of 10^3 times. The C_i and E_c values were almost invariant before electric field cycling of 10^3 times, whereas they significantly increased after the electric field cycling of 10^3 times. The increase in C_i and E_c values could be understood from the t-to-o phase transition as in the case of the $Hf_{0.5}Zr_{0.5}O_2$ film in addition to the increase in the area of thin film portion to the switching. Their retardation up to switching cycles of 10^3 could be attributed to the relatively low free energy of t-phase compared to o-phase in the $Hf_{0.4}Zr_{0.6}O_2$ film.

Finally, the scaling strategy for dynamic random access memory (DRAM) capacitors using the MPB of o- and t-phase in HZO films was suggested. From the C-V characterizations, the extraordinary ε_r values could be observed in the morphotropic phase boundary (MPB), and the composition of films changed with changing film thickness. The Zr contents for MPB decreased with decreasing film thickness owing to the relative decrease of the free energy of the o-phase compared to that of t-phase. The minimum t_{ox} of 0.59 nm could be achieved for 8.7nm-thick $Hf_{0.4}Zr_{0.6}O_2$ films.

This thesis presents a new pathway for the next-generation ferroelectric memory by exploring the new material system of $Hf_{1-x}Zr_xO_2$ films and by suggesting the scaling technology for DRAM capacitors using MPB of the o- and the t- phase. Even though the ferroelectric memory is still far from the adoption as a universal memory, the results in this thesis could shed light on this field by suggesting new pathways different from the conventional approach.

Curriculum Vitae

Han Joon Kim

Department of Materials Science and Engineering
College of Engineering
Seoul National University
1 Gwanak-ro, Gwanak-gu, 08826, Seoul, Korea

E-mail: june110@snu.ac.kr
Tel.: +82-2-880-8923
Fax.: +82-2-874-6414

I. Educations

2007.03. - 2012.02. B.S.
Department of Materials Science and Engineering
Seoul National University, Seoul, Korea

2012.03. – 2018.02 Integrated M. S. & Ph. D. Course
Department of Materials Science and Engineering
Seoul National University, Seoul, Korea

II. Research Areas

1. Ferroelectric and Antiferroelectric HfO_2-based films

- The effect of grain size of HfO_2-based films and its influence on electrical characteristics.
- The structural analysis on the polycrystalline HfO_2-based films by Pohang accelerator laboratory synchrotron X-ray scattering methods.
- The wake-up effect of thin HfO_2-based films by repetitive electric field cycles.
- The competition of polymorphs in thin HfO_2-based films with the change of film thickness and composition.
- The first order phase transition in thin HfO_2-based films.
- The observation of abnormal high dielectric constant based on morphotropic phase boundary for the capacitive layer in dynamic random access memory.

2. Domain Switching Kinetics of Ferroelectric Thin Film

- Domain switching kinetics of ferroelectric thin films
- Characterization of electronic properties of ferroelectric thin films
- Domain structure analysis
- Pulse switching system for ferroelectric capacitor
- Negative capacitance theory

III. Experimental Skills

1. Deposition methods

- Atomic layer deposition for fabrication of dielectric materials (Al_2O_3, HfO_2, ZrO_2, SiO_2) by thermal ALD (using traveling wave type)
- DC & RF magnetron sputtering for fabrication of electrode materials (Pt, TiN, RuO_2)
- E-beam evaporation for metal electrode
- Handling and maintenance of high vacuum equipment

2. Analysis methods

- X-Ray Fluorescence Analyzer (XRF, Thermo scientific, ART Quant'X EDXRF) for analysis of composition and layer density of the film.
- X-ray Diffractometer (XRD, PANalytical, X'Pert PRO MPD) for measurement of X-ray diffraction, X-ray reflection (XRR) and reciprocal space mapping.
- Transmission Electron Microscopy (TEM, JEOL, JEM-2100F, JEM-3000F, JEM-200CX) for analysis of cross-sectional images.
- Energy Dispersive Spectroscopy (EDS, Oxford Instrument, AZtec) incorporated by Scanning Transmission Electron Microscopy (STEM, JEOL, JEM-2100F, JEM-3000F) for elemental analysis.
- Atomic Force Microscopy (AFM, JEOL, JSPM-5200) for analysis of the topography
- Spectroscopic Ellipsometer (SE, J.A. Woollam, M-2000) for analysis of optical properties and thicknesses of thin films
- Four points probe for resistivity measurement of metals and conducting

materials

- Pulse/pattern generator (Agilent, 81110A/81111A) and digital oscilloscope for pulse switching measurement of ferroelectric materials
- TF 2000 analyzer (aixACCT) for ferroelectric characterization.
- HP4194A for C-V and impedance measurement of capacitors
- HP4140B and HP4145B for I-V measurement of capacitors
- Characterizing thin films by XPS, AES, ToF-SIMS

IV. Academic Honors

1. "Best Poster Award", The 21st Korean Conference on Semiconductors (2014. 02. 25.)
2. "장려상", 제 6회 서울대학교 기초과학동동기기원 유저논문상 (2015. 04. 09.)
3. "최우수논문상", 제 23회 한국반도체학술대회 (2017. 02. 14)

List of publications

1. Refereed Journal Articles (SCI)

1.1 Domestic

1.2. International

1. Min Hyuk Park, **Han Joon Kim**, Yu Jin Kim, Woongkyu Lee, Hyo Kyeom Kim, and Cheol Seong Hwang, "Effect of forming gas annealing on the ferroelectric properties of $Hf_{0.5}Zr_{0.5}O_2$ thin films with and without Pt electrodes", Applied Physics Letters, 11, 102, 112914 (2013)
2. Min Hyuk Park, **Han Joon Kim**, Yu Jin Kim, Woongkyu Lee, Taehwan Moon, and Cheol Seong Hwang, "Evolution of phases and ferroelectric properties of thin $Hf_{0.5}Zr_{0.5}O_2$ films according to the thickness and annealing temperature", Applied Physics Letters, 24, 102, 242905 (2013)
3. Min Hyuk Park, **Han Joon Kim**, Yu Jin Kim, Taehwan Moon and Cheol Seong Hwang, "The effects of crystallographic orientation and strain of thin $Hf_{0.5}Zr_{0.5}O_2$ film on its ferroelectricity", Applied Physics Letters, 104, 072901 (2014)
4. Min Hyuk Park, **Han Joon Kim**, Yu Jin Kim, Woojin Jeon, Taehwan Moon and Cheol Seong Hwang, "Ferroelectric properties and switching endurance of $Hf_{0.5}Zr_{0.5}O_2$ films on TiN bottom and TiN or RuO_2 top electrodes", Physica Status Solidi R.R.L., 6, 8, 532-535 (2014)
5. Min Hyuk Park, **Han Joon Kim**, Yu Jin Kim, Taehwan Moon, Keum Do Kim, and Cheol Seong Hwang, "Thin $Hf_xZr_{1-x}O_2$ Films: A New Lead-Free System for Electrostatic Supercapacitors with Large Energy Storage Density and Robust Thermal Stability", Advanced Energy Materials, 16, 4, 1400610 (2014)

6. Min Hyuk Park, **Han Joon Kim**, Yu Jin Kim, Taehwan Moon, Keum Do Kim, and Cheol Seong Hwang, "Effect of the annealing temperature of thin $Hf_{0.3}Zr_{0.7}O_2$ films on their energy storage behavior", Physica Status Solid R.R.L., 10, 8, 857-861 (2014)
7. Min Hyuk Park, **Han Joon Kim**, Yu Jin Kim, Woongkyu Lee, Taehwan Moon, Keum Do Kim, and Cheol Seong Hwang, "Study on the degradation mechanism of the ferroelectric properties of thin $Hf_{0.5}Zr_{0.5}O_2$ films on TiN and Ir electrodes", Applied Physics Letters, 7, 105, 072902 (2014)
8. **Han Joon Kim**, Min Hyuk Park, Yu Jin Kim, Young Hwan Lee, Woojin Jeon, Taehong Gwon, Taehwan Moon, Keum Do Kim, and Cheol Seong Hwang, "Grain size engineering for ferroelectric $Hf_{0.5}Zr_{0.5}O_2$ films by an insertion of Al_2O_3 interlayer", Applied Physics Letters, 19, 105, 192903 (2014)
9. Min Hyuk Park, **Han Joon Kim**, Yu Jin Kim, Taehwan Moon, Keum Do Kim and Cheol Seong Hwang, "Toward a multifunctional monolithic device based on pyroelectricity and the electrocaloric effect of thin antiferroelectric $Hf_xZr_{1-x}O_2$ films", Nano Energy, 12, 131-140 (2015)
10. Min Hyuk Park, Young Hwan Lee, **Han Joon Kim**, Yu Jin Kim, Taehwan Moon, Keum Do Kim, Johannes Müller, Alfred Kersch, Uwe Schroeder, Thomas Mikolajick and Cheol Seong Hwang, "Ferroelectricity and Antiferroelectricity of Doped Thin HfO_2-Based Films", Advanced Materials, 11, 27, 1811-1831 (2015)

11. Woongkyu Lee, Woojin Jeon, Cheol Hyun An, Min Jung Chung, **Han Joon Kim**, Taeyong Eom, Sheby Mary George, Bo Keun Park, Jeong Hwan Han, Chang Gyoun Kim, Taek-Mo Chung, Sang Woon Lee, and Cheol Seong Hwang, "Improved Initial Growth Behavior of SrO and $SrTiO_3$ Films Grown by Atomic Layer Deposition Using $\{Sr(demamp)(tmhd)\}_2$ as Sr-Precursor", Chemistry of Materials, 11, 27, 3881-3891 (2015)
12. Min Hyuk Park, **Han Joon Kim**, Yu Jin Kim, Taehwan Moon, Keum Do Kim, Young Hwan Lee, Seung Dam Hyun and Cheol Seong Hwang, "Study on the internal field and conduction mechanism of atomic layer deposited ferroelectric $Hf_{0.5}Zr_{0.5}O_2$ thin films", Journal of Materials and Chemistry C, 3, 6291-6300 (2015)
13. Woongkyu Lee, Sijung Yoo, Woojin Jeon, Yeon Woo Yoo, Cheol Hyun An, Min Jung Chung, **Han Joon Kim**, SangWoon Lee, and Cheol Seong Hwang, "Reducing the nano-scale defect formation of atomic-layer-deposited $SrTiO_3$ films by adjusting the cooling rate of the crystallization annealing of the seed layer", Thin Solid Films, 589, 723-729 (2015)
14. Min Hyuk Park, **Han Joon Kim**, Yu Jin Kim, Young Hwan Lee, Taehwan Moon, Keum Do Kim, Seung Dam Hyun and Cheol Seong Hwang, "Study on the size effect in $Hf_{0.5}Zr_{0.5}O_2$ films thinner than 8 nm before and after wake-up field cycling", Applied Physics Letters, 19, 107, 192907 (2015)

15. Yu Jin Kim, Min Hyuk Park, Woojin Jeon, **Han Joon Kim**, Taehwan Moon, Young Hwan Lee, Keum Do Kim, Seung Dam Hyun, and Cheol Seong Hwang, "Interfacial charge-induced polarization switching in Al_2O_3/Pb(Zr,Ti)O_3 bi-layer", Journal of Applied Physics, 22, 118, 224105 (2015)
16. **Han Joon Kim**, Min Hyuk Park, Yu Jin Kim, Young Hwan Lee, Taehwan Moon, Keum Do Kim, Seung Dam Hyun and Cheol Seong Hwang, "A study on the wake-up effect of ferroelectric $Hf_{0.5}Zr_{0.5}O_2$ films by pulse-switching measurement", Nanoscale, 8, 1383-1389 (2016)
17. Min Hyuk Park†, **Han Joon Kim**†, Young Hwan Lee, Yu Jin Kim, Taehwan Moon, Keum Do Kim, Seung Dam Hyun and Cheol Seong Hwang, "Two-step polarization switching mediated by a nonpolar intermediate phase in $Hf_{0.4}Zr_{0.6}O_2$ thin films", Nanoscale, 8, 13898-13907 (2016)
18. Yu Jin Kim, Min Hyuk Park, Young Hwan Lee, **Han Joon Kim**, Woojin Jeon, Taehwan Moon, Keum Do Kim, Doo Seok Jeong, Hiroyuki Yamada and Cheol Seong Hwang, "Frustration of Negative Capacitance in Al_2O_3/$BaTiO_3$ Bilayer Structure", Scientific Reports, 6, 19039 (2016)
19. Seul Ji Song†, Yu Jin Kim†, Min Hyuk Park, Young Hwan Lee, **Han Joon Kim**, Taehwan Moon, Keum Do Kim, Jung-Hae Choi, Zhihui Chen, Anquan Jiang and Cheol Seong Hwang, "Alternative interpretations for decreasing voltage with increasing charge in ferroelectric capacitors", Scientific Reports, 6, 20825 (2016)

20. Yu Jin Kim, Hiroyuki Yamada, Taehwan Moon, Young Jae Kwon, Cheol Hyun An, **Han Joon Kim**, Keum Do Kim, Young Hwan Lee, Seung Dam Hyun, Min Hyuk Park, and Cheol Seong Hwang, "Time-Dependent Negative Capacitance Effects in $Al_2O_3/BaTiO_3$ Bilayers", Nano Letters, 16, 7, 4375-4381 (2016)
21. Min Hyuk Park, **Han Joon Kim**, Yu Jin Kim. Young Hwan Lee, Taehwan Moon, Keum Do Kim, Seung Dam Hyun, Franz Fengler, Uwe Schroeder, and Cheol Seong Hwang, "Effect of Zr Content on the Wake-Up Effect in $Hf_{1-x}Zr_xO_2$ Films", ACS Applied Materials & Interfaces, 8 (24), 15466-15475 (2016)
22. Keum Do Kim, Min Hyuk Park, **Han Joon Kim**, Yu Jin Kim, Taehwan Moon, Young Hwan Lee, Seung Dam Hyun, Taehong Gwon, and Cheol Seong Hwang, "Ferroelectricity in undoped-HfO_2 thin films induced by deposition temperature control during atomic layer deposition", Journal of Materials Chemistry C, 4, 6864-6872 (2016)
23. Min Hyuk Park, **Han Joon Kim**, Yu Jin Kim, Taehwan Moon, Keum Do Kim, Young Hwan Lee, Seung Dam Hyun, and Cheol Seong Hwang, "Giant Negative Electrocaloric Effects of $Hf_{0.5}Zr_{0.5}O_2$ Thin Films", Advanced Materials, 28, 36, 7956-7961 (2016)
24. Taehwan Moon, Hae Jun Jung, Yu Jin Kim, Min Hyuk Park, **Han Joon Kim**, Keum Do Kim, Young Hwan Lee, Seung Dam Hyun, Hyeon Woo Park, Sang Woon Lee and Cheol Seong Hwang, "Diode performance of the Pt/Al_2O_3/two-dimensional electron gas/$SrTiO_3$ structure and its time-dependent resistance evolution", APL Materials, 5, 042301 (2017)

25. Hae Jin Kim, Kyung Jean Yoon, Tae Hyung Park, **Han Joon Kim**, Young Jae Kwon, Xing Long Shao, Dae Eun Kwon, Yu Min Kim and Cheol Seong Hwang, "Filament Shape Dependent Reset Behavior Governed by the Interplay between the Electric Field and Thermal Effects in the Pt/TiO_2/Cu Electrochemical Metallization Device", Advanced Electronic Materials, 3, 2, 1600404 (2017)
26. Young Hwan Lee, **Han Joon Kim**, Taehwan Moon, Keum Do Kim, Seung Dam Hyun, Hyeon Woo Park, Yong Bin Lee, Min Hyuk Park, and Cheol Seong Hwang, "Preparation and characterization of ferroelectric $Hf_{0.5}Zr_{0.5}O_2$ thin films grown by reactive sputtering", Nanotechnology, 28, 30, 305703 (2017)
27. Min Hyuk Park, Young Hwan Lee, **Han Joon Kim**, Tony Schenk, Woongkyu Lee, Keum Do Kim, Franz P. G. Fengler, Thomas Mikolajick, Uwe Schroeder, and Cheol Seong Hwang, "Surface and grain boundary energy as the key enabler of ferroelectricity in nanoscale hafnia-zirconia: a comparison of model and experiment", Nanoscale, 9, 9973-9986 (2017)
28. Keum Do Kim, Young Hwan Lee, Taehong Gwon, Yu Jin Kim, **Han Joon Kim**, Taehwan Moon, Seung Dam Hyun, Hyeon Woo Park, Min Hyuk Park, Cheol Seong Hwang, "Scale-up and optimization of HfO_2-ZrO_2 solid solution thin films for the electrostatic supercapacitors", Nano Energy, 39, 390-399 (2017)

29. Yu Jin Kim†, Hyeon Woo Park†, Seung Dam Hyun, **Han Joon Kim**, Keum Do Kim, Young Hwan Lee, Taehwan Moon, Yong Bin Lee, Min Hyuk Park, and Cheol Seong Hwang, "Voltage Drop in a Ferroelectric Single Layer Capacitor by Retarded Domain Nucleation", Nano Letters, DOI: 10.1021/acs.nanolett.7b04008 (2017)

2. CONFERENCES

2.1 Domestic

1. Min Hyuk Park, Hyun Ju Lee, Gun Hwan Kim, Yu Jin Kim, Jeong Hwan Kim, Jong Ho Lee, **Han Joon Kim** and Cheol Seong Hwang, "Novel tri-states memory using ferroelectric-insulator-semiconductor hetero-junctions for fifty percent increased data storage", 제8차 강유전체 연합 심포지엄, 무주, 2012년 2월 12일-14일, Poster
2. Yu Jin Kim, Min Hyuk Park, Hyun Ju Lee, Hyung-Suk Jung, **Han Joon Kim** and Cheol Seong Hwang, "Polarization switching in ferroelectric thin films with interposed interfacial layer", 제8차 강유전체 연합 심포지엄, 무주, 2012년 2월 12일-14일, Poster

3. 김유진, 박민혁, 정형석, **김한준**, 황철성, “The observation of Negative Capacitance at Room Temperature from Switching Domains of Ferroelectric Thin Films”, 제 20회 한국 반도체 학술대회, 성우리조트, 2013년 2월 4일-6일, Oral
4. **Han Joon Kim**, Min Hyuk Park, Yu Jin Kim, Hyo Kyeom Kim, Il-Hyuk Yu, and Cheol Seong Hwang, “Examination on the ferroelectric properties and reliability of $Hf_xZr_{1-x}O_2$ films on Ir substrates”, 제 20회 한국 반도체 학술대회, 성우리조트, 2013년 2월 4일-6일, Poster
5. Min Hyuk Park, **Han Joon Kim**, Yu Jin Kim, Hyo Kyeom Kim, Woongkyu Lee, Il-Hyuk Yu, and Cheol Seong Hwang, “The effects of grain size on the electrical properties of ferroelectric $Hf_{1-x}Zr_xO_2$ thin films”, 제 20회 한국 반도체 학술대회, 성우리조트, 2013년 2월 4일-6일, Oral
6. Min Hyuk Park, **Han Joon Kim**, Yu Jin Kim, Taehwan Moon, and Cheol Seong Hwang, “The Factros that Determine the Ferroelectricity in Thin $Hf_{0.5}Zr_{0.5}O$= Films”, 제 10차 강유전체연합심포지엄, 2014년 2월 16일-18일, Poster
7. **Han Joon Kim**, Min Hyuk Park, Yu Jin Kim, Taehwan Moon, and Cheol Seong Hwang, “Grain size engineering for ferroelectric $Hf_{0.5}Zr_{0.5}O_2$ films with Al_2O_3 inter-layer”, 제 10차 강유전체연합심포지엄, 2014년 2월 16일-18일, Poster
8. **Han Joon Kim**, Min Hyuk Park, Yu Jin Kim, Taehwan Moon, and Cheol Seong Hwang, “Deposition of Thicker Ferroelectric $(Hf,Zr)0_2$ Thin Films using Al_20_3 Inter-Layer”, 제 21회 한국 반도체 학술대회, 한양대학교, 2014년 2월 24일-26일, poster

9. Yu Jin Kim, Min Hyuk Park, **Han Joon Kim**, Tae Hwan Moon, and Cheol Seong Hwang, “Stabilization of Negative Capacitance in Ferroelectric Thin Films”, 제 21 한국 반도체 학술대회, 한양대학교, 2014년 2월 24일-26일, oral
10. Min Hyuk Park, **Han Joon Kim**, Yu Jin Kim. Woongkyu Lee, Taehwan Moon, and Cheol Seong Hwang, “Evolution of Phases and Ferroelectric Properties of Thin $Hf_{0.5}Zr_{0.5}O_2$ Films According to the Thickness and Annealing Temperature”, 제 21 한국 반도체 학술대회, 한양대학교, 2014년 2월 24일-26일, oral
11. M. H. Park, **H. J. Kim**, Y. J. Kim, T. Moon, K. D. Kim, Y. H. Lee, and C. S. Hwang, “Antiferroelectric $Hf_xZr_{1-x}O_2$ thin films for the energy-related applications”, 제 11차 강유전체 연합심포지엄, 무주리조트, 2015년 2월 1-3일, oral
12. Y. J. Kim, M. H. Park, Y. H. Lee, **H. J. Kim**, W. Jeon, T. Moon, K. D. Kim, D. S. Jeong, H. Yamada, and C. S. Hwang, “A New Approach to the Negative Capacitance of Ferroelectric Thin Films”, 제 11차 강유전체 연합심포지엄, 무주리조트, 2015년 2월 1-3일, poster
13. **H. J. Kim**, M. H. Park, Y. J. Kim, T. Moon, K. D. Kim, Y. H. Lee, and C. S. Hwang, “Study on the wake-up phenomenon of ferroelectric $Hf_{0.5}Zr_{0.5}O_2$ thin films by polarization switching and discharge behavior”, 제 11차 강유전체 연합심포지엄, 무주리조트, 2015년 2월 1-3일, poster
14. Min Hyuk Park, **Han Joon Kim**, Yu Jin Kim, Taehwan Moon, Keum Do Kim, Young Hwan Lee, and Cheol Seong Hwang, “Thin $Hf_xZr_{1-x}O_2$ Films (x=0.1-0.4) for a Monolithic Device for Various Energy-related Applications”, 제 22회 한국반도체학술대회, 송도컨벤시아, 2015년 2월 10일-12일, oral

15. **Han Joon Kim**, Min Hyuk Park, Yu Jin Kim, Young Hwan Lee, Taehwan Moon, Keum Do Kim, and Cheol Seong Hwang, “Ferroelectric $Hf_{0.5}Zr_{0.5}O_2$ Thin Films with Al_2O_3 inter-layer as a Serial Resistor on Ferroelectric Switching”, 제 22회 한국반도체학술대회, 송도컨벤시아, 2015년 2월 10일-12일, oral
16. Young Hwan Lee, Min Hyuk Park, Yu Jin Kim, **Han Joon Kim**, Taehwan Moon, Keum Do Kim, Seung Dam Hyun, Cheol Seong Hwang, “Characterization of Ferroelectric $Hf_{0.5}Zr_{0.5}O_2$ Films by RF-sputtering Method” 제12차 유전체 연합 심포지엄, 무주 덕유산리조트, 2016. 1. 31.~2. 2., poster
17. **Han Joon Kim**, Min Hyuk Park, Young Hwan Lee, Yu Jin Kim, Taehwan Moon, Keum Do Kim, Seung Dam Hyun, Cheol Seong Hwang, “Study on the Two Step Polarization switching in $Hf_{0.4}Zr_{0.6}O_2$ Thin Film Based on the First Order Phase Transition Theory”, 제12차 유전체 연합 심포지엄, 무주 덕유산리조트, 2016. 1. 31.~2. 2., poster
18. Keum Do Kim, Min Hyuk Park, Yu Jin Kim, **Han Joon Kim**, Taehwan Moon, Young Hwan Lee, Seung Dam Hyun, Cheol Seong Hwang, “Ferroelectric Engineered HfO_2 Films Induced by Gran Size Engineering through Atomic Layer Deposition Temperature Control”, 제12차 유전체 연합 심포지엄, 무주 덕유산리조트, 2016. 1. 31.~2. 2., poster

19. Taehwan Moon, Hae Jun Jung, Min Hyuk Park, Yu Jin Kim, **Han Joon Kim**, Keum Do Kim, Young Hwan Lee, Seung Dam Hyun, Sang Woon Lee and Cheol Seong Hwang, “Influence of O_3 treatment on carrier density of two-dimensional electron gas at a-Al_2O_3/$SrTiO_3$ interface”, 제 23회 한국반도체학술대회, 강원도 하이원리조트, 2016년 2월 22일-24일, poster
20. **Han Joon Kim**, Min Hyuk Park, Yu Jin Kim, Taehwan Moon, Keum Do Kim, Young Hwan Lee, Seung Dam Hyun, and Cheol Seong Hwang, “Decreasing Interfacial Layers of The Ferroelectric $Hf_{0.5}Zr_{0.5}O2$ Film Capacitors by Wake-Up Effect”, 제 23회 한국반도체학술대회, 강원도 하이원리조트, 2016년 2월 22일-24일, oral
21. Seung Dam Hyun, Yu Jin Kim, Min Hyuk Park, **Han Joon Kim**, Teahwan Moon, Keum Do Kim, Young Hwan Lee, and Cheol Seong Hwang, “Study on the Ferroelectric Domain Switching Kinetics in Dielectric/Ferroelectric Capacitors”, 제 23회 한국반도체학술대회, 강원도 하이원리조트, 2016년 2월 22일-24일, poster
22. Keum Do Kim, Min Hyuk Park, Yu Jin Kim, **Han Joon Kim**, Taehwan Moon, Young Hwan Lee, Seung Dam Hyun, and Cheol Seong Hwang, “Analysis on the Evolution of the Ferroelectricity in Undoped HfO_2 Films Prepared by Atomic Layer Deposition”, 제 23회 한국반도체학술대회, 강원도 하이원리조트, 2016년 2월 22일-24일, poster

23. Yu Jin Kim, Min Hyuk Park, **Han Joon Kim**, Taehwan Moon, Keum Do Kim, Cheol Hyun An, Young Hwan Lee, Seung Dam Hyun, and Cheol Seong Hwang, “Interface Charge Controlled Negative Capacitance in Dielectric/Ferroelectric Thin Films”, 제 23회 한국반도체학술대회, 강원도 하이원리조트, 2016년 2월 22일-24일, poster
24. Young Hwan Lee, Min Hyuk Park, Yu Jin Kim, **Han Joon Kim**, Taehwan Moon, Keum Do Kim, Seung Dam Hyun, and Cheol Seong Hwang, “Preparation and Characterization of Ferroelectric $Hf_{0.5}Zr_{0.5}O_2$ Films by RF-Sputtering Method”, 제 23회 한국반도체학술대회, 강원도 하이원리조트, 2016년 2월 22일-24일, poster
25. Keum Do Kim, Min Hyuk Park, Yu Jin Kim, **Han Joon Kim**, Taehwan Moon, Seung Dam Hyun, Hyeonwoo Park, and Cheol Seong Hwang, “Stabilization of tetragonal phase in $Hf_{0.5}Zr_{0.5}O_2$ thin films induced by low deposition temperature during atomic layer deposition”, 제 24회 한국반도체학술대회, 강원도 대명비발디파크, 2017년 2월 13일-15일, oral
26. **Han Joon Kim**, Min Hyuk Park, Young Hwan Lee, Yu Jin Kim, Taehwan Moon, Keum Do Kim, Seung Dam Hyun, and Cheol Seong Hwang, “Involvement of an intermediate nonpolar phase during polarization switching in the $Hf_{0.4}Zr_{0.6}O_2$ thin Films”, 제 24회 한국반도체학술대회, 강원도 대명비발디파크, 2017년 2월 13일-15일, oral

27. Hae Jin Kim, Kyung Jean Yoon, Tae Hyung Park, **Han Joon Kim**, Young Jae Kwon, Xing Long Shao, Dae Eun Kwon, Yu Min Kim, and Cheol Seong Hwang, "Resistive switching behavior of $Pt/TiO_2/Cu$ electrochemical metallization device governed by the interplay between the field and thermal effects", 제 24회 한국반도체학술대회, 강원도 대명비발디파크, 2017년 2월 13일-15일, poster

28. Taehwan Moon, Hae Jun Jung, Yu Jin Kim, Min-Hyuk Park, **Han Joon Kim**, Keum Do Kim, Young Hwan Lee, Seung Dam Hyun, Hyeon Woo Park, Sang Woon Lee, and Cheol Seong Hwang, "Diode Characteristics of the $Pt/Al_2O_3/SrTiO_3$ Structure with Two-Dimensional Electron Gas and Its Time-Dependent Resistance Evolution", 제 24회 한국반도체학술대회, 강원도 대명비발디파크, 2017년 2월 13일-15일, oral

29. Yu Jin Kim, Hyeon woo Park, Hiroyuki Yamada, Taehwan Moon, Young Jae Kwon, Cheol Hyun An, **Han Joon Kim**, Keum Do Kim, Young Hwan Lee, Seung Dam Hyun, Min Hyuk Park, and Cheol Seong Hwang, "Non-hysteretic Negative Capacitance in $Al_2O_3/BaTiO_3$ Bilayers", 제 24회 한국반도체학술대회, 강원도 대명비발디파크, 2017년 2월 13일-15일, poster

30. Seung Dam Hyun, Min Hyuk Park, Yu Jin Kim, **Han Joon Kim**, Taehwan Moon, Keum Do Kim, Young Hwan Lee, Hyeonwoo Park, Yong Bin Lee, and Cheol Seong Hwang, "Study on ferroelectric switching kinetics in polycrystalline $Hf_{0.5}Zr_{0.5}O_2$ films", 제 24회 한국반도체학술대회, 강원도 대명비발디파크, 2017년 2월 13일-15일, poster

2.2 International

1. Min Hyuk Park, Hyun Ju Lee, Yu Jin Kim, Jong Ho Lee, Woongkyu Lee, **Han Joon Kim**, and Cheol Seong Hwang, "Diode-Embedded Resistive Memory Using Stacked Ferroelectric/Dielectric Layer", WoDiM, Dresden, Germany, June 25-27 (2012), Poster
2. Yu Jin Kim, Min Hyuk Park, **Han Joon Kim**, Doo Seok Jeong, Anquan Jiang and Cheol Seong Hwang, "DIRECT OBSERVATION OF TRANSIENT NEGATIVE CAPACITANCE IN DOMAIN WALL OF FERROELECTRIC THIN FILMS", Nature Conference 2012, Aachen, Germany, June 17-20 (2012), Poster
3. Min Hyuk Park, **Han Joon Kim**, Yu Jin Kim, Hyo Kyeom Kim, Il-Hyuk Yu, and Cheol Seong Hwang, "Examination on the ferroelectricity in $Hf_xZr_{1-x}O_2$ thin film", KJC-FE09, Ulsan, August 7-10 (2012)
4. Yu Jin Kim, Min Hyuk Park, **Han Joon Kim**, Doo Seok Jeong, Anquan Jiang, and Cheol Seong Hwang, "Transient Negative Capacitance in Domain Wall of Ferroelectric Thin Films", KJC-FE09, Ulsan, August 7-10 (2012), Poster
5. **Han Joon Kim**, Min Hyuk Park, Yu Jin Kim, Hyo Kyeom Kim, Il-Hyuk Yu, and Cheol Seong Hwang, "Effect of Composition on the ferroelectric properties of $Hf_xZr_{1-x}O_2$ thin film", KJC-FE09, Ulsan, August 7-10 (2012), Poster

6. Yu Jin Kim, Min Hyuk Park, **Han Joon Kim**, and Cheol Seong Hwang, "Transient Negative Capacitance in switching domain of ferroelectric thin films", The 8th Asian Meeting on Ferroelectrics(AMF-8), Pattaya, Thailand, December 9-14 (2012)
7. Min Hyuk Park, **Han Joon Kim**, Yu Jin Kim, Woonkyu Lee, Hyo Kyeom Kim, Il-Hyuk Yoo and Cheol Seong Hwang, "Examination on the ferroelectricity of $Hf_xZr_{1-x}O_2$ thin film on various substrates", The 8th Asian Meeting on Ferroelectrics(AMF-8), Pattaya, Thailand, December 9-14 (2012), Oral
8. Yu Jin Kim, Min Hyuk Park, Hyung-Suk Jung, **Han Joon Kim**, and Cheol Seong Hwang, "Direct Observation of Transient Negative Capacitance in Switching Domains of Ferroelectric/Dielectric Bi-layer Structure", The 8th Asian Meeting on Ferroelectrics(AMF-8), Pattaya, Thailand, December 9-14 (2012), Oral
9. **Han Joon Kim**, Min Hyuk Park, Yu Jin Kim, Hyo Kyeom Kim, Il-Hyuk Yu, and Cheol Seong Hwang, "Investigation on ferroelectric properties of $Hf_xZr_{1-x}O_2$ thin film with various compositions", The 8th Asian Meeting on Ferroelectrics(AMF-8), Pattaya, Thailand, December 9-14 (2012), Poster
10. Yu Jin Kim, Min Hyuk Park, **Han Joon Kim**, Doo Seok Jeong, Cheol Seong Hwang, "Negative capacitance in ferroelectric oxides", CECAM-Workshop Functional oxides for emerging technologies, Bremen University, Bremen, Germany, October 14-18 (2013)

11. **Han Joon Kim**, Min Hyuk Park, Yu Jin Kim, Taehwan Moon and Cheol Seong Hwang, "Grain size engineering for ferroelectric (Hf,Zr)O_2 films by insertion of thin Al_2O_3 layer", MRS SPRING MEETING & EXHIBIT, San Francisco, California, April 21-25 (2014), poster
12. Min Hyuk Park, Ju-Young Cho, **Han Joon Kim**, Yu Jin Kim, Deok Yong Cho, Hyo Kyeom Kim, Woongkyu Lee, Il-Hyuk Yu, Taehwan Moon, Tae Yeong Koo, Young-Chang Joo, and Cheol Seong Hwang, "The origin of the ferroelectricity in thin $Hf_{1-x}Zr_xO_2$ films: microstructure and in-plane tensile stress formed during island coalescence", MRS SPRING MEETING & EXHIBIT, San Francisco, California, April 21-25 (2014), oral
13. Min Hyuk Park, **Han Joon Kim**, Yu Jin Kim, Woongkyu Lee, Taehwan Moon, and Cheol Seong Hwang, "Ferroelectricity in HfO_2-based films", Electroceramics XIV, Bucharest Romania, June 16-20 (2014)
14. M. H. Park, **H. J. Kim**, Y. J. Kim, W. Lee, T. Moon, K. D. Kim, and C. S. Hwang, "Comparative study on the ferroelectric properties of thin $Hf_{0.5}Zr_{0.5}O_2$ films on TiN and Ir electrodes", 14th Annual Non-Volatile Memory Technology Symposium, Jeju, Korea, October 27-29 (2014), poster
15. **H. J. Kim**, M. H. Park, Y. J. Kim, T. Moon, K. D. Kim, W. Jeon, T. Gwon and C. S. Hwang, "Incorporation of Al_2O_3 inter-layer to ferroelectric $Hf_{0.5}Zr_{0.5}O_2$ films for controlling grain size and leakage current" 14th Annual Non-Volatile Memory Technology Symposium, Jeju, Korea, October 27-29 (2014), poster

16. Min Hyuk Park, **Han Joon Kim**, Yu Jin Kim, Taehwan Moon, Keum Do Kim, Young Hwan Lee, and Cheol Seong Hwang, "Thin $Hf_xZr_{1-x}O_2$ Films: A New Lead-free Material for Electrostatic Supercapacitors", HyMAP2014, Busan, Korea, November 10-14 (2014), oral
17. Min Hyuk Park, **Han Joon Kim**, Yu Jin Kim, Taehwan Moon, Keum Do Kim, Young Hwan Lee, and Cheol Seong Hwang, "Toward a multifunctional monolithic device based on pyroelectricity and the electrocaloric effect of thin antiferroelectric $Hf_xZr_{1-x}O_2$ films" MRS Spring Meeting&Exhibit, San Francisco, CA, April 6-10 (2015), oral
18. Taehwan Moon, Min Hyuk Park, Yu Jin Kim, **Han Joon Kim**, Keum Do Kim, Young Hwan Lee, Sang Woon Lee and Cheol Seong Hwang, "Carrier density control of 2-dimensional electron gas at a-Al_2O_3/$SrTiO_3$ interface by ALD using O_3 treatment", ISAF-ISIF-PFM-2015, Singapore, May 24-27 (2015)
19. Lee, Young Hwan, Min Hyuk Park, **Han Joon Kim**, Yu Jin Kim, Taehwan Moon, Keum Do Kim and Cheol Seong Hwang, "The Ferroelectric and Antiferroelectric Properties of HfO_2/ZrO_2 Nanolaminate Systems", ISAF-ISIF-PFM-2015, Singapore, May 24-27 (2015)
20. **Han Joon Kim**, Min Hyuk Park, Yu Jin Kim, Taehwan Moon, Keum Do Kim, Young Hwan Lee, and Cheol Seong Hwang, "An analysis for the wake-up phenomenon of ferroelectric $Hf_{0.5}Zr_{0.5}O_2$ thin films by transient switching current", ISAF-ISIF-PFM-2015, Singapore, May 24-27 (2015)

21. Keum Do Kim, Min Hyuk Park, Yu Jin Kim, **Han Joon Kim**, Taehwan Moon, Young Hwan Lee, Seung Dam Hyun and Cheol Seong Hwang, “Evolution of the Ferroelectricity in undoped HfO_2 films through Deposition Temperature Control during Atomic Layer Deposition”, 1st International Symposium on Emerging Functional Materials, 송도 컨벤시아, November 4-6 (2015), poster
22. **Han Joon Kim**, Min Hyuk Park, Yu Jin Kim, Taehwan Moon, Keum Do Kim, Young Hwan Lee, Seung Dam Hyun and Cheol Seong Hwang, “Analysis on the wake-up behavior of ferroelectric $Hf_{0.5}Zr_{0.5}O_2$ films by pulse-switching measurement”, 1st International Symposium on Emerging Functional Materials, 송도 컨벤시아, November 4-6 (2015), poster
23. Min Hyuk Park, **Han Joon Kim**, Yu Jin Kim, Taehwan Moon, Keum Do Kim,Young Hwan Lee, Seung Dam Hyun, Uwe Schroeder, and Cheol Seong Hwang, “Current understanding of ferroelectricity and field-induced ferroelectricity in $(Hf,Zr)O_2$ films based on first order phase transition theory", Novel High-k workshop, Technical University Dresden, March 14-15 (2016), oral
24. Min Hyuk Park, **Han Joon Kim**, Yu Jin Kim, Taehwan Moon, Keum Do Kim, Young Hwan Lee, Seung Dam Hyun, Franz Fengler, Thomas Mikolajick, Uwe Schroeder, and Cheol Seong Hwang, “Optimization of dielectric and ferroelectric properties in $Hf_{1-x}Zr_xO_2$ for non-volatile ferroelectric memory applications”, WoDIM 2016, Hotel Baia Verde, Catania, ITALY, June 30, 2016, Oral

25. Keum Do Kim. Min Hyuk Park, Yu Jin Kim, **Han Joon Kim**, Taehwan Moon, Seung Dam Hyun, Hyeonwoo Park, and Cheol Seong Hwang, "Ferroelectric to antiferroelectric transition in $Hf_{0.5}Zr_{0.5}O_2$ thin films induced by deposition temperature control during atomic layer deposition", KJC-FE11, Sungkyunkwan University, Seoul, Korea, August 9th 2016, poster
26. Seung Dam Hyun, Yu Jin Kim, Min Hyuk Park, Young Hwan Lee, **Han Joon Kim**, Taehwan Moon, Keum Do Kim, Hyeonwoo Park, and Cheol Seong Hwang, "Study on ferroelectric switching kinetics affected by wake up effect in $Hf_{0.5}Zr_{0.5}O_2$ films", KJC-FE11, Sungkyunkwan University, Seoul, Korea, August 9th 2016, poster
27. Young Hwan Lee, Min Hyuk Park, Yu Jin Kim, **Han Joon Kim**, Taehwan Moon, Keum Do Kim, Seong Dam Hyun, and Cheol Seong Hwang, "Preparation and characterization of ferroelectric $Hf_{0.5}Zr_{0.5}O_2$ films by RF-sputtering method", KJC-FE11, Sungkyunkwan University, Seoul, Korea, August 9th 2016, poster
28. **Han Joon Kim**, Min Hyuk Park, Young Hwan Lee, Yu Jin Kim, Taehwan Moon, Keum Do Kim, Seung Dam Hyun, and Cheol Seong Hwang, "Two-step polarization switching mediated by a nonpolar intermediate phase in $Hf_{0.4}Zr_{0.6}O_2$ thin films", ISAF/ECAPD/PFM Conference 2016, Darmstadt, August 21-25, 2016, oral
29. Keum Do Kim, Min Hyuk Park, Yu Jin Kim, **Han Joon Kim**, Taehwan Moon, Young Hwan Lee, Seung Dam Hyun, Taehong Gwon, Cheol Seong Hwang, "Ferroelectric Engineered HfO_2 thin film prepared by low temperature atomic layer deposition", ISAF/ECAPD/PFM Conference 2016, Darmstadt, August 21-25, 2016, poster

30. Seung Dam Hyun, Yu Jin Kim, Young Hwan Lee, Min Hyuk Park, **Han Joon Kim**, Taehwan Moon, Keum Do Kim, Hyun Woo Park, and Cheol Seong Hwang, "Study on the Ferroelectric Switching Kinetics of $Hf_{0.5}Zr_{0.5}O_2$ films after wake-up effect", ISAF/ECAPD/PFM Conference 2016, Darmstadt, August 21-25, 2016, poster
31. Young Hwan Lee, Min Hyuk Park, Yu Jin Kim, **Han Joon Kim**, Taehwan Moon, Keum Do Kim, Seung Dam Hyun, and Cheol Seong Hwang, "Examination on the effects of various sputter deposition conditions on ferroelectric $Hf_{0.5}Zr_{0.5}O_2$ films", ISAF/ECAPD/PFM Conference 2016, Darmstadt, August 21-25, 2016, poster
32. Keum Do Kim, Min Hyuk Park, Young Hwan Lee, Yu Jin Kim, **Han Joon Kim**, Taehwan Moon, Seung Dam Hyun, Hyeon Woo Park, and Cheol Seong Hwang, "Suppression of crystallization in the as-deposited $Hf_{0.5}Zr_{0.5}O_2$ thin films by controlling deposition temperature during atomic layer deposition", Novel high-k Application Workshop 2017, Dresden, Germany, Mar. 9th, poster
33. Seung Dam Hyun, Yu Jin Kim, Min Hyuk Park, **Han Joon Kim**, Taehwan Moon, Keum Do Kim, Young Hwan Lee, Hyeon Woo Park, Yong Bin Lee, and Cheol Seong Hwang, "Study on Ferroelectric Switching Kinetics in Polycrystalline $Hf_{0.5}Zr_{0.5}O_2$ Films", Novel high-k Application Workshop 2017, Dresden, Germany, Mar. 9th, poster

34. Hyeon Woo Park, Yu Jin Kim, Hiroyuki Itoi, Taehwan Moon, Young Jae Kwon, Cheol Hyun Ahn, **Han Joon Kim**, Keum Do Kim, Young Hwan Lee, Seung Dam Hyun, Min Hyuk Park, Young Bin Lee, and Cheol Seong Hwang, "Study on Hysteresis of Negative Capacitance in $Al_2O_3/BaTiO_3$ Bilayers", Novel high-k Application Workshop 2017, Dresden, Germany, Mar. 9th, poster

Abstract (in Korean)

HfO_2 기반의 강유전체 메모리는 2011년 독일 드레스덴에 있는 NaMLab 이란 연구소에서 처음 발표가 되었다. 기본 페로브스카이트 구조의 강유전체와는 달리 Fluorite 구조를 갖고 있는 HfO_2에 Si을 doping 하였더니 강유전성이 나타났다. 기존의 두꺼웠던 강유전체와는 달리 두께가 10nm 수준으로 매우 얇기 때문에 강유전체 커뮤니티에 새로운 도전을 불러일으켰다. 또한 HfO_2 산화막은 밴드갭이 5.5 eV로 매우 커서 누설 전류 특성에 유리하기 때문에 메모리로 적용하기 우수한 물질이다. 게다가 얇은 박막 두께로 인해서 3차원 구조로 제작할 수 있다는 강점이 있다. 주로 Titanium Nitride 전극을 사용하고, Si 과의 호환성이 좋기 때문에 기존 메모리 공정에 적용할 수 있어 대표적인 산업친화적인 물질이라고 할 수 있다. 이렇듯, 강유전 HfO_2 박막은 차세대 메모리로 적용하기에 있어 우수한 점들이 많고, 흥미로운 결과가 나타나기 때문에 많은 연구가 진행되고 있다. 한편, HfO_2 박막은 Non-centrosymmetric한 Orthorhombic $Pca2_1$ phase인 결정 구조를 지닐 때 강유전성이 나타난다고 알려져 있다. 하지만 이러한 결정 구조를 갖기 위해서 박막을 어떻게 제작해야 할 지에 대한 연구는 아직 부족한 실정이다.

따라서 본 연구에서는 HfO_2가 강유전성을 나타내는 근원을 내부 구조에 대한 연구를 통해서 밝혀내고자 하였다. HfO_2 기반의

강유전체가 갖는 좋은 특징들로 인해 여러 Dopant들에 관한 연구가 진행되었다. 대표적인 Dopant로 Si, Zr, Y, Al, Gd, Sr, La 등이 연구되었다. 여러 Dopant들 가운데, Zr을 Doping 하였을 때 강유전성이 나타나는 조성 범위가 가장 넓었다. 또한, Orthorhombic phase로 결정화시키기 위한 열처리 온도도 500도 정도로 가장 작았기 때문에 강유전성 발현 메커니즘을 분석하는 데에 있어서 가장 유리한 후보라고 할 수 있다.

그 중 첫 번째로, $Hf_{0.5}Zr_{0.5}O_2$ 박막 두께가 증가할수록 강유전성이 열화되는 효과에 대해서 다뤘다. 기존 연구 결과에서는 박막 두께가 10nm 일 때 가장 우수한 강유전성이 나타났는데, 박막 두께가 20nm 이상으로 커지게 되면 점점 강유전성이 사라지기 시작한다. 이 때 결정 구조 분석을 통해 non-ferroelectric monoclinic phase로 결정화가 된 것을 확인하였다. 한편 일반적인 박막 성장 이론에 따르면, 박막 두께가 증가할수록 박막을 이루고 있는 grain의 크기도 함께 커진다. Grain의 크기는 표면 에너지와 부피 에너지의 관계에 영향을 주기 때문에 박막의 결정 구조를 결정하는데 큰 역할을 한다. 따라서 박막 두께가 증가함에도 강유전성의 열화를 막기 위해서는 grain의 크기를 조절하는 것이 중요하다. 본 연구에서는 두꺼운 $Hf_{0.5}Zr_{0.5}O_2$ 박막 중간에 1nm의 Al_2O_3 중간막을 삽입함으로써, grain의 크기를 조절하는데 성공하였다. Al_2O_3 중간막은 하부에 있는 grain의 연속 성장을 방해하기 때문에 원하는 크기로 제어할 수 있었고, 그 결과

40nm 두께의 $Hf_{0.5}Zr_{0.5}O_2$ 박막에서도 강유전성의 열화를 성공적으로 억제할 수 있었다.

다음으로, 강유전 HfO_2에서 나타나는 “wake-up effect” 로 불리는 흥미로운 현상에 대해 다루었다. 이는 반복적으로 전기적 자극을 계속 가하면 강유전성이 점점 더 좋아지는 현상으로, “fatigue effect”와 반대되는 현상이다. 이런 현상이 나타나는 원인은 박막 내부에 orthorhombic phase가 균일하게 생성되지 않고, 전극과의 계면 부근에서도 tetragonal phase로 결정화가 이루어지기 때문이다. 하지만 반복적인 전계를 통해 불완전한 영역들이 균일한 ferroelectric orthorhombic phase로 상전이가 일어나게 되고, 분극 switching에 기여함에 따라 “wake-up effect”가 나타나는 것이다. 이러한 원인을 밝히기 위해서는 Pulse-switching 측정을 하였고, 이를 통해 박막 내부의 저항과 계면의 캐패시턴스를 추적함으로써 반복 전계가 가해질 때 박막 내부의 구조를 확인하였다.

또한, $Hf_{0.4}Zr_{0.6}O_2$ 박막에서는 “Broken Ferroelectric Hysteresis Loop” 이 나타났는데, 이를 1차 상전이 이론에 따라 해석하였다. 이 이론에 따르면 강유전 물질은 온도에 따라 특성 변화가 나타나는데, $Hf_{1-x}Zr_xO_2$ 박막의 경우 조성에 따라서 Curie 온도가 다르게 나타나기 때문에 상온에서 나타나는 특성 역시 다르다. $Hf_{0.4}Zr_{0.6}O_2$ 박막은 상온에서 두 번에 걸친 분극 switching이 나타나는데, 이를 앞서 설명한 1차 상전이 이론으로 해석할 수 있다. 또한, 이러한 현상을

Pulse-switching 측정을 통해 정량적으로 분석하였는데, 결론적으로 두 번에 걸친 분극 switching이 나타나기 위해서는 non-polar 중간상의 존재가 필연적 임을 이해할 수 있다.

마지막으로 $Hf_{1-x}Zr_xO_2$ 박막이 갖는 특성을 이용해서 DRAM 캐패시터로 활용할 수 있는 방법에 대해서 고찰하였다. DRAM 캐패시터는 집적도를 높이기 위해 높은 유전율을 갖고 얇은 두께를 갖는 물질이 후보군으로 대두되었다. 하지만 일반적으로 높은 유전율을 갖는 물질의 경우 밴드갭이 작기 때문에 누설전류 측면에서 취약해서 박막 두께를 얇게 만드는데 한계가 있다. 따라서 이러한 트레이드-오프 관계를 극복하기 위해서는 일반적인 접근이 아닌, 특별히 나타나는 이상 현상을 시도해 볼 수 있다. $Hf_{1-x}Zr_xO_2$ 박막은 두께가 얇아지면서 Orthorhombic phase에서 Tetragonal phase로 상전이가 일어난다. 이 경계를 Morphotropic Phase Boundary라고 부르는데, 이때 계에서 비정상적으로 유전율이 높아지는 현상이 나타난다. 따라서 이러한 현상을 DRAM 캐패시터 물질로 적용하려는 연구를 진행하였고, 그 결과 8.1 nm 두께의 $Hf_{0.4}Zr_{0.6}O_2$ 박막에서 0.59 nm의 등가산화막 두께를 얻을 수 있었다.

주요어: 강유전체, HfO_2, $(Hf,Zr)O_2$, ZrO_2, $Pca2_1$, Wake-up effect, 1차 상전이 이론, 강유전 메모리, 캐패시터, 비휘발성 메모리, 원자층 증착 방법

학번: 2012 - 24158

김 한 준